THE ROLE OF ENVIRONMENTAL FACTORS IN REGIONAL AND LOCAL SCALE

VARIABILITY IN PERMAFROST THERMAL REGIME

By

William Lambert Cable

RECOMMENDED:

_____
Dr. Kenji Yoshikawa

_____
Dr. Bo Elberling

_____
Dr. Hanne H. Christiansen

_____
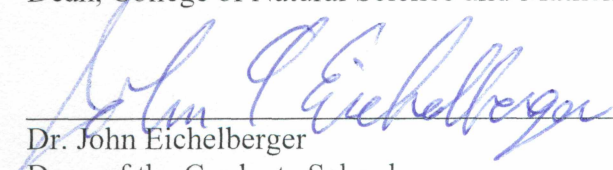Dr. Vladimir E. Romanovsky
Advisory Committee Chair

_____
Dr. Michael Whalen
Chair, Department of Geosciences

APPROVED:

_____
Dr. Paul Layer
Dean, College of Natural Science and Mathematics

_____
Dr. John Eichelberger
Dean of the Graduate School

_____
Date   18 August 2016

THE ROLE OF ENVIRONMENTAL FACTORS IN REGIONAL AND LOCAL SCALE

VARIABILITY IN PERMAFROST THERMAL REGIME

A

THESIS

Presented to the Faculty

of the University of Alaska Fairbanks

in Partial Fulfillment of the Requirements

for the Degree of

MASTER OF SCIENCE

By

William Lambert Cable, B.A.

Fairbanks, AK

August 2016

Abstract

Global climate change is a topic of great concern and research interest because there are still many components of the Earth System which we do not fully understand and cannot predict how they will respond to this change. One of these components is the permafrost that underlies approximately 24% of the Northern Hemisphere land surface. Permafrost is a thermal condition, found primarily at higher latitudes and elevations, in which subsurface material remains below 0 °C for at least two, but often up to thousands of years. As such, permafrost can accumulate large amounts of carbon in the form of organic material that remains frozen, unavailable for decomposition. However, as the climate warms, permafrost warms and thaws, slowly making this stored carbon available for decomposition into greenhouse gases, which have the potential to create a large positive feedback to climatic warming.

A major challenge in permafrost research is that it is not possible to directly obtain spatial information about permafrost through remote sensing alone. This means that we must infer the presence or absence of permafrost and its thermal state based on other remotely sensible parameters such as vegetation, land surface temperature, and topography using a combination of modelling and remote sensing. To do this, we must understand the effects of different environmental factors, such as vegetation, hydrology, topography, and snow on the ground thermal regime and permafrost.

In this thesis, the effects of these environmental factors are examined in relation to permafrost presence or absence and the ground thermal regime on a regional and local scale. The regional scale study focuses on the use of vegetation communities, ecotypes, as integrators of variation in environmental factors to influence the ground thermal regime. At the local scale, the microtopography created by ice-wedge polygons is examined as a cause of variations in environmental factors and the impact this has on the permafrost thermal regime of these features. We find that at both scales, remotely sensible parameters such as ecotypes and microtopography show great promise in the efforts to scale-up both field measurements and modelling results.

Table of Contents

List of Figures

List of Tables

List of Appendices

Acknowledgements

Introduction

Climate change research has shown unequivocally that the climate is warming and will continue to do so if anthropogenic greenhouse gas emissions are not reduced. In the Arctic though, environments are changing much more quickly, as the climate is warming twice as fast as the global average (IPCC, 2014). This has thrust the Arctic into the spotlight for climate change research to understand how these sensitive areas are responding and will respond to continued warming. One area of particular interest has become the permafrost that underlies approximately 24% of the Northern Hemisphere exposed land area (Zhang et al., 2008). The term permafrost was first defined by S. W. Muller (1947) as:

> Permanently frozen ground or permafrost is defined as a thickness of soil or other superficial deposit, or even bedrock, at a variable depth beneath the surface of the earth in which a temperature below freezing has existed continually for a long time (from two [years] to tens of thousands of years). Permanently frozen ground [permafrost] is defined exclusively on the basis of temperature, irrespective of texture, degree of induration, water content, or lithologic character.

Current interest in permafrost stems from the fact that it contains large amounts of organic carbon that has accumulated slowly over thousands of years (Tarnocai et al., 2009). The amount of carbon stored in permafrost regions is approximately 1300 Pg; however, only ~800 Pg is stored within the permafrost itself (Hugelius et al., 2014). To put this in perspective, the concentration of CO_2 in 2005 was 380 ppm or about 805 Pg of carbon (Houghton, 2007). Since permafrost temperatures are coupled to the atmosphere through the surface energy balance, as the climate warms, so does permafrost, leading to permafrost thaw. As a result of climate warming, increases in permafrost temperatures across the Northern Hemisphere have already observed (Romanovsky et al., 2010). As permafrost thaws it becomes part of the seasonally frozen layer above permafrost, the active layer, where almost all biological activity in permafrost underlain landscapes takes place. Carbon in the active layer is then available for decomposition into the greenhouse gases carbon dioxide and methane. This creates the potential for a strong positive feedback that would continue or even accelerate climate warming (Koven et al., 2011; Schaefer et al., 2014; Schuur et al., 2015).

The challenge is to understand how permafrost is responding and will respond to a warming climate. However, in this complex system it cannot simply be assumed that a warming climate will

cause the same amount of warming and thawing of permafrost everywhere. This is because the degree to which permafrost is coupled to the atmosphere is influenced by many factors and surface conditions such as vegetation, hydrology, snow, soil composition, and topography. These factors act to moderate or amplify the effect of climate on the permafrost temperature and amount of thawing. Additionally, there are numerous interactions among these factors, where a change to one often results in changes in the others.

Snow for example, is an excellent insulator, and when sufficient accumulation of snow occurs mean annual ground temperatures can be increased by several degrees (Goodrich, 1982). The timing of snow accumulation is also of importance, as early season snow accumulation impacts the rate at which the active layer refreezes (Goodrich, 1982; Romanovsky and Osterkamp, 1995). Accumulation of snow is influenced by vegetation structure, such as interception of snowfall in spruce canopies (Viereck, 1970) and trapping of snow by shrubs in more windy environments (Sturm et al., 2001).

It has also been long known that vegetation alone plays an important role in the surface energy balance (Dingman and Koutz, 1974; Stoeckeler, 1949; Viereck, 1970). Vegetation regulates the flux of energy into and out of the ground by controlling the accumulation of organic soil layers and moss, and interception of solar radiation (Viereck, 1970) for instance. Viereck (1970) studied the formation of permafrost in a successional floodplain environment in central Alaska. He found that permafrost usually develops concurrently with the successional changes in vegetation and begins to appear as white spruce establishment creates conditions favorable for moss growth.

The importance of hydrology and soil moisture in permafrost systems arises from some of the unique properties of water during the freezing and thawing processes. The most unique property of water is its high latent heat of fusion (334 J/g), the energy associated with phase change between liquid and solid. Compared to the specific heat capacity (4.2 J/gK) for liquid water (Williams and Smith, 1991), this is about 80 times the amount of energy required to raise the temperature of the same amount of water by 1 °C. Thus, as water freezes, this latent energy is released, slowing the cooling and freezing process. Melting of ice requires the same input of latent energy, slowing the melting process. Consequently, a moist or saturated soil in the active layer requires a large amount of energy during the thawing process and releases a lot of energy during the freezing process, which can have a considerable buffering effect. Additionally, when water freezes, its thermal conductivity increases by a factor of four, while its specific heat capacity decreases by half (Gold

and Lachenbruch, 1973). The presence of permafrost also effects the local hydrology as it often creates an impermeable layer, causing hydrologic processes to be confined to the active layer or the portion of the active layer that is thawed (Hinzman et al., 1991).

A major challenge in permafrost research is that unlike many parts of the cryosphere and climate system it is not possible to remotely sense permafrost or permafrost temperature directly (National Research Council, 2014; Westermann et al., 2014). This presents a problem for modelling exercises needed to understand how permafrost will respond to climate change because direct spatial information about permafrost is unavailable. However, since permafrost thermal regime depends on the factors discussed above, they can be used as proxies to assess spatial variation in the permafrost thermal regime.

In this thesis, the variation in permafrost thermal regime will be evaluated on both local and regional scales in relation to these environmental factors. At a regional scale, the ground thermal regime in Western Alaska will be evaluated in relation to vegetation communities (ecotypes) to determine their suitability for use in scaling-up ground thermal regime (Chapter 1). In Western Alaska, and much of Interior Alaska, the permafrost is discontinuous (Brown et al., 1997) and the vegetation communities in these areas often play a critical role in permafrost development and protection (Jorgenson et al., 2010). At a much smaller, local, scale the variation in permafrost thermal regime across different types of ice-wedge polygons, on the Arctic Coastal Plain near Barrow, Alaska, will be examined to determine how variation in microtopography, and the factors it influences, control the thermal regime of permafrost (Chapter 2). The continuous permafrost of the Alaskan Arctic Coastal Plain is considerably colder than that of the Interior Alaska (Romanovsky et al., 2010) and ice-wedge polygon landforms are widespread (Brown, 1967). Recent publications have shown that degradation of these ice-wedges is accelerating (Jorgenson et al., 2006; Liljedahl et al., 2016), impacting the local hydrology (Liljedahl et al., 2012, 2016) and making it important to understand the thermal regime of this landform.

Chapter 1 Scaling-up Permafrost Thermal Measurements in Western Alaska using an Ecotype Approach[1]

Abstract. Permafrost temperatures are increasing in Alaska due to climate change and in some cases permafrost is thawing and degrading. In areas where degradation has already occurred the effects can be dramatic, resulting in changing ecosystems, carbon release, and damage to infrastructure. Yet in many areas we lack baseline data, such as subsurface temperatures, needed to assess future changes and potential risk areas. Besides climate, the physical properties of the vegetation cover and subsurface material have a major influence on the thermal state of permafrost. These properties are often directly related to the type of ecosystem overlaying permafrost. In this paper we demonstrate that classifying the landscape into general ecotypes is an effective way to scale up permafrost thermal data collected from field monitoring sites. Additionally, we find that within some ecotypes the absence of a moss layer is indicative of the absence of near surface permafrost. As a proof of concept, we used the ground temperature data collected from the field sites to recode an ecotype landcover map into a map of mean annual ground temperature ranges at 1 m depth based on analysis and clustering of observed thermal regimes. The map should be useful for decision making with respect to land use and understanding how the landscape might change under future climate scenarios.

1.1 Introduction

Interest in permafrost as a potential source of the greenhouse gasses carbon dioxide and methane has increased, as we are beginning to understand the magnitude of the amount of carbon stored in these frozen soils (Koven et al., 2011; Schuur et al., 2015). However, measurements of the thermal state of permafrost, one of the main indicators of its stability, are sparse given the immense area underlain by permafrost (Romanovsky et al., 2010). It would be advantageous to use remote sensing and modeling to expand upon the direct measurements that are currently available. Satellite remote sensing of permafrost, however, is complicated by the fact that currently there are no sensors that can penetrate the subsurface deep enough to make direct measurements of

permafrost (National Research Council, 2014; Westermann et al., 2014). Instead, the presence or absence of permafrost and its thermal state must be inferred based on other parameters that can be remotely sensed such as land surface temperature (LST), topography, and vegetation through a combination of modeling and remote sensing.

Shur & Jorgenson (2007) have proposed a classification scheme for the formation and stability of permafrost based on the role of climate and ecosystem properties. This classification scheme points to the intimate relationship that exists between ecosystems and permafrost. The connection between permafrost and the atmosphere (in lowland areas) is not direct, rather its thermal state is influenced by vegetation, snow, surface water, soil properties, topography, and numerous interactions between these components and by their interactions with permafrost (Jorgenson et al., 2010). It has long been known that vegetation plays an important role in the development and preservation of permafrost (Dingman and Koutz, 1974; Rieger et al., 1963; Stoeckeler, 1949; Viereck, 1970). Vegetation regulates the flux of energy into and out of the ground by controlling things such as the accumulation of organic layers and moss, and interception of solar radiation (Viereck, 1970). Viereck (1970) studied the formation of permafrost in a successional floodplain environment in central Alaska and found that permafrost developed concurrently with the successional vegetation and began to appear as white spruce created conditions favorable for moss growth.

Mosses play an important role in permafrost formation and preservation due to their change in thermal conductivity depending on their moisture content and whether they are frozen or not. O'Donnell et al. (2009) found that dry live mosses had thermal conductivities between 0.02 and 0.04 W m^{-1} K^{-1}, while water saturated mosses had thermal conductivities approaching that of water, 0.56 W m^{-1} K^{-1} at 0°C (Lide, 2009), a more than tenfold increase. When frozen, the ice in these mosses would have a conductivity of 2.2 W m^{-1} K^{-1} at 0°C (Lide, 2009), a fourfold increase. This makes mosses more effective insulators during the summer than during the winter (Viereck, 1970). During the summer moss layers dry out, lowering their thermal conductivity and evaporation during this period also lowers the surface temperature. Then, during the fall as the air temperature cools, evaporation decreases, the moss layers become water saturated with late rainfall and early snowfall events. As these saturated moss layers become frozen during the winter their thermal conductivity increases and this in turn increasing energy loss during the early winter before substantial snowfall accumulates (Viereck, 1970).

Snow is an excellent insulator, having thermal conductivity values between 0.08 W m^{-1} K^{-1} for new snow and 0.29 W m^{-1} K^{-1} for wind slab (Sturm et al., 2002). When sufficient accumulation of snow occurs mean annual ground temperatures can be increased by several degrees (Goodrich, 1982). However, total end of season snow depth is not the only thing that is important. Early season snow accumulation is particularly important as this is when large amounts of latent heat are released as the active layer refreezes (Goodrich, 1982; Romanovsky and Osterkamp, 1995). The vegetation structure also influences snow accumulation through interception, primarily in spruce canopies (Viereck, 1970), and in the presence of wind through trapping of blowing snow (Sturm et al., 2001). Additionally, Sturm et al. (2001) found the deepest snow occurred in areas with the tallest, densest shrubs and that even small differences in the density of shrubs could have significant effects on snow depth.

Aside from vegetation and snow, other properties are also important in controlling the way the overriding climate is translated to belowground temperatures including: hydrology, subsurface material, topography. These factors are often strongly associated with each other making it possible to identify distinct ecosystems and on a local scale these ecosystems can be classified into ecotypes (Jorgenson, 2000; Jorgenson et al., 2009). Ecotypes can be mapped from remotely sensed data, such as Enhanced Thematic Mapper Plus and Thematic Mapper from Landsat, using the different spectral signatures created by vegetation composition and structure (Jorgenson et al., 2009). Thus, it seems reasonable that ecotypes could be used to infer properties of the underlying permafrost (or lack of permafrost).

The objectives of this paper are: (1) describe an established network of ground temperature monitoring sites in the Selawik area of north-west Alaska; (2) assess the climate gradient across the sites; (3) analyse the ground thermal regimes; and (4) develop a ground temperature map based on relationships between ground thermal regimes and ecotypes.

1.2 Research Area and Ecotype Delineation

As an evaluation of ecotypes to infer permafrost characteristics, the Selawik National Wildlife Refuge (SNWR) in Western Alaska (Figure 1.1) was selected, as previously a high resolution ecotype map had been created for this area (Jorgenson et al., 2009). In addition, western Alaska in general, and the broad area centered on the SNWR and adjacent Bureau of Land Management (BLM) and National Park Service (NPS) lands in particular, were poorly represented in the

network of permafrost temperature measurements developed in Alaska during the last 30 to 40 years by several scientific organizations. The permafrost temperature in this region has only been monitored in two relatively deep boreholes located near Nome and Kotzebue (60 and 29 m deep respectively). During the last several years, a network of shallow (2 to 6 m) boreholes has been established in the villages in this region as a part of the University of Alaska Fairbanks K-12 outreach program (Yoshikawa, 2013). However, this network is limited to locations near to local schools and does not represent the wide local variation in permafrost conditions in the region. Based on existing data, permafrost mean annual temperatures in Western Alaska vary generally between 0 and -4°C (most of existing data fall in the range between 0 and -2°C) and the permafrost spatial distribution changes from continuous in the north to no permafrost in the south (Figure 1.1). Existing observations show that as a result of recent warming local permafrost degradation has already started near the boundary of continuous and discontinuous permafrost, not only in Alaska but also in Siberia (Romanovsky et al., 2010). Present and future thawing of permafrost in these regions will have a dramatic effect on the ecosystems in this area because the permafrost generally has a high ice content, as a result of preservation of old, Late Pleistocene, ground ice in these relatively cold regions even during the warmer time intervals of the Holocene. The high vulnerability of the ecosystems to permafrost degradation in these transitional regions largely dictated our decision to begin establishment of a distributed permafrost observatory on the SNWR and adjacent BLM lands.

1.3 Methods

1.3.1 Establishment of Study Sites

Our study area, the SNWR, is located in Western Alaska (Figure 1.1). The SNWR covers 2.15 million acres and is named for the Selawik River that meanders through the middle of the refuge (U.S. Fish & Wildlife Service, 2003). In the fall of 2011, sites for installation in summer 2012 were selected based on integrative analysis of the existing data on generalized ecotype classes (Figure 1.1), soil landscapes, and vegetation type distribution as documented in Jorgenson et al. (2009). Sites were selected to represent the most abundant ecotypes according to coverage dominance within the SNWR and to provide replication within the most abundant ecotypes (Table 1.1). In total, locations for 18 sites covering 11 of the 43 ecotypes and two burned ecotypes were

selected, representing 62.4% land area of the ecotypes within the SNWR. In addition to these 18 sites, three additional sites outside of the SNWR, previously installed in 2011, were included as they are within a similar climatic region as the SNWR. While we would have liked to include more measurement locations in order to cover more ecotypes and increase replication within ecotypes, this was not possible due to logistical and financial constraints. As there is no road access to SNWR, access during the summer is mostly by boat, airplane on floats, or helicopter. To be able to access all areas of the refuge and not be limited to areas near waterways, we used a small helicopter (Robinson R44) to access most of our sites for installation of equipment and collection of data.

1.3.2 Measurement Design

Our measurement design consisted of a two-tiered site layout of core and distributed sites. The first tier of core sites, collected high temporal and vertical resolution temperature data. These sites comprised a CR1000 data logger (Campbell Scientific, Logan, UT) that collected and saved data from the attached sensors measuring air temperature, snow depth, a high vertical resolution thermistor probe with 16 thermistors spaced exponentially to 1.5 m depth, and three deeper soil temperature sensors (2.0, 2.5 and 3.0 m in most cases). All temperature sensors were installed by drilling a small hole, approximately 2.5 cm in diameter, using a portable handheld hammer drill. The temperatures were measured every 5 minutes and hourly averages were stored on the data logger. The reported accuracy of the temperature sensors is 0.10 °C; however, an ice bath calibration was carried out prior to sensor installation, improving the accuracy for temperatures near 0 °C to approximately 0.02 °C. The core sites were also equipped for remote communications using Iridium satellite transceivers or cellular modems and data was collected daily or weekly. Established in a transect from west to east, moving away from the ocean, and to cover a small elevational gradient (Figure 1.1, stars), these three sites allowed us to characterize any climatic dissimilarities that might be present within the study area.

To further characterize the climate within the area and to put our monitoring years in a historical context, we used daily summarized climate data from the Kotzebue Airport (OTZ) (Menne et al., 2012a, 2012b) located just to the west of the SNWR (Figure 1.1). Daily summarized air temperature and snow depth are available from this station beginning in 1946.

The second tier of distributed sites were deployed to capture the spatial variability in ground temperatures in the region (Figure 1.1). These sites consisted of a U-12 data logger (Onset, Cape Cod, Massachusetts) and four soil temperature sensors located at 3, 50, 100, and 150 cm depth. At six sites it was not possible to drill to 150 cm due to rocks so the maximum sensor depth is 100 cm at four sites, 115 cm at one site, and 75 cm at one site. These data loggers record an instantaneous temperature every 4 hours. The reported accuracy of these temperature sensors is 0.25 °C; however, an ice bath calibration was performed prior to installation, improving the accuracy for temperatures near 0 °C to approximately 0.03 °C. Data from these sites has been collected manually once per year.

In 2013 during site visits to collect data, a small soil pit, approximately 30 by 30 cm, was excavated down to the top of permafrost or at least 75 cm at sites without near-surface permafrost. A general description of the soil profile was made for each site by dividing the soil layers into: living moss, litter, fibric organic material (slightly decomposed), humic organic material (moderate or highly decomposed), and mineral soil.

1.3.3 Data Analysis

Data analysis was conducted using MATLAB (R2013a, MathWorks Inc.). All raw data were first adjusted using a zero-offset that had been determined for each temperature sensor using an ice bath calibration in the lab before sensor installation. Erroneous values in the raw (hourly and 4 hour) data, due to sensor malfunctions, were detected visually and removed. Gaps in the raw data of up to 4 hours were filled using an average of the point's preceding and following the gap. Daily averages, minimums, and maximums were calculated from the raw data for days with at least 75% data coverage; gaps of two days or less in the time series of daily averages were filled using linear interpolation of the previous and following points. Gap filling of both raw and daily data was performed in only a few cases as most data was continuous and without erroneous values. Yearly averages, minimums, and maximums were calculated from the daily data only when 99% of the data was available to insure the data were not biased. A summary period from August 1st to July 31st of the following year was selected as this gave us a full year of data for analysis since the sites were installed in late July (summary periods 2011–2012 and 2012–2013). However, because in 2014 the sites were visited in late July, 10 July 2013 to 9 July 2014 was used as the 2013–2014 summary period in order to have a full year of data for this year.

Thaw depth was calculated from the daily mean subsurface temperatures at each site by first applying a 29 day moving average to smooth the data. The moving average acted to stabilize the near surface temperature (3 cm), but had little effect on the deeper depths as they were already filtered due to the natural damping of temperature variations that occurs with depth in the soil. Then, thaw depth was estimated daily at each site by fitting a piecewise cubic hermite polynomial to the daily temperatures with depth and evaluated at 0 °C for the depth of thaw penetration. This approach forced the temperature profile interpolation to pass through each measurement point, while preserving the shape of the temperature profile (Figure 1.2). It is important that the function fit to the data pass through each measurement point because at these points we know the temperature with the most certainty. Active layer thickness was defined as the maximum depth of the 0 °C isotherm for the entire warm (thawing) period of the year. To test the precision of this technique, the active layer thickness was computed at the three core sites using only 4 of the 16 temperature measurement depths. The resulting active layer thickness corresponded very well to what was estimated from the higher vertical resolution temperature measurements at these sites. An example of this comparison on the date of maximum thaw penetration (11 September 2013) at this site is shown in Figure 1.2, on the right the active layer thickness calculated using all 16 temperature sensors and on the left using only the 4 depths at the 2nd tier sites. The difference between two estimates in 2013 was 1 cm at the Kugurak Cabin (KC1) site and 3 cm at the Selawik Village (SV1). In 2012 the difference between the estimates was 1 cm at all three core sites. Furthermore, this validation shows that our choice of measurement depths, particularly with a measurement at 50 cm, is optimal for this area because the active layer thickness is often near 50 cm.

The timing of the active layer freeze-up was estimated to within a few days. The initiation of the freeze-back period was defined as the date when the daily mean temperature at the near surface (3 cm) dropped and remained below a threshold of -0.3°C for the rest of the season. This threshold was chosen because it has been shown in our previous investigations the temperature interval between 0 and -0.3°C represents the temperatures of major changes in the physical state of water during the freezing process in silty and organic soils (Romanovsky and Osterkamp, 2000). The end of the freeze-back period (time when the active layer was considered to be completely frozen) was defined as the date when all the temperature measurements had gone below this same threshold (e.g., 3 cm, 50 cm, 100 cm etc.).

To objectively evaluate the degree to which our sites were similar (or dissimilar) in terms of ground temperature dynamics, a cluster analysis was performed. A cluster analysis is a data based approach used to objectively classify data into groups where the within group dissimilarity is minimized and the between group similarly is maximized (Liao, 2005). This is in contrast to a more commonly used rule-based approach where groups are first defined arbitrarily for each measured quantity or quantities and then each measurement location is placed into a group (Fovell, 1997). One advantage of the data-based cluster analysis is that the classification rules do not have to be predefined, thus biases of the researcher are removed. For example, Fovell (1997) used this approach to delineate climate zones in the United States based on temperature and precipitation time-series data. Using the time-series of daily mean temperatures at 1 m from each of our sites and with missing data excluded, the pair-wise Euclidian distance between each site was computed. Then, the unweighted average Euclidian distance was used to create an agglomerative hierarchical cluster tree that could be visualized as a dendrogram. The total length of the U-shaped branches connecting two sites indicates the similarity of the datasets, where sites with small distances are most similar and sites with large distances are most dissimilar.

N-factors, which were originally developed by engineers as a way of estimating the freezing and thawing depth (Carlson, 1952; Lunardini, 1978), have also been applied in many studies of the natural environment (Jorgenson and Kreig, 1988; Kade et al., 2006; Karunaratne and Burn, 2004; Klene et al., 2001; Taylor, 1995). The n-factor, $n = DD_s / DD_a$, was calculated as the ratio of the degree-day sums of surface temperature (DD_s) to the degree-day sums of air temperature (DD_a). From our datasets, thawing and freezing n-factors were calculated using daily average air temperature and daily average surface temperature (3 cm depth) for each site and measurement period.

1.3.4 Ground Temperature Map Development

Based on the cluster analysis and the mean annual ground temperature (MAGT) at 1m depth from each ecotype, a map of MAGT was created using the ecotype delineations from Jorgenson et al. (2009). First, using ArcMap (version 10.1, ESRI) each ecotype was recoded with the group number from the cluster analysis. For ecotypes where we did not have any measurements we used the vegetation and soil descriptions in Jorgenson et al. (2009) to group them with their most similar ecotype. Each cluster group was then assigned a range of expected MAGT at 1m depth: -4 to -1

°C, -2 to -1 °C, -1 to 0 °C, and greater than 0 °C. These ranges were chosen to accommodate the majority of MAGT ranges for each ecotype observed during our measuring period. Additionally, a fifth, unknown, category was added for ecotypes that we were not comfortable classifying due to lack of information. Two versions of the MAGT map for the SNWR were created, one with all the ecotypes and one with only the ecotypes for which we made measurements.

1.4 Results

1.4.1 Climate Assessment

Measurements of the air temperature from our three core sites Selawik Village (SV1), Kugurak Cabin (KC1), and Selawik Thaw Slump (STS) (Figure 1.1) allow for comparison of how this parameter changes from the west to the east within the study area. This comparison shows that the seasonal changes in the air temperature are very similar for the SV1 and KC1 sites. The difference in mean monthly temperatures between these two sites does not exceed 2°C and is typically less than 1°C (Figure 1.3 & Figure 1.4, top). Comparison of the monthly means for our three sites to the monthly means for the Kotzebue airport (OTZ) show good agreement during this measurement period (1 August 2012 to 31 July 2014). Unfortunately our STS site stopped functioning in August 2013 due to wildlife damage so we do not have data for the 2013–2014 summary period. Mean annual air temperature calculated from OTZ and our three core sites show that on an annual basis temperatures are similar between sites (Table 1.2). The temperature at STS, however, is a little warmer compared to the other sites, which may be explained by slightly higher elevation of this site and presence of temperature inversions. The air temperature varies substantially from year to year, however. The 2011–2012 measurement period was the coldest on average with temperatures close to the long-term (1981–2010) mean for OTZ with the exception of January 2012, which was considerably colder than the long-term mean. Air temperature during the 2012–2013 summary period shows that most months could be considered normal, with the exception of a cooler than normal November and December 2012 and slightly warmer June 2013 (Figure 1.3). During the 2013–2014 summary period, mean annual air temperatures were considerably warmer (Table 1.2), due in large part to the considerably warmer months of October 2013 and January 2014, and slightly warmer April 2014 (Figure 1.4).

13

In contrast to the air temperatures, available records from all three core sites show that the snow depths were anomalously low during the winter seasons of 2012–2013 and 2013–2014 (Figure 1.3 & Figure 1.4). These measurements agree well with the snow depth reported at OTZ and are well below the long-term (1981-2010) average. In 2012, the first substantial snowfall came very late in the season (mid-December) and by this time the active layer was already completely frozen at most sites. In 2013, the first substantial snowfall also came later (early-November), but due to the warmer than average October the active layer at most sites had just began to freeze. In contrast, during the 2011-1012 summary period the snow depth reported at OTZ was much higher than the long-term average (not shown).

1.4.2 Ground Thermal Regime Analysis

Ground temperature dynamics, as expected, were variable between sites and between measurement periods. For example, the time-series of daily average ground temperature (3, 50, 100, and 150 cm depth) from two years (1 August 2012 to 31 July 2014) for three of our sites (KCF, KC1, and SV1) is presented in Figure 1.5. The time-series begins in August and surface temperatures (3 cm) are warm as the thaw depth approaches its maximum. As the surface temperature cools, the point at which it becomes negative signifies the beginning of the freeze-back period (Figure 1.5, red dashed line). The progression of the freezing front continues from the surface downward and the temperature at each depth remains constant, near 0 °C, until the freezing front has passed. This effect of constant near-zero ground temperatures during the freezing period is termed the 'zero curtain'. When the freezing front passes a particular depth, the temperature at that depth decreases more rapidly, as almost all the liquid water at that depth has been converted to ice. Freeze-back is complete when all temperatures are below a threshold of -0.3°C (Figure 1.5, blue dashed line), indicating that the majority of liquid water has been frozen in the soil profile to the depth of our measurements. Finally, the point at which the 3-cm temperature becomes and stays positive signals the beginning of the thawing period and the cycle begins again.

In this example of time-series data (Figure 1.5) distinct differences and similarities can be seen among sites and between years. For example, sites KC1 (Figure 1.5, B) and KCF (Figure 1.5, A) were only about 200 m apart, but were quite different in terms of their magnitude of temperature response and the timing of the active-layer refreezing. At site KC1 (Figure 1.5, B) freeze-back of the active layer was complete well before KCF (Figure 1.5, A). In contrast, sites KC1 (Figure 1.5,

B) and SV1 (Figure 1.5, C) were much more similar with respect to the magnitude of their temperature response and the date of active-layer refreezing, even though these sites were ~45 km apart. There were also differences between years within the same site, for example, in the winter of 2012–2013 the active layer at our three example sites was completely refrozen by early to mid-December; however, in the winter of 2013–2014 it didn't freeze back until mid-January or late-February. Thus, each time-series is like a unique fingerprint that is a result of the materials and processes occurring between the depth of the temperature measurement and atmosphere above.

To determine the similarity and differences of ground temperature regimes among sites, independent of the ecotype classification, a hierarchical cluster analysis was performed. This analysis included all available daily averages of 1m ground temperature data from each of the 21 sites. The product was four distinct groups or clusters (Figure 1.6). Figure 1.8 and Figure 1.9 show temperature range, MAGT, and active layer thickness sorted according to the dendrogram and reveal that while groups tend to have similar MAGT, the active layer thickness is somewhat more variable. With only one exception all sites of the same ecotype fell into the same cluster group, and we use this order for subsequent figures.

The freezing and thawing n-factors (Figure 1.7) are used to divide the effect of the vegetation and snow cover on the surface temperatures into freezing and thawing seasons. An n-factor near one indicates there is little difference between the air and surface temperatures, while a thawing n-factor above one indicates a surface that is warmer than the air and a thawing n-factor below one indicates a surface that is colder than the air. The opposite is true for the freezing n-factor. In most natural systems n-factors are less than one due to the insulating effects and albedo of vegetation and snow (Taylor, 1995) and due to evaporation from the ground surface. The thawing n-factor gives us a relative sense of the amount of heat absorbed by the ground during the warm part of the year. While complicated to interpret, the freezing n-factor is related to the timing, thickness, and density of the snowpack. A thick snowpack would tend to keep the ground warmer producing a low freezing n-factor, while a thin or late snowpack would allow the surface temperature to more closely match the air temperature resulting in a freezing n-factor closer to 1. Figure 1.7 shows that the thawing n-factors for our sites generally fall between 0.8 and 1.0 and that between year differences for a given site are small. Thus, the insulative and cooling effects of the vegetation are more or less constant from year to years. The freezing n-factors show a much wider range of variation and a pronounced difference between our two measurement periods. The freezing n-

15

factor in 2013–2014 for all sites was considerably lower than in 2012–2013, likely due to the late arrival of snow in winter 2012-2013. The freezing n-factors point to the importance of both the timing and depth of the snowpack in controlling the thermal regime.

The first group in the cluster analysis, with the coldest MAGT's, is composed mostly of the Upland Dwarf Birch-Tussock Shrub (TS) ecotype, which is abundant within the SNWR (28.4% areal coverage). The group also includes the Lowland Sedge Fen ecotype (SFL, 3.6% areal coverage) and Riverine Birch-Willow Low Shrub ecotype (BWR, 3.3% areal coverage), making the coverage of this grouping approximately 35% within the SNWR and the largest areal coverage of all the cluster groups. The vegetation within all of these ecotypes is primarily sedges and low shrubs, and with usually a thick moss layer (3–6 cm) that is underlain by a thick organic layer (fibric and humic) that often makes up most or all of the active layer (Figure 1.10). In 2012–2013, the MAGT at 1 m varied between -4.6 and -3.5 °C, while during 2013–2014 the MAGT was considerably warmer and varied between -2.8 and -0.8 °C (Table 1.3). The active layer was variable, but averaged 52 cm during both periods with the exception of the Tussock Post Burn site (S2-PB), which averaged 82 cm for the two years (Table 1.3). In 2012–2013, freeze-back of the active layer was complete by late November or early December, while in 2013–2014 freeze-back occurred in January or as late as March at one site (Table 1.3). The freezing n-factors (Figure 1.7) for these sites are the highest of all the cluster groups, indicating these sites have the best coupling to the atmosphere during the freezing season.

The second group identified by the cluster analysis was composed of three different ecotypes: Lowland Birch-Ericaceous Shrub (BEL, 7.3% areal coverage), Upland White Spruce-Ericaceous Forest (WSE, 4.8% areal coverage), and Upland Alder-Willow Tall Shrub (AWU, 4.4% areal coverage). Together, these ecotypes cover approximately 17% of the SNWR. The vegetation within this group was mostly low to medium shrubs with some sites having white spruce trees. The soil profile at these sites, like the first group, also tended to have a thick moss layer, but was underlain by somewhat thinner organic layers (fibric and humic). However, one site within the Lowland Birch-Ericaceous Shrub ecotype (site KCF) had only a thin (2 cm) leaf litter layer with no moss layer (Figure 1.10). The sites within this group have similar MAGT at 1 m, with a range of -3.2 to -2.4 °C in 2012–2013 and -2.0 to -0.7 °C in 2013–2014 (Figure 1.8 & Figure 1.9), making them slightly warmer than the first group. The calculated active layer depths within this group were variable, averaging 66 cm in 2012–2013 and 46 cm in 2013–2014 (Table 1.3). The end of

the freeze-back period was generally the same as group one, occurring by late November or early December in 2012–2013 and occurring later in 2013–2014 (Table 1.3). The freezing n-factors (Figure 1.7) for these sites are similar but slightly lower than in the first group, indicating that sites in this group are also well coupled to the atmosphere during the freezing season.

The third group, with the warmest permafrost, was made up of only two ecotypes; the Lowland Alder-Willow Tall Shrub ecotype (AWL, 4.0% areal coverage) and the Upland Birch-Ericaceous Shrub ecotype (BEU, 3.2% areal coverage). Together these ecotypes occupy approximately 7% of the SNWR and formed the smallest group with near-surface permafrost. Generally, the vegetation within these ecotypes had low to medium height shrubs and these sites had either a very thin or no moss layer underlain by organic layers similar in thickness to that of the second group (Figure 1.10). The MAGT at 1 m for these sites ranged from -1.9 to -1.1 °C in 2012–2013 and from -0.6 to -0.2 °C in 2013–2014 (Figure 1.8 and Figure 1.9). The active layer thickness and freeze back duration at these sites was variable (Table 1.3). The freezing n-factors (Figure 1.7) for these sites are lower than both of the first two groups and indicate that these sites are more decoupled from the atmosphere during the freezing season, likely due to a thicker snowpack.

The fourth group identified in the cluster analysis included only the sites where we did not observe near-surface permafrost. This group is also the greatest distance from the other groups according to the cluster analysis (Figure 1.6). These sites belong to the Upland White Spruce-Willow Forest ecotype (WSW, 1.8% areal coverage), Upland Birch Forest (BFU, 0.6% areal coverage), and one site from the Upland Alder-Willow Tall Shrub (AWU, 4.4% areal coverage). Also included in this group is a White Spruce site that had previously burned (WSB). All these sites lack a moss layer on the surface and have a relatively thin organic layer (Figure 1.10). The freezing n-factors (Figure 1.7) at these sites are the lowest off all our sites and indicate they are the most decoupled from the atmosphere during the freezing season, likely due to a thicker and possibly earlier snowpack. Unfortunately, many of these sites had equipment malfunctions, making it difficult to calculate yearly summary statics (Figure 1.8, Figure 1.9 & Table 1.3). However, the ground temperature dynamics reflected in the available time-series data for these sites indicates that permafrost is likely absent in the upper 1.5 m. Additionally, their clustering with sites known to lack near-surface permafrost lends support to this conclusion.

Based on our measurements freeze-back begins at approximately the same time across all sites, however, the duration often differs. During the 2012–2013 period the active layer began to freeze

back in early October 2012 and freeze-up was complete at most sites by the beginning of December 2012 (Table 1.3). The very late and shallow snow-cover and related early freeze-up of the active layer resulted in low winter, and thus annual, mean ground temperatures. During the 2013–2014 period freeze-back began much later (early-December 2013) and at some sites lasted until late-February or early-March 2014 (Table 1.3). Analysis of the mean annual ground temperatures at 1 m depth obtained from the measurement sites that were established in 2011 shows that the mean annual temperatures at this depth were lower in the 2012-2013 measurement period than in 2011-2012 by 1.5 to 1.8°C (Table 1.4). During the 2013–2014 measurement period MAGT at 1 m was the warmest of the three years (Table 1.4), which corresponds to the warmest mean annual air temperature. In general, the variation in MAGT at 1 m seen between years is as large as the variation among ecotypes.

1.4.3 Ground Temperature Map

As a proof of concept we used the range of MAGT at 1m depth measured across these different ecotypes (Table 1.3) and the clustering results to recode the ecotype map from Jorgenson et al. (2009) into a map of MAGT classes. Fortunately, our two main study years (2012–2013 and 2013–2014) included both a relatively cold (2012–2013) and warm (2013–2014) year allowing us to assess variability among years. We are confident these years bracket the longer-term mean ground temperature (and deeper permafrost temperature) because in 2012–2013 the slope of MAGT with depth was negative (Figure 1.8), indicating colder than average MAGT and mean annual air temperature (MAAT). While, in 2013–2014 the slope of MAGT with depth was positive (Figure 1.9), indicating warmer than average MAGT and MAAT. While our measurements only covered 11 of the 43 ecotypes present in the SNWR, these ecotypes covered 62.4% of the land area in the SNWR. Two versions of the MAGT map for the SNWR were created, one with all the ecotypes (Figure 1.11) and one where the ecotypes we did not make any measurements in are masked out (Figure 1.12).

1.5 Discussion

A moss layer, which strongly affects soil temperatures, was not found in all of our ecotypes and this is possibly related to the presence of shrubs and trees in those ecotypes. When the density of deciduous trees and shrubs becomes sufficiently high, the annual leaf litter from these trees and

shrubs can inhibit the growth of mosses (Viereck, 1970) by covering the ground and preventing the mosses from receiving light. However, this is not the case with coniferous species, which retain their needles for longer periods of time.

We found that within the Upland Alder-Willow Shrub (AWU) ecotype and ecotypes containing White Spruce (WSW & WSE) there was a positive relationship between the presence of moss and the presence of near-surface permafrost. For example, within the White Spruce ecotypes the n-factors (Figure 1.7) can help us understand the difference between these sites. Within the Upland White Spruce-Willow Forest (WSW) ecotype our site (S1-WS), with no moss layer and no near-surface permafrost, had low n_f values; while the values of n_t were similar to that of the Upland White Spruce Ericaceous (WSE) site (SS-WS), with a thick moss layer and permafrost. The WSE site, however, had much higher n_f values, indicating that it was less insulated during the winter and was able to loose heat accumulated during the summer more readily. The same effect is likely occurring between our two AWU sites, but unfortunately we did not have sufficient surface temperature data from the AWU site without near-surface permafrost to calculate n-factors. The moss layer is important within other ecotypes as well because it acts as an insulator during the summer keeping the thawing front from penetrating too deeply.

Tussocks in the Dwarf Birch-Tussock Shrub (TS) ecotype also have an important effect on the permafrost thermal regime. During the winter the tussocks stick up above the snow surface until enough snow has fallen to cover them completely. This creates holes in the snow cover, which would normally be a very good insulator, and allows heat to be removed from the ground surface by convecting air, cooling the ground. Additionally, these same tussocks have a shading effect during the summer, reducing the warming of the ground surface and permafrost. These factors work together to make tussock shrub ecotypes one of the coldest.

While there is some variability in n-factor values (Figure 1.7) within the cluster groups there are observations that can be made based on these values. We see that n_t values generally range between 0.6 and 1.0 and there does not seem to be any relationship between ecotypes or cluster groups. The n_f values however show a decreasing trend with increasing MAGT at 1 m. Cluster one, with the coldest MAGT, tends to have the highest n_f values; while cluster four, with no near-surface permafrost, tends to have the lowest n_f values. This indicates that the MAGT of an ecotype in this region depends more on how well it is able to release accumulated summer heat during the winter. There are exceptions to this generalization. Some sites in cluster one have low n_f values; however,

these sites also tend to have low n_t values that would tend to offset this. There is also some variability between the two measurement periods, but almost all of this variability occurs during the freezing season. In fact, all the n_f values are lower in 2013–2014 than they were in the previous year. This could be related to the late snowfall and early freeze-up of the active layer in 2012. With the active layer refrozen earlier in 2012 it would be a better conductor of heat to the surface for longer than during the following year, when the snow arrived earlier and the active layer refroze later.

The MAGT at 1m depth maps (Figure 1.11 and Figure 1.12) show that large areas of the SNWR, mainly the lowlands, are covered by ecotypes belonging to the coldest groups. These areas are probably more stable under a warming climate. However, areas along the rivers and streams and in the more upland areas tend to have warmer permafrost or lack permafrost entirely and are probably much more sensitive to any additional warming or disturbance. Evidence of areas with warmer permafrost can be found in the form of permafrost thaw features. One such feature, the Selawik Retrogressive Thaw Slump (RTS), is located along the Selawik River to the east and approximately 100 km upstream from Selawik (and near our site STS, Figure 1.11). The Selawik RTS formed in 2004 (USFWS, 2007) and the headwall has retreated at a rate of about 20 m/yr (Barnhart and Crosby, 2013). Closer inspection of the map in the area of the RTS indicates large areas classified as the warmest permafrost with smaller spots classified as no permafrost. Thus, maybe we can expect more of these features in this area as the climate continues to warm.

Closer inspection of the MAGT map around the Selawik River (e.g. inset in Figure 1.11) shows that areas immediately adjacent to the river belong either to the warmest permafrost group or lack near-surface permafrost. These areas, more recently modified by the meandering of the river, are in the early stages of vegetational succession and permafrost development. While areas that have not been modified by the river recently are classified into the colder permafrost groups. This agrees with what Viereck (1970) found in Interior Alaska, that newly fluvial modified surfaces did not have permafrost. However, as the vegetation succession progresses, it begins to favor the formation of permafrost in later successional stages. It is uncertain though whether the climate will continue to favor the development of permafrost in these areas.

20

1.6 Conclusion

In this paper we have shown that ecotypes, which partition the variability in both vegetation and soil characteristics, are a reliable way to scale up observed ground thermal regimes from point to regional scale. This provides not only an opportunity for the scaling up of the ground thermal regime observed at field research sites but also for improved resolution of models of ground thermal regime. Accordingly, we recommend that future permafrost modeling efforts consider using an ecotype approach rather than more traditional grid-based approaches. Additional, future efforts to collect baseline ground temperature data should be focused on improving spatial coverage by establishing distributed sites in different ecotypes within a region.

Classification of the temperature time-series from our sites using a cluster analysis yielded four groups with distant properties. The first, coldest permafrost group, consisted mainly of ecotypes with sedges and low shrubs that tended to have thick moss and organic layers. The second, warmer permafrost group, contained mostly ecotypes with shorter shrubs or white spruce and also had a thick moss layer, but thinner organic layers than the first group. The third, warmest permafrost group, consisted mostly of ecotypes with tall shrubs and tended to have very thin or no moss layer and thinner organic layers. The fourth group, lacking permafrost within the top 1.5 m, had ecotypes with tall shrubs but lacked a moss layer and had thin organic layers. Thus, we find that an insulative moss layer is an important positive permafrost predictor. Warmer ground temperatures were associated with ecotypes with denser deciduous shrubs or trees, presumably because the shrubs and trees trap snow during the winter, which increases the snowpack, and generate more leaf litter, which reduces moss growth.

We used our results to generate a map of MAGT at 1m depth for the SNWR based on the ecotype landcover map produced by Jorgenson et al. (2009). This map shows that large areas in the lowlands of the SNWR are underlain by colder permafrost, while upland areas and areas adjacent to the rivers tend to be underlain by warmer or no permafrost at all.

Additionally, we collected a baseline of ground thermal data for the SNWR and surrounding areas which were previously underrepresented. We plan to continue collecting data from these sites as long as funding permits. The data used in this paper have been archived and are publicly accessible on the ACADIS Gateway[2].

---

[2] https://www.aoncadis.org/dataset/Permafrost_Western_AK_Selawik_NWR.html

Acknowledgements

Figure 1.1: Location Map

Figure 1.1 The map of the location of our research sites in the study area, the SNWR, north-west Alaska. The ecotype map (Jorgenson et al. 2009) is shown in the background where available.

Figure 1.2: Temperature Depth Profiles
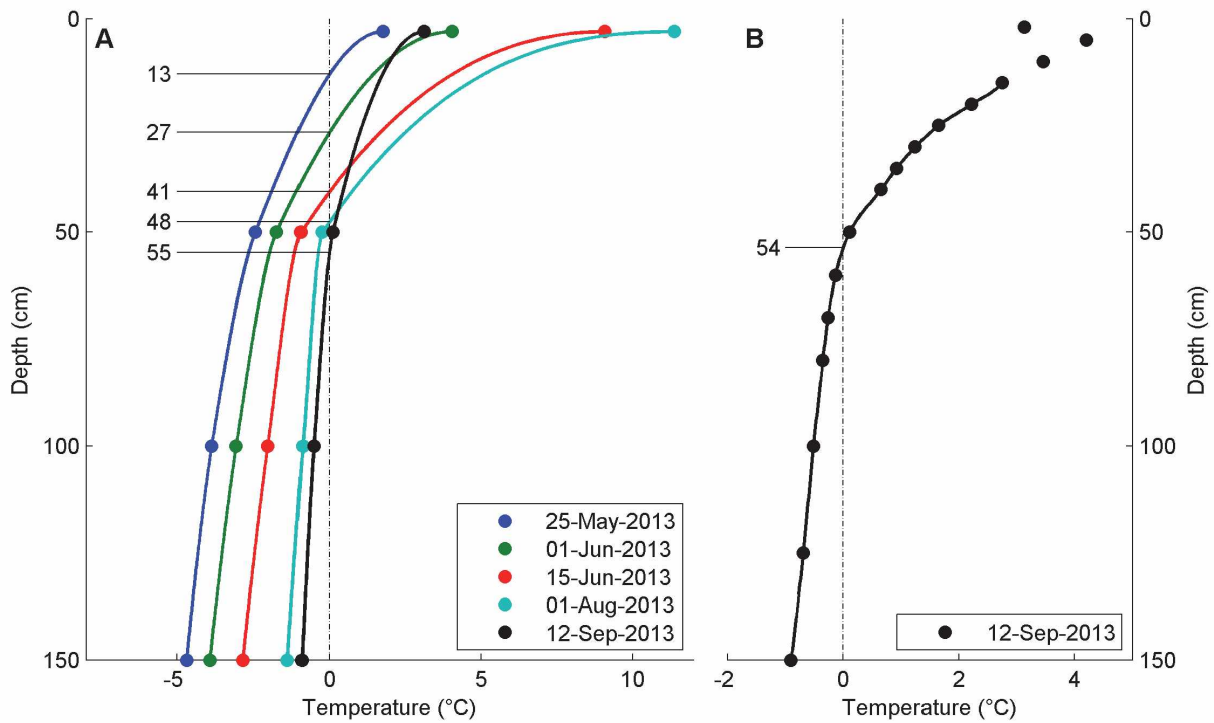
Figure 1.2 Temperature depth profiles from site KC1. (A) Shows temperature depth profiles using only 4 depths for selected days with the estimated thaw depth to the left. (B) Shows the temperature depth profile with all 16 temperature measurements for the date near maximum thaw depth.

Figure 1.3: Climate Summary 2012-2013
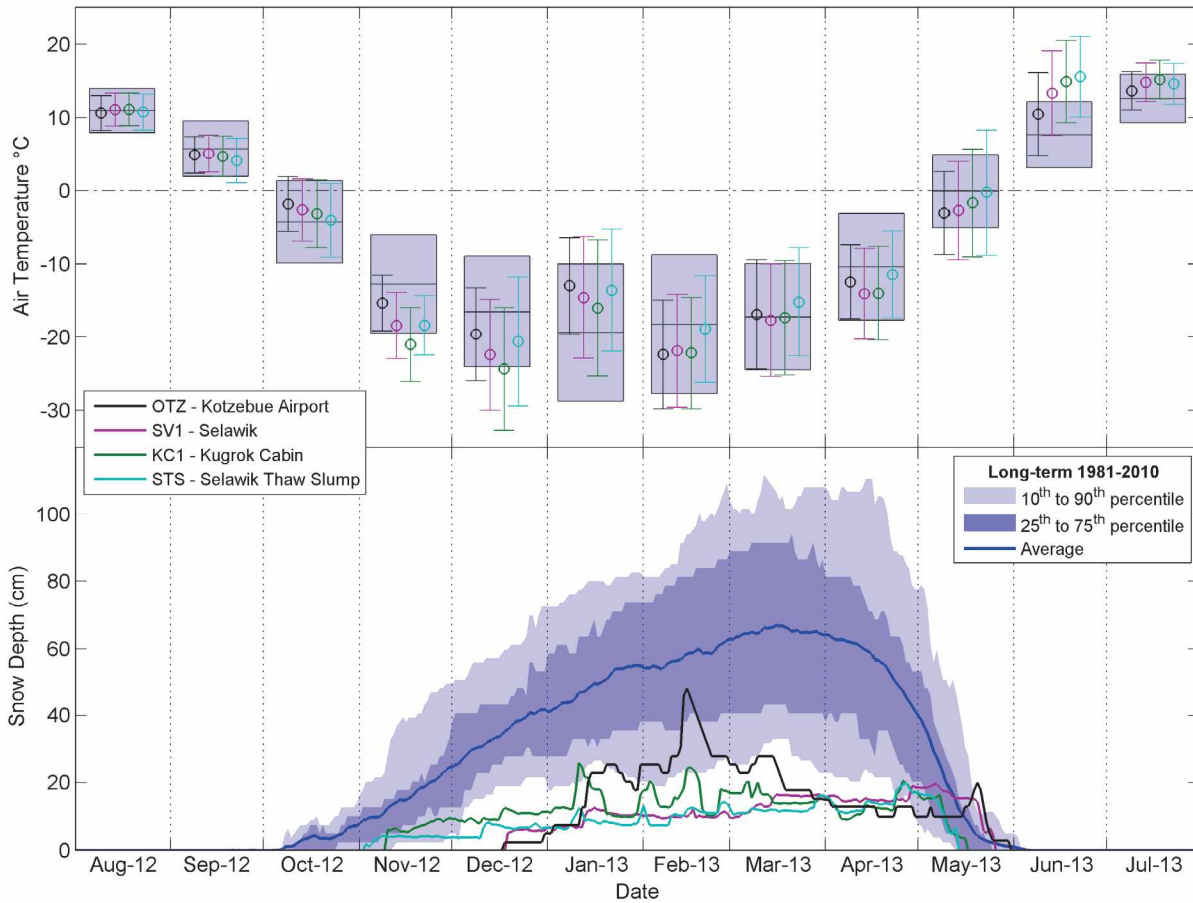
Figure 1.3 Summary of air temperatures and snow depths for the period August 2012 to July 2013. The top panel shows the mean monthly air temperatures and standard deviations for our core sites and the Kotzebue (OTZ) airport; the blue boxes show the long-term (1981–2010) monthly means and standard deviations from the Kotzebue airport. The bottom panel shows the snow depths on the ground for our core sites and Kotzebue airport, with daily summary statistics for the same long-term period.

Figure 1.4: Climate Summary 2013-2014
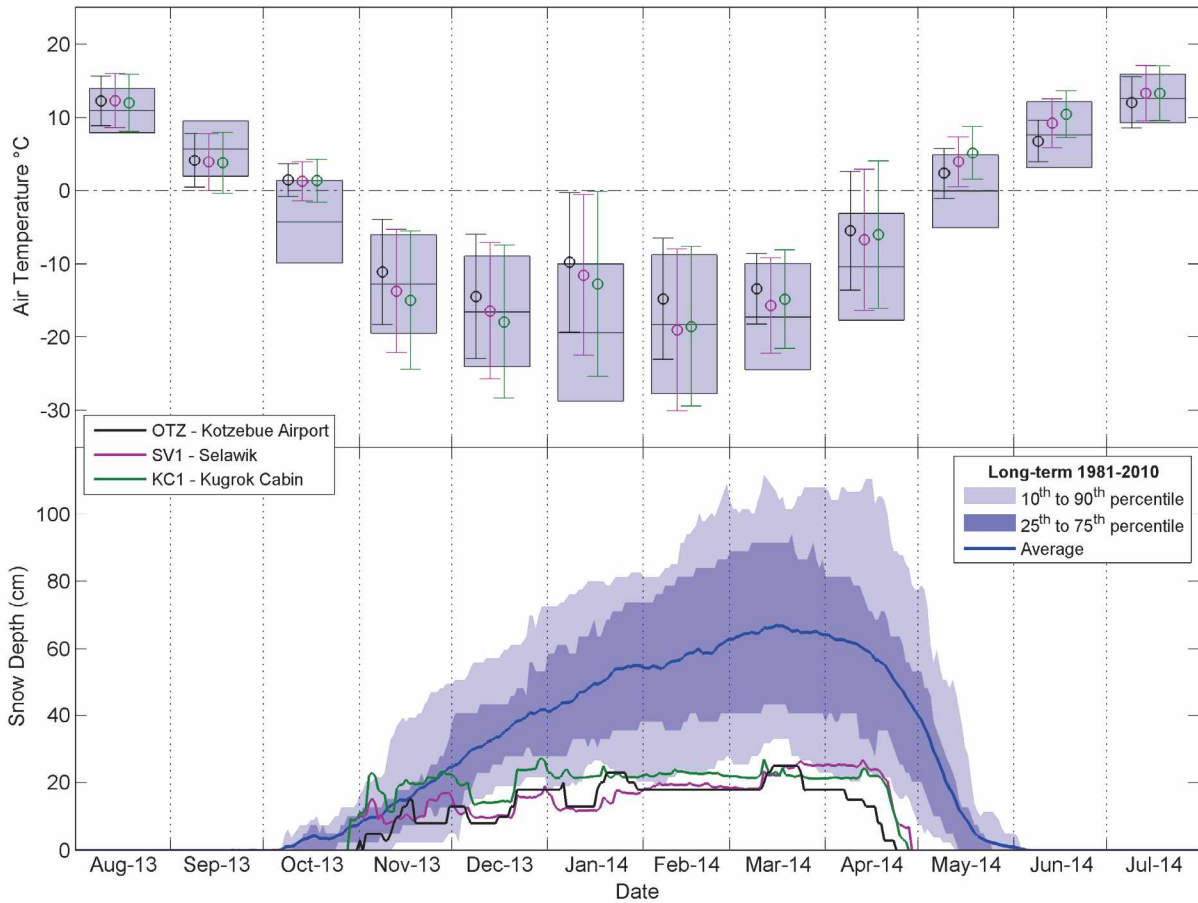
Figure 1.4 Summary of air temperatures and snow depths for the period August 2013 to July 2014. The top panel shows the mean monthly air temperatures and standard deviations for our core sites and the Kotzebue (OTZ) airport; the blue boxes show the long-term (1981–2010) monthly means and standard deviations from the Kotzebue airport. The bottom panel shows the snow depths on the ground for our core sites and Kotzebue airport, with daily summary statistics for the same long-term period.

Figure 1.5: Ground Thermal Regime Example
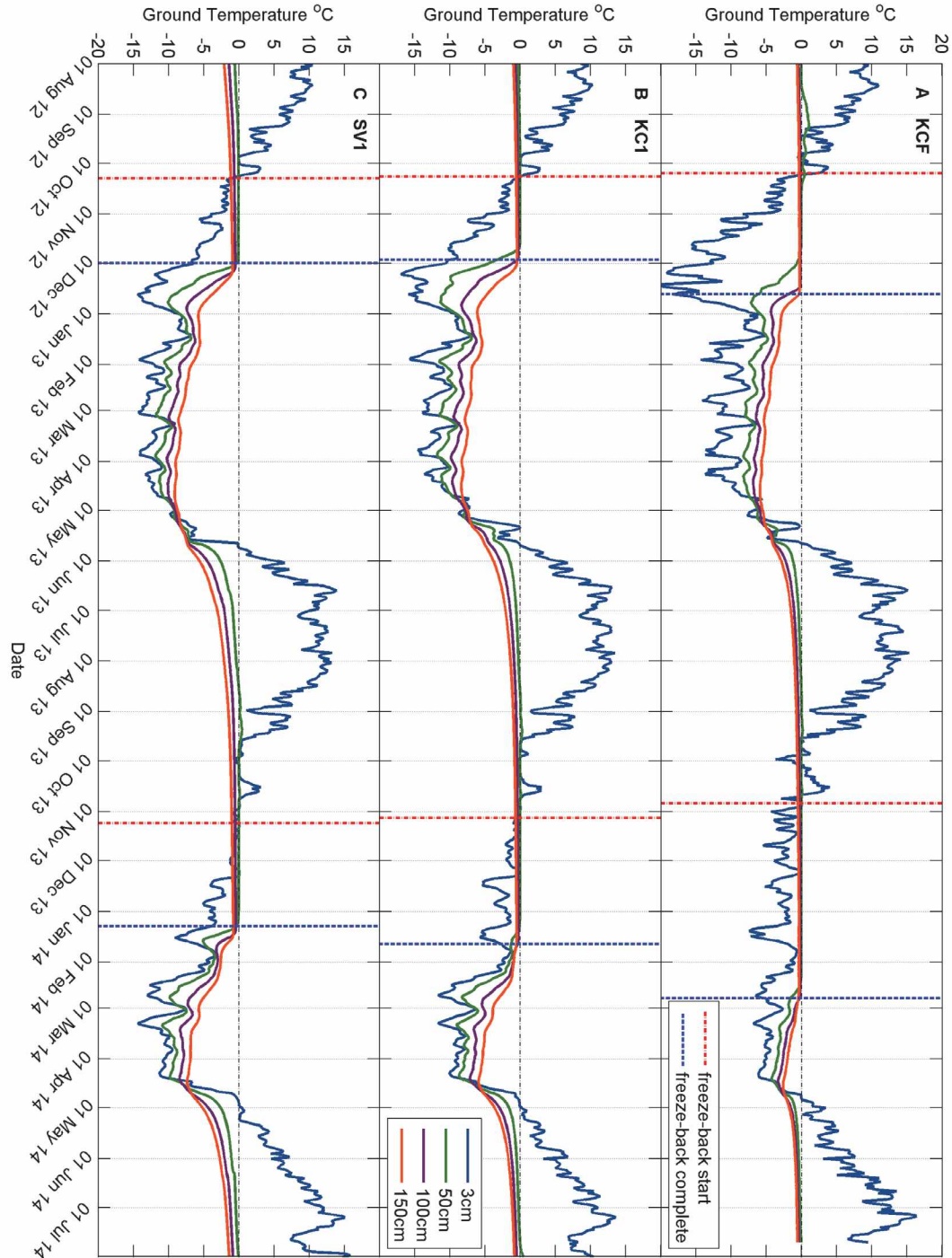
Figure 1.5 Daily average temperatures at four depths from two years (Aug. 2012 to July 2014) is shown for three sites (A: KCF, B: KC1, & C: SV1). The start (red) and end (blue) of the freeze-back periods are identified.

Figure 1.6: Cluster Analysis Dendrogram
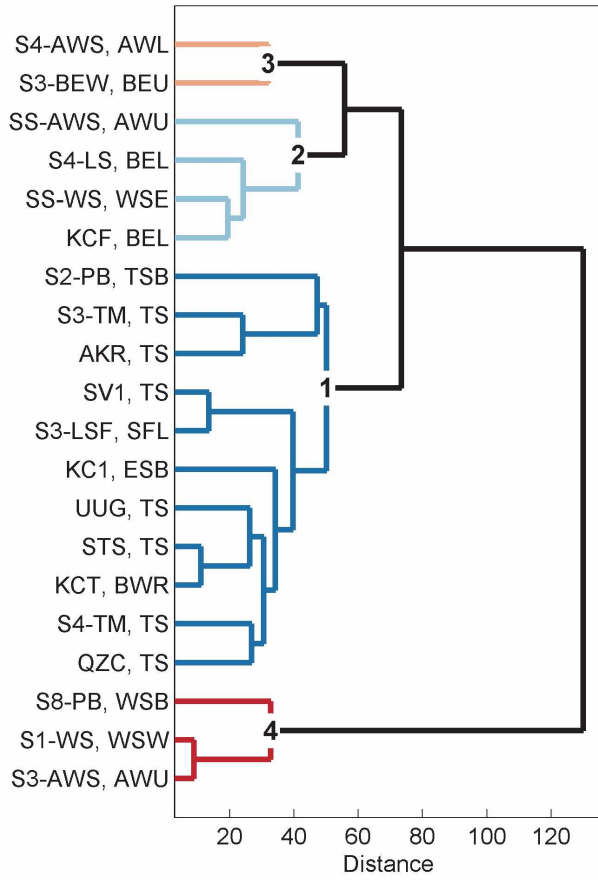
Figure 1.6 The results of the cluster analysis are shown as a dendrogram.

Figure 1.7: Thawing and Freezing N-Factors
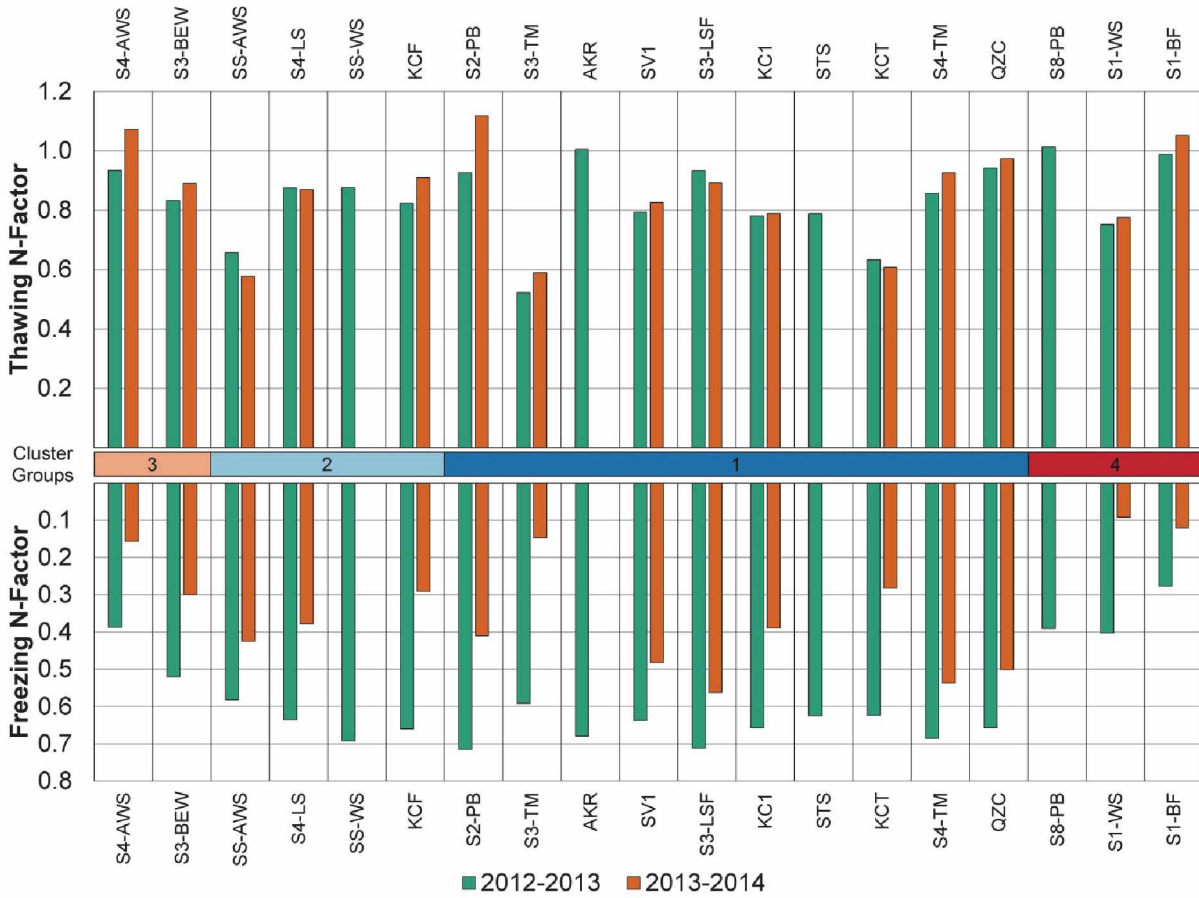
Figure 1.7 Thawing n-Factors (top) and freezing n-Factors (bottom) for each site and measurement period.

Figure 1.8: Ground Thermal Regime Summary 2012-2013
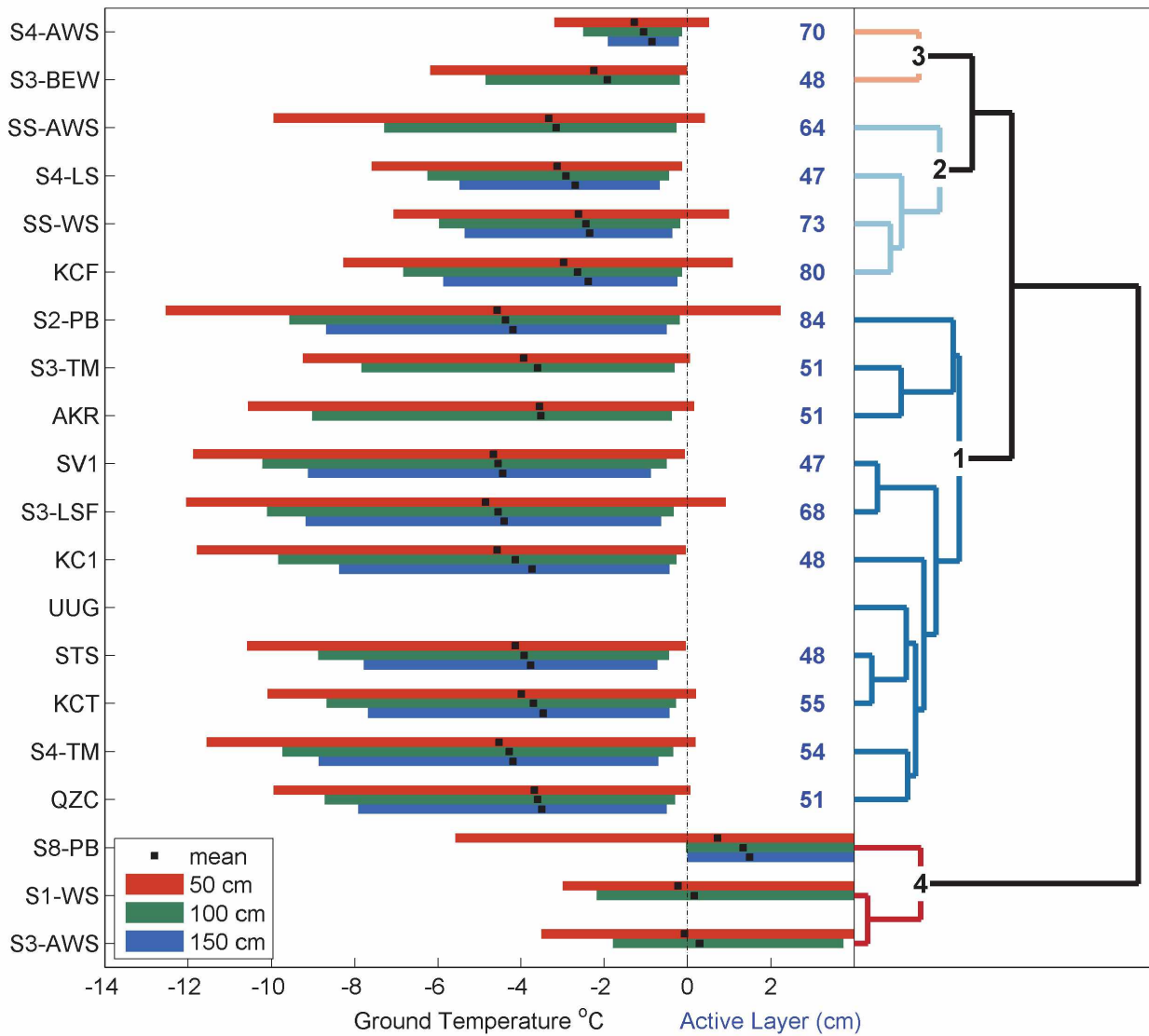
Figure 1.8 Annual summarized data for the period from 1 August 2012 to 31 July 2013. On the left is the annual mean (black squares) and range from daily averages (colored bars) for 3 depths from each site; in the center is the calculated active layer depth; and on the right the cluster analysis dendrogram for reference.

Figure 1.9: Ground Thermal Regime Summary 2013-2014
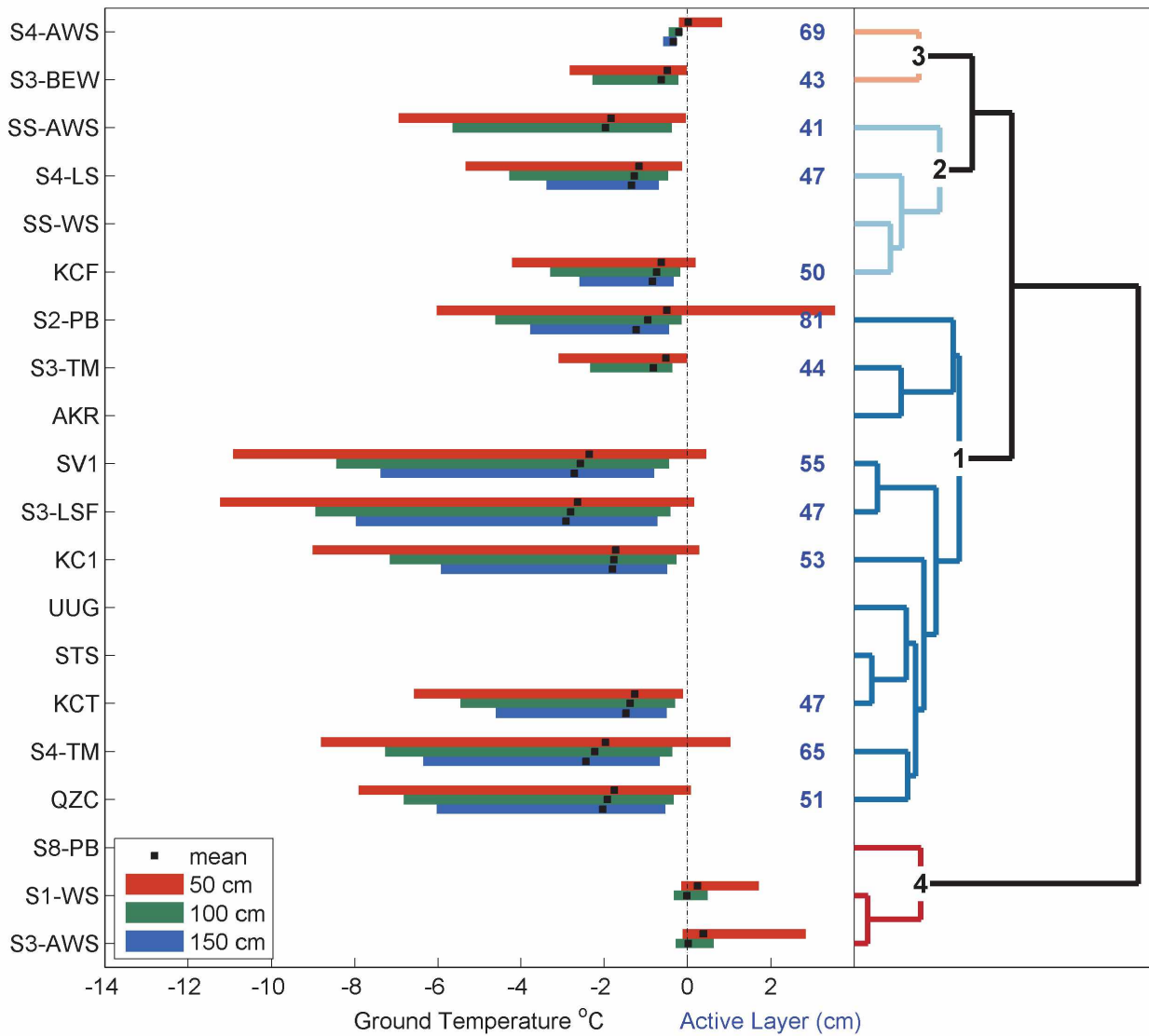
Figure 1.9 Annual summarized data for the period from 1 August 2013 to 31 July 2014. On the left is the annual mean (black squares) and range from daily averages (colored bars) for 3 depths from each site; in the center is the calculated active layer depth; and on the right the cluster analysis dendrogram for reference.

Figure 1.10: Active Layer Soil Profile Summary
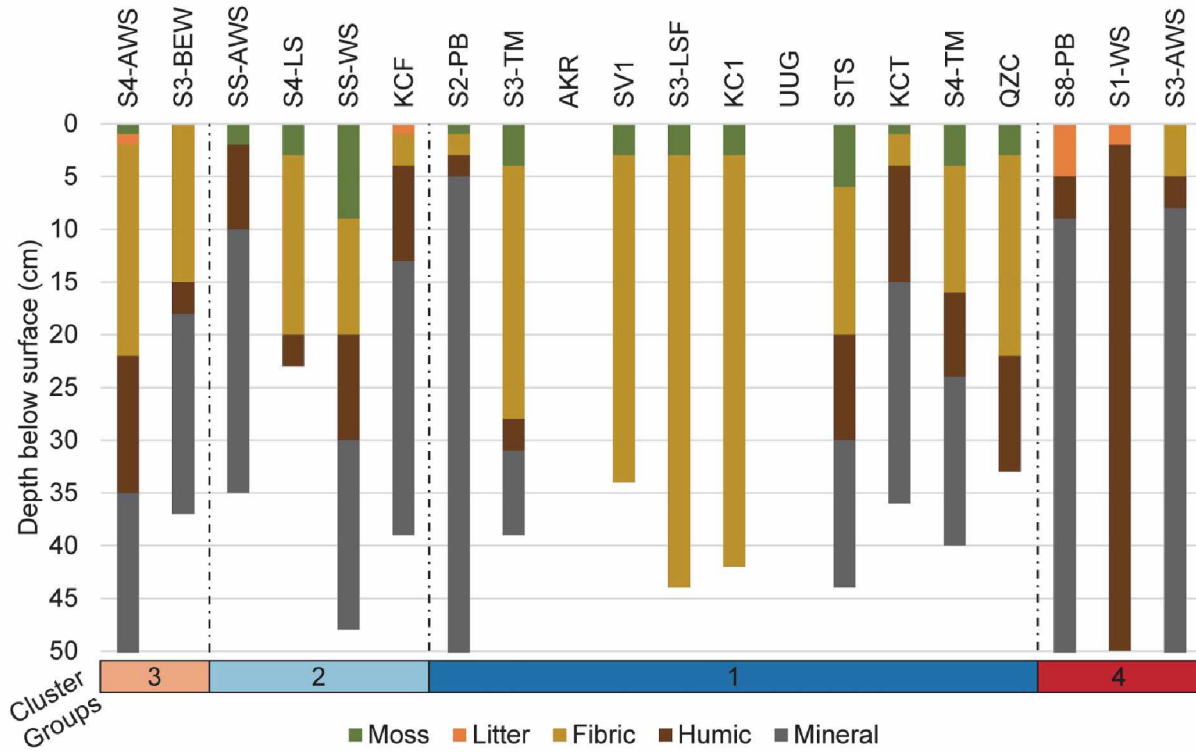
Figure 1.10 The profiles of soil layers in the active layer at each site, organized according to the cluster analysis are shown.

Figure 1.11: Mean Annual Ground Temperature Map with Estimates
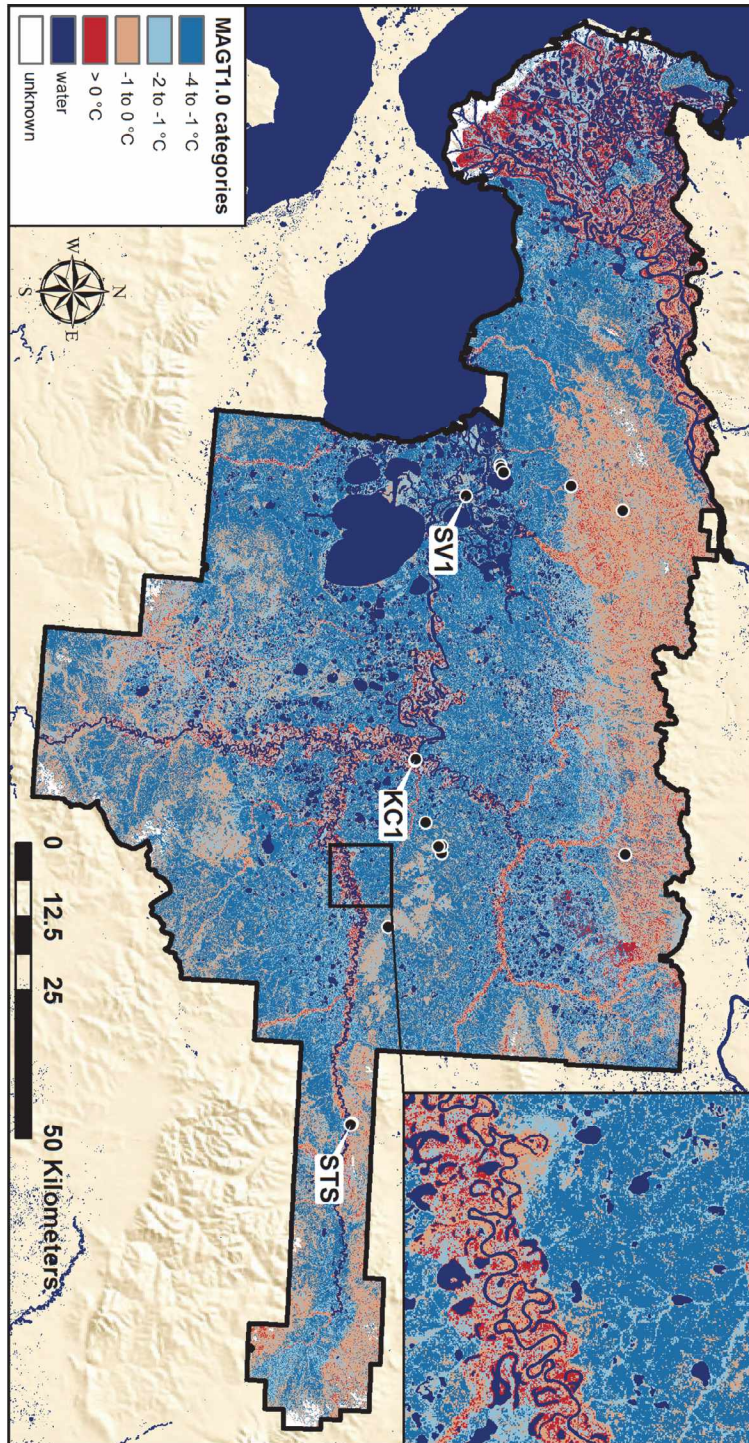
Figure 1.11 Map of MAGT at 1m depth for the SNWR including estimates for unmeasured ecotypes.

Figure 1.12: Mean Annual Ground Temperature Map without Estimates
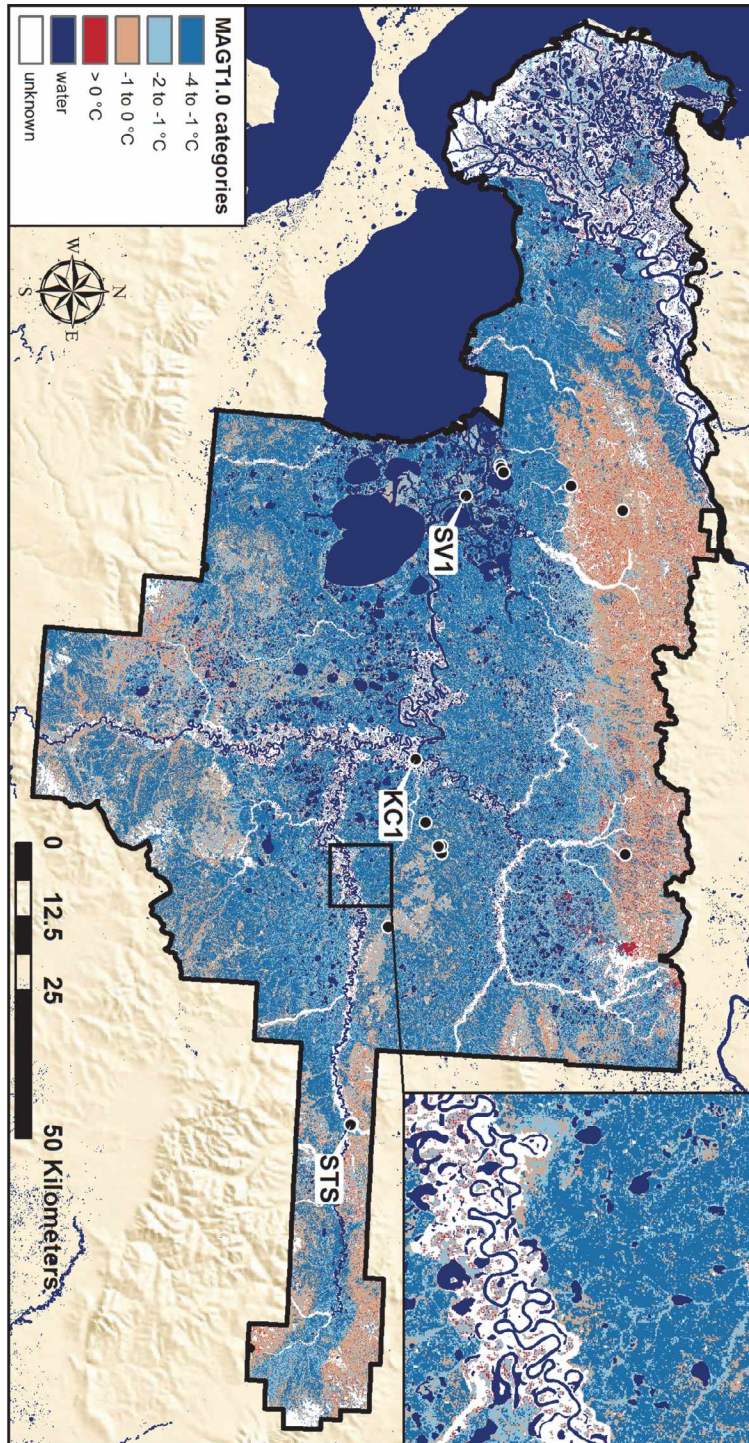
Figure 1.12 Map of MAGT at 1m depth for the SNWR using only ecotypes for which we made measurements.

Table 1.1: Site Location

The ecotype, ecotype areal coverage, and location of each site is shown in this table. Site codes in italics were installed in 2011 and are outside the SNWR. Site codes in bold are core sites.

Site Code	Ecotype	Ecotype Code	Ecotype % Cover	Latitude	Longitude
AKR	Upland Dwarf Birch-Tussock Shrub	TS	28.4	64.917500	-160.728144
QZC	Upland Dwarf Birch-Tussock Shrub	TS	28.4	65.547459	-161.403238
S3-TM	Upland Dwarf Birch-Tussock Shrub	TS	28.4	66.612523	-158.655397
S4-TM	Upland Dwarf Birch-Tussock Shrub	TS	28.4	66.659274	-160.121866
STS	Upland Dwarf Birch-Tussock Shrub	TS	28.4	66.501157	-157.607440
SV1	Upland Dwarf Birch-Tussock Shrub	TS	28.4	66.605569	-160.019213
UUG	Upland Dwarf Birch-Tussock Shrub	TS	28.4	65.055433	-159.473368
KCF	Lowland Birch-Ericaceous Low Shrub	BEL	7.3	66.561726	-159.000179
S4-LS	Lowland Birch-Ericaceous Low Shrub	BEL	7.3	66.655085	-160.136155
SS-WS	Upland White Spruce-Ericaceous Forest	WSE	4.8	66.499779	-157.604170
S3-AWS	Upland Alder-Willow Tall Shrub	AWU	4.4	66.611343	-158.683565
SS-AWS	Upland Alder-Willow Tall Shrub	AWU	4.4	66.501420	-157.609424
S4-AWS	Lowland Alder-Willow Tall Shrub	AWL	4.0	66.653454	-160.148182
S3-LSF	Lowland Sedge Fen	SFL	3.6	66.584576	-158.768248
KCT	Riverine Birch-Willow Low Shrub	BWR	3.3	66.562135	-159.003357
S3-BEW	Upland Birch-Ericaceous Low Shrub	BEU	3.2	66.607057	-158.679527
S1-WS	Upland White Spruce-Willow Forest	WSW	1.8	66.845685	-160.017046
KC1	Lowland Ericaceous Shrub Bog	ESB	1.0	66.562380	-159.004640
S1-BF	Upland Birch Forest	BFU	0.6	66.763641	-160.092071
S2-PB	Upland Burned Tussock Shrub	TSB		66.538220	-158.362833
S8-PB	Upland Burned White Spruce	WSB		66.891180	-158.700893

Table 1.2: Mean Annual Air Temperature Summary

A summary of mean annual air temperature (MAAT) for our 3 study years from the Kotzebue Airport (OTZ), our Selawik Village site (SV1), Kugurak Cabin site (KC1), and Selawik Thaw Slump site (STS). The long-term average for OTZ is also shown.

Year(s)	OTZ	SV1	KC1	STS
1981–2010	-5.09			
2011–2012	-6.90			
2012–2013	-5.30	-5.74	-6.05	-4.69
2013–2014	-2.41	-3.14	-3.14	

Table 1.3: Mean Annual Ground Temperature Summary

A summary of the MAGT at 3 and 100 cm, the active layer depth, and the freeze-back date, for all study sites and for our two main measurement periods.

Site Code	Ecotype Code	Cluster Group	2012-2013 Measurement Period				2013-2014 Measurement Period			
			MAGT at 3cm (°C)	MAGT at 100cm (°C)	Active Layer (cm)	Freeze-Back Date	MAGT at 3cm (°C)	MAGT at 100cm (°C)	Active Layer (cm)	Freeze-Back Date
S4-AWS	AWL	3	-0.15	-1.05	70	27-Dec	3.00	-0.20	69	
S3-BEW	BEU	3	-1.66	-1.92	48	11-Dec	1.66	-0.63	43	3-Mar
SS-AWS	AWU	2	-2.82	-3.15	64	28-Nov	-0.38	-1.96	41	22-Dec
S4-LS	BEL	2	-2.53	-2.92	47	24-Nov	0.97	-1.27	47	16-Jan
SS-WS	WSE	2	-3.02	-2.44	73	6-Dec				
KCF	BEL	2	-2.92	-2.64	80	20-Dec	1.62	-0.74	50	23-Feb
S2-PB	TSB	1	-3.05	-4.38	84	30-Nov	1.68	-0.95	81	23-Feb
S3-TM	TS	1	-3.38	-3.60	51	30-Nov	1.29	-0.81	44	14-Mar
AKR	TS	1	-2.46	-3.52	51	5-Dec				
SV1	TS	1	-2.83	-4.55	47	1-Dec	0.20	-2.57	55	10-Jan
S3-LSF	SFL	1	-3.00	-4.56	68	22-Nov	-0.03	-2.80	47	9-Jan
KC1	ESB	1	-3.06	-4.13	48	29-Nov	0.60	-1.76	53	21-Jan
UUG	TS	1								
STS	TS	1	-2.74	-3.92	48	1-Dec				
KCT	BWR	1	-3.27	-3.70	55	6-Dec	0.57	-1.37	47	10-Feb
S4-TM	TS	1	-3.03	-4.29	54	26-Nov	0.45	-2.23	65	11-Jan
QZC	TS	1	-2.49	-3.61	51	6-Dec	0.62	-1.92	51	29-Dec
S8-PB	WSB	4								
S1-WS	WSW	4	-0.92	0.17			2.29	-0.01		
S3-AWS	AWU	4		0.30				0.02		
S1-BF	BFU	4	1.02				3.14			

Table 1.4: Mean Annual Ground Temperature at 1 m Three Year Summary

The MAGT at 1 m depth for the three sites, installed in 2011, from which we have three years of data.

	MAGT at 1 m depth		
Site	2011–2012	2012–2013	2013–2014
QZC	-2.9	-3.6	-1.9
KCT	-2.0	-3.7	-1.4
KCF	-0.8	-2.6	-0.7

References

Barnhart, T. B. and Crosby, B. T.: Comparing two methods of surface change detection on an evolving thermokarst using high-temporal-frequency terrestrial laser scanning, Selawik River, Alaska, Remote Sens., 5(6), 2813–2837, doi:10.3390/rs5062813, 2013.

Carlson, H.: Calculation of depth of thaw in frozen ground, in Highway Research Board Special Report, pp. 192–223, Washington DC, United States., 1952.

Dingman, S. and Koutz, F.: Relations among vegetation, permafrost, and potential insolation in central Alaska, Arct. Alp. Res., 6(1), 37–47, 1974.

Fovell, R. G.: Consensus Clustering of U.S. Temperature and Precipitation Data, J. Clim., 10(6), 1405–1427, doi:10.1175/1520-0442(1997)010<1405:CCOUST>2.0.CO;2, 1997.

Goodrich, L.: The influence of snow cover on the ground thermal regime, Can. Geotech. J., 1982.

Jorgenson, M. T.: Hierarchial organisation of ecosystems at multiple spatial scales on the Yukon-Kuskokwim Delta, Alaska, USA, Arct. Antarct. Alp. Res., 32(3), 221–239, doi:10.2307/1552521, 2000.

Jorgenson, M. T. and Kreig, R. A.: A Model for Mapping Permafrost Distribution Based on Landscape Component Maps and Climatic Variables, in 5th International Conference on Permafrost, edited by K. Senneset, pp. 176–182, Tapir Publishers, Trondheim, Norway., 1988.

Jorgenson, M. T., Roth, J. E., Miller, P. F., Macander, M. J., Duffy, M. S., Pullman, E. R., Attanas, L. B., Wells, A. F. and Talbot, S.: An Ecological Land Survey and Landcover Map of the Selawik National Wildlife Refuge, Kotzebue, AK., 2009.

Jorgenson, M. T., Romanovsky, V. E., Harden, J., Shur, Y., O'Donnell, J., Schuur, E. a. G., Kanevskiy, M. and Marchenko, S.: Resilience and vulnerability of permafrost to climate change, Can. J. For. Res., 40(7), 1219–1236, doi:10.1139/X10-060, 2010.

Kade, A., Romanovsky, V. E. and Walker, D. A.: The N-factor of nonsorted circles along a climate gradient in Arctic Alaska, Permafr. Periglac. Process., 17(4), 279–289, doi:10.1002/ppp.563, 2006.

Karunaratne, K. C. and Burn, C. R.: Relations between air and surface temperature in discontinuous permafrost terrain near Mayo, Yukon Territory, Can. J. Earth Sci., 41(12), 1437–1451, doi:10.1139/e04-082, 2004.

Klene, A. E., Nelson, F. E., Shiklomanov, N. I. and Hinkel, K. M.: The N-Factor in Natural Landscapes: Variability of Air and Soil-Surface Temperatures, Kuparuk River Basin, Alaska, U.S.A., Arctic, Antarct. Alp. Res., 33(2), 140–148, 2001.

Koven, C. D., Ringeval, B., Friedlingstein, P., Ciais, P., Cadule, P., Khvorostyanov, D., Krinner, G. and Tarnocai, C.: Permafrost carbon-climate feedbacks accelerate global warming., Proc. Natl. Acad. Sci. U. S. A., 108(36), 14769–14774, doi:10.1073/pnas.1103910108, 2011.

Liao, T. W.: Clustering of time series data - A survey, Pattern Recognit., 38(11), 1857–1874, doi:10.1016/j.patcog.2005.01.025, 2005.

Lide, D. R., Ed.: CRC Handbook of Chemistry and Physics, 90th ed., CRC Press/Taylor and Francis, Boca Raton, FL., 2009.

Lunardini, V. J.: Theory of N-Factors and Correlation of Data, in 3rd International Conference on Permafrost, Vol. 1, pp. 40–46, Edmonton, Alberta, Canada., 1978.

Menne, M. J., Durre, I., Vose, R. S., Gleason, B. E. and Houston, T. G.: An Overview of the Global Historical Climatology Network-Daily Database, J. Atmos. Ocean. Technol., 29(7), 897–910, doi:10.1175/JTECH-D-11-00103.1, 2012a.

Menne, M. J., Durre, I., Korzeniewski, B., McNeal, S., Thomas, K., Yin, X., Anthony, S., Ray, R., Vose, R. S., E.Gleason, B. and Houston, T. G.: Global Historical Climatology Network - Daily (GHCN-Daily), Version 3. [USW00026616, Kotzebue Ralph Wein Memorial Airport AK], , doi:10.7289/V5D21VHZ, 2012b.

National Research Council: Opportunities to Use Remote Sensing in Understanding Permafrost and Related Ecological Characteristics, National Academies Press, Washington, D.C., 2014.

O'Donnell, J. A., Romanovsky, V. E., Harden, J. W. and McGuire, A. D.: The Effect of Moisture Content on the Thermal Conductivity of Moss and Organic Soil Horizons From Black Spruce Ecosystems in Interior Alaska, Soil Sci., 174(12), 646–651, doi:10.1097/SS.0b013e3181c4a7f8, 2009.

Rieger, S., Dement, J. A. and Sanders, D.: Soil survey of Fairbanks area, Alaska, Washington, DC., 1963.

Romanovsky, V. E. and Osterkamp, T. E.: Interannual variations of the thermal regime of the active layer and near-surface permafrost in northern Alaska, Permafr. Periglac. Process., 6(4), 313–335, doi:10.1002/ppp.3430060404, 1995.

Romanovsky, V. E. and Osterkamp, T. E.: Effects of unfrozen water on heat and mass transport processes in the active layer and permafrost, Permafr. Periglac. Process., 11(3), 219–239, doi:10.1002/1099-1530(200007/09)11:3<219::AID-PPP352>3.0.CO;2-7, 2000.

Romanovsky, V. E., Smith, S. L. and Christiansen, H. H.: Permafrost thermal state in the polar Northern Hemisphere during the international polar year 2007-2009: a synthesis, Permafr. Periglac. Process., 21(2), 106–116, doi:10.1002/ppp.689, 2010.

Schuur, E. A. G., McGuire, A. D., Schädel, C., Grosse, G., Harden, J. W., Hayes, D. J., Hugelius, G., Koven, C. D., Kuhry, P., Lawrence, D. M., Natali, S. M., Olefeldt, D., Romanovsky, V. E., Schaefer, K., Turetsky, M. R., Treat, C. C. and Vonk, J. E.: Climate change and the permafrost carbon feedback, Nature, 520(7546), 171–179, doi:10.1038/nature14338, 2015.

Shur, Y. and Jorgenson, M. T.: Patterns of permafrost formation and degradation in relation to climate and ecosystems, Permafr. Periglac. Process., 19(December 2006), 7–19, doi:10.1002/ppp, 2007.

Stoeckeler, E. G.: Investigation of airfield construction in arctic and subarctic regions: identification and evaluation of Alaskan vegetation from airphotos with reference to soil, moisture and permafrost conditions : a preliminary paper, St. Paul, Minn., 1949.

Sturm, M., McFadden, J. and Liston, G.: Snow-shrub interactions in arctic tundra: A hypothesis with climatic implications., J. Clim., 14, 336–344, 2001.

Sturm, M., Perovich, D. K. and Holmgren, J.: Thermal conductivity and heat transfer through the snow on the ice of the Beaufort Sea, J. Geophys. Res., 107(C21), 19.1–19.17, doi:10.1029/2000JC000409, 2002.

Taylor, A. E.: Field measurements of n-factors for natural forest areas, Mackenzie Valley, Northwest Territories., 1995.

U.S. Fish & Wildlife Service: Selawik National Wildlife Refuge, Kotzebue, AK, USA, 26 [online] Available from: http://www.fws.gov/uploadedFiles/Region_7/NWRS/Zone_2/Selawik/PDF/selawik_brochure.pdf, 2003.

U.S. Fish & Wildlife Service: Selawik National Wildlife Refuge Newsletter, Kotzebue, AK, USA. [online] Available from: http://www.fws.gov/uploadedFiles/Region_7/NWRS/Zone_2/Selawik/PDF/Selawik Newsletter Spring 2007.pdf, 2007.

Viereck, L. A.: Forest Succession and Soil Development Adjacent to the Chena River in Interior Alaska, Arct. Alp. Res., 2(1), 1–26, 1970.

Westermann, S., Duguay, C. R., Grosse, G. and Kääb, A.: Remote sensing of permafrost and frozen ground, in Remote Sensing of the Cryosphere, pp. 307–344., 2014.

Yoshikawa, K.: Permafrost in our time : community-based permafrost temperature archive, 1st ed., University of Alaska Fairbanks Permafrost Outreach Program., 2013.

Chapter 2 The Impact of Microtopography on Ground Thermal Regime in an Ice-Wedge Polygon Landscape[1]

Abstract. Ice-wedge polygons are perhaps the most dominant permafrost related features in the Arctic landscape. The microtopography of these features, that includes rims, troughs, and high and low polygon centers, alters the local hydrology, as water tends to collect in the low areas. During winter, wind redistribution of snow leads to an increased snowpack depth in the low areas, while the slightly higher areas often have very thin snow cover, leading to differences across the landscape in vegetation communities and soil moisture between higher and lower areas. These differences in local surface conditions lead to spatial variability of the ground thermal regime in the different microtopographic areas and between different types of ice-wedge polygons. We studied four different ice-wedge polygon developmental stages in a space for time substitution using intensive two-dimensional subsurface temperature measurements.

We found snow cover, timing and depth, and active layer soil moisture to be major controlling factors in the observed thermal regimes. In troughs and in the centers of low-center polygons, the combined effect of typically saturated soils and increased snow accumulation resulted in the highest mean annual ground temperatures (MAGT). Additionally, these areas were the last part of the polygon to refreeze during the winter. However, increased active layer thickness was not necessarily found in areas of higher MAGT. Active layer thickness does not appear to be correlated to mean annual air temperature but rather is a function of summer air temperature or thawing degree-days. While the refreezing of the active layer initiated at nearly the same time for all locations and polygons, we find differences in the proportion of top-down versus bottom-up freezing and the length of time required to complete the refreezing process.

Examination of the daily temperature dynamics using interpolated two-dimensional temperature fields reveal that during the summer, the predominate temperature gradient is vertical while the isotherms tend to follow the topography. However, as the active layer begins to refreeze and snow accumulates, the thermal regime diverges. The fall shows an increased temperature gradient horizontally with landscape positions containing higher soil moisture and/or snow depth (low

---

[1] Cable, W.L., Romanovsky, V. E., and Busey, R. C. The Impact of Microtopography on Ground Thermal Regime in an Ice-Wedge Polygon Landscape, prepared for submission to The Cryosphere.

centers and troughs) cooling more slowly than the adjacent ground (rims and high centers). This two-dimensional effect is greatest as the active layer refreezes and persists until mid-winter, by which time the temperature gradients are again mostly vertical and the isotherms follow the topography. Our findings demonstrate the complexity and two-dimensionality of the temperature dynamics in these landscapes.

2.1 Introduction

The Arctic is currently warming at twice the rate of the global average and projected to continue warming faster than the global average (IPCC, 2014). As permafrost temperatures are directly coupled to the atmosphere through the surface energy balance, this warming has already lead to permafrost warming and thawing in many areas (Romanovsky et al., 2010). One of the biggest concerns related to permafrost thawing is due to the large amounts of carbon it contains (Tarnocai et al., 2009). As permafrost thaws, these vast stocks of carbon become exposed to decomposition by micro-organisms, producing the greenhouse gasses carbon dioxide and methane. This creates the potential for a strong positive feedback that would further accelerate global warming (Koven et al., 2011; Schaefer et al., 2014; Schuur et al., 2015). Thus, it has become imperative that we understand the ground thermal regime and active layer dynamics in the Arctic and how they might respond to further warming.

One of the most visible and dominate permafrost related landforms in the Arctic are ice-wedge polygons and in northern Alaska they cover almost 65% of the land surface (Brown, 1967). These unique features result from contraction cracking in the winter and the subsequent filling of these cracks with snowmelt water, which quickly freezes, in the spring. This process repeats year after year, with contraction cracks forming in the same locations, allowing the ice-wedges to grow slowly over hundreds and thousands of years creating large bodies of clear ice (Lachenbruch, 1962; Leffingwell, 1915). As the ice-wedges grow, the permafrost and active layer are slowly, plastically deformed often creating rims on either side of the ice-wedge and leaving a trough over the ice-wedge. This process creates microtopographic relief in often, otherwise flat landscapes, such as the Arctic Coastal Plain of Alaska. Normally, ice-wedges are protected by a thin layer of soil and organic material above them; however, occasionally, during relatively warm periods, when the maximum thaw depth exceeds the thickness of this protective layer, the tops of the ice wedges can be melted. When this happens, the ground above the ice wedges settles and the relief becomes

more pronounced (Jorgenson et al., 2006). The formation of microtopography creates microsites with different hydrology, snow, vegetation, and soil properties.

The change in local hydrology is one first and most visible effects of microtopographic change and is mostly due to the impermeable permafrost layer below which creates a perched water table, causing ponding of water in low areas. In the case of polygon troughs, interconnected drainage pathways can also be formed, drastically altering the hydrology of the area (Liljedahl et al., 2012, 2016). The centers of low-centered polygons tend to trap and pond water, while high-centered polygons tend to have reduced near-surface soil moisture in their centers (Liljedahl et al., 2012). Thus, we find that near-surface soil moisture in ice-wedge polygon landscapes is largely controlled by microtopography (Engstrom et al., 2005). As near surface soil moisture has a large impact on the near surface soil conductivity, it is also a key factor in terms of active layer dynamics and ground thermal regime.

Another major impact of microtopography is on the spatial distribution of snow. Wind is the dominate force in redistributing snow across the Arctic landscape and with no shrubs or trees to slow the blowing snow, it becomes trapped in low areas (Dingman et al., 1980) such as troughs and low centers as it blows across the surface. As the winter progresses, the low areas are preferentially infilled with snow, masking the underlying microtopography so it is no longer visible on the snow surface. Thus, deep troughs tend to accumulate a thick snowpack while the polygon rims and the centers of high-centered polygons can have very thin snowpack (Gusmeroli et al., 2012). As snow is an effective insulator, it can lead to significant differences in below ground winter temperatures (Goodrich, 1982).

Changes in vegetation and moss communities often accompany changes in microtopography and result largely from the changes in hydrology and soil moisture (Jorgenson et al., 2015; Minke et al., 2009). Additionally, it has been found that in areas where the microtopography plays a significant role in determining the soil moisture, that a strong correlation exists between vegetation greenness (NDVI) and soil moisture (Engstrom et al., 2008). Thus, microtopography not only exerts control over the vegetation composition but also the vegetation productivity within these landscapes.

All of these parameters (hydrology, snow, vegetation) influenced by microtopography, act together to influence the surface energy balance and the degree to which the air temperature is coupled to the ground temperature at depth. The interaction is further complicated by the different time scales

45

and parts of the year that these parameters exert their influence. While many studies have focused on various aspects of ice-wedge polygons, relatively few of them have examined, in-depth, the ground thermal regime using in-situ measurements. Thus, the goals of this paper are: 1) to show how variation in microtopographic influenced parameters of ice-wedge polygon landscapes creates variation in active layer dynamics and ground thermal regime and 2) show how this variation might be important with respect to future climate change.

2.2 Methods

2.2.1 Site Description

Our study area is a meadow tundra situated mostly between two drained lake basins (Hinkel et al., 2003) in the Barrow Experimental Observatory (BEO, 156°36.3'W, 71°16.9'N) approximately 6 km to the east of Barrow. This is one of the main study sites of the Department of Energy sponsored, Next Generation Ecosystem Experiment (NGEE) Arctic. The goal of the NGEE Arctic project is to improve climate model predictions in the Arctic through in-depth understanding of the coupled processes. This area provides a good setting to study different growth and thermokarst phases of ice-wedge polygons as there many different phases represented within close proximity (Figure 2.1). Following the ice-wedge polygon classification of MacKay (2000) the youngest growth phase is an incipient polygon (IP), Site D (Figure 2.1), located in a medium aged (50-300 years) drained lake basin (Hinkel et al., 2003). This site has very little microtopographic relief and its low centers are typically flooded with water. Site A (Figure 2.1) is a low-centered polygon (LCP) and has a greater amount of microtopographic relief that has developed as the ice-wedges have grown and deformed the surface. Site C (Figure 2.1) is an example of a walled polygon (WP) and is the result of melting ice-wedges during the thermokarst development phase. The low center of the WP is probably a result of thawing of ice-rich permafrost in the polygon center (MacKay, 2000). Site B (Figure 2.1) is a high-centered polygon (HCP) and an example of the most degraded ice-wedges in our study area. These sites form a gradient from young ice-wedges (IP) with very little microtopographic relief, to old, degrading ice-wedges (HCP) with much more topographic relief. The presence of all these ice-wedge polygons phases allows for a substitution of space for time across this sequence.

The soils in the Barrow area have been formed primarily through the processes of ice segregation and cryoturbation, leading to the formation of Gelisols. With the exception of raised polygon rims and centers of high center polygons, the soils generally remain saturated due to the low hydraulic gradient and impermeable permafrost table generally within 1 m of the surface (Bockheim et al., 2001).

2.2.2 Field Instrumentation

A temperature transect on each of the four polygons was established with five vertical array thermistor probes (VATP), distributed to cover the features of each particular polygon type but generally extending from the center of the polygon through the trough to the rim of the adjacent polygon. The VATP's were constructed by affixing thermistors to a strip of nylon, inserting this nylon strip into a clear 19 cm by 1.5 m tenite butyrate tube, and filling the tube with urethane potting compound (http://permafrost.net.gi.alaska.edu/content/thermistor-probe-construction). The spacing of the thermistors followed a semi logarithmic distribution (2, 5, 10, 15, 20, 25, 30, 35, 40, 50, 60, 70, 80, 100, 125, and 150 cm) with more thermistors near the surface and less with depth. The probes were installed with their tops flush with the ground surface and at the end of each summer the amount of probe protruding from the surface (heave) was measured so the actual thermistor locations could be determined.

In addition to the thermal transects, at most sites two small soil pits were excavated to install soil moisture, soil temperature, thermal conductivity, and heat flux sensors. Soil moisture was measured at three depths using the Hydra Probe II (Stevens Water Monitoring Systems, Portland, OR, USA) and paired with a self-made thermistor probe using the same type of thermistors as the VATP. Thermal conductivity was measured once per day at the same depths as soil moisture and temperature using thermal conductivity sensors from East 30 Sensors (Pullman, WA, USA). At the bottom of the soil pit, near the top of the permafrost table, a heat flux sensor (HFP01; Hukseflux Thermal Sensors, Manorville, NY, USA) was installed horizontally. The depths of the soil moisture, temperature, and thermal conductivity sensors were selected based upon the visible soil layers of each pit. All the subsurface data is archived with NGEE-Arctic (Cable and Romanovsky, 2014).

Temperature data from both the VATP and soil pit thermistor probes were adjusted using a zero-offset that had been determined before installation using an ice bath calibration in the lab following

Wise (1988). The offsets were typically within 0.10 °C from zero, the stated tolerance for this thermistor (PS103J2; U.S. Sensor Corp, Orange, CA, USA). The zero-offset adjustment was performed on the data logger and increased our confidence in the measured temperatures near zero, giving us an accuracy of approximately 0.02 °C.

Above ground at each polygon a full suite of micrometeorological measurements were made, including air temperature and relative humidity, wind speed and direction, net radiation, and snow depth (Busey et al., 2014a, 2014b). Most polygons had multiple snow depth sensors positioned to capture the variability in snow depth due to the microtopography of the polygon (i.e. center vs trough). All above and below ground sensors at each polygon were connected to a CR1000 data logger (Campbell Scientific, Logan, UT, USA) and data was transmitted to the University of Alaska Fairbanks for storage and analysis. Data collection from most of these sites began in September, 2012 and is ongoing.

2.2.3 Data Analysis

The data analyses in this paper were conducted with Matlab (2015b, Mathworks Inc.). Before any analyses were conducted the raw data were inspected visually and erroneous values, due to sensor malfunctions, were removed from. Then any gaps in the raw hourly data up to two hours were filled using a linear interpolation with the point preceding and following the gap. From these gap filled hourly datasets, daily average datasets were produced for days with at least 83% data coverage. Gaps of up to two days in the daily datasets were filled using a linear interpolation of the point preceding and following the gap. Monthly average datasets were produced from the daily datasets for months that had at least 80% data coverage. Finally, yearly datasets were produced from the daily datasets for all sensors that had at least 98% daily data coverage. All yearly statistics were calculated for a year beginning 1 October through 30 September the following year. Additional gap filling was performed on the daily average snow depth data using linear relationships between sensors with correlation coefficients of at least 90% and highly significant p-vlaues (<0.01). This allowed filling gaps in snow sensor data larger than two days that resulted from sensor failure during the winter.

2.2.3.1 Two-Dimensional Cross-sections

To get a complete picture of the temperature field within each polygon, two-dimensional cross-sections of each polygon were created using the temperature data from each VATP. The temperature values from daily and annual averages were interpolated, linearly, onto a grid using the depths converted to elevation and the horizontal distance between VATP. Animations were created using the daily cross-sections to aid in the initial data interpretation and quickly get a sense of the two-dimensional ground thermal dynamics within each polygon. Using the two-dimensional temperature field, the temperature gradient was calculated and added to these figures as arrows representing the direction and magnitude of the temperature gradient. These animations for each polygon are included as short videos in the supplementary material.

2.2.3.2 Thaw Depth and Active Layer Parameters

Calculation of thaw depth from a vertical profile of temperatures requires determination of the temperature at which soil water undergoes phase change from liquid to solid or vice versa. Due to interaction between soil particles and liquid water, this phase change takes place over a range of temperatures, typically between 0 °C and -0.5 °C (Osterkamp and Romanovsky, 1997; Romanovsky and Osterkamp, 2000). For our analyses, a phase change temperature of -0.15 °C was selected by examining temperature vs volumetric water content curves (e.g. Figure 2.2) from our sites and looking for the inflection point at which a further temperature increase resulted in rapidly increasing water content.

The daily thaw depth was calculated for each VATP by fitting a piecewise cubic hermite polynomial to the daily average temperature data. The piecewise cubic hermite polynomial was selected as it passes through every point while maintaining the shape of the temperature profile (Figure 2.3). This polynomial was then evaluated at the phase change temperature of -0.15 °C to locate all the freezing/thawing fronts in the profile. The deepest freezing/thawing front was take to be the bottom of the active layer and upward freezing front, while the second deepest, when present, indicated the downward freezing front (Figure 2.4). Based on this daily thaw depth other important parameters can be determined such as: start of the thaw period, depth and date of maximum thaw (active layer thickness), initiation of upward freezing, initiation of downward freezing, and complete freeze-up of the active layer. The beginning of the thaw period was defined as the date when the daily average surface (2 cm) temperature was greater than and remained above

zero. The depth and date of maximum thaw, active layer thickness, was defined as the maximum daily thaw depth for a given thaw season and its date of occurrence. Following the date of maximum thaw depth, upward freezing of the active layer initiates. The beginning of top down freezing was taken to be the date when the daily average surface temperature (2 cm) became and stayed below -0.15 °C. The point at which the downward and upward freezing fronts met defined the proportion of downward and upward freezing and the timing of the completion of freeze-up.

2.2.3.3 Topographic Wetness Index

Since it was not possible to measure the soil moisture at every VATP location, the topographic wetness index (TWI) was calculated for each probe location using the open source software package, System for Automated Geoscientific Analyses (SAGA) (Conrad et al., 2015). Fortunately, a 0.25 m horizontal resolution digital elevation model (DEM) produced from airborne laser altimetry taken in July 2013 was available for our study area (Wilson and Altmann, 2013). This DEM was used as the basis for determining the TWI; however, first a mesh denoising filter (Sun et al., 2007) was used to remove some noise and speckling from the DEM. This denoising filter has been previously evaluated on elevation datasets (Stevenson et al., 2010) and found to provide good noise removal without compromising features. The denoised DEM was then used to calculate the TWI following the modified approach of Böhner and Selige (2006), which offers improved performance in flat terrain. Finally, the TWI values from the 5 closest pixels were averaged for each VATP and soil pit location to use in subsequent analyses.

In order to validate the TWI for the general area of our field sites, a dataset collected on 30 June 2014 from Hubbard and Peterson (2016) was used. The dataset included 65 point measurements of percent saturation in the top 15cm of the soil profile using a Trace TDR probe. The data were collected along a 35 m transect that represented all of the polygon positions and moisture conditions present at our research site. A least squares regression between the point percent saturation and TWI gave a R^2 value of 0.60 (p < 0.01), giving confidence that TWI could be used to represent surface wetness.

2.3 Results

2.3.1 Climate Assessment

To access the climate in the Barrow area, historical data was obtained from the NOAA National Climatic Data Center for the Barrow Airport (Menne et al., 2012). The long-term mean annual air temperature (MAAT, 1981–2010) for the Barrow Airport is -11.2°C (Table 2.1). The MAAT's from our sites from 2012-2015 show a cold bias compared to the Barrow airport so we cannot compare them directly; however, these 3 years were all warmer than the long-term average by over 1°C (Table 2.1). Since the early-1990's, the mean annual air temperature (MAAT) in Barrow has been increasing from near -12°C to over -10°C in 2015 (Figure 2.5). While the thawing degree days (TDD), related to how warm the summer is, have only increased slightly, during this period (Figure 2.5). The freezing degree days (FDD) however, have increased considerably during this period (Figure 2.5), indicating that the increase in MAAT is due more to increasing winter-time than summer-time temperatures (Zhang et al., 1996). In fact, the winters of 2014 and 2015 had the highest FDD in the almost 100 year temperature record, while the TDD in these years were closer to average, indicating warm winters and more average summers. The five years preceding 2014 (2009-2013) however, had some of the highest TDD values in recent history and certainly the longest stretch of high TDD in recent history (Figure 2.5).

2.3.2 Ground Thermal Regime

The mean annual ground temperatures (MAGT) at 1 m depth for our four sites follow the trend in MAAT during our study period (Figure 2.6) with 2012–2013 being the coldest year. Within a given year, the range in MAGT at 1 m is approximately 2.5 °C with the center of the HCP always being the coldest and the center of the LCP being the warmest. It is difficult to determine which polygon type is the warmest and coldest because calculating the spatial average is problematic. However, since the centers of the polygons usually represent the largest area, it appears that the IP and LCP have the highest and the HCP and WP have the lowest MAGT at 1 m (Figure 2.6). The relationship between polygon positions tends to hold constant between years with the whole group getting warmer or colder together (Figure 2.6). The mean annual surface temperatures (MAST, not shown) are very similar to the MAGT at 1 m with only the spread of values being larger.

To compare the MAGT with depth from each polygon side-by-side, two-dimensional cross-sections were created for each polygon and year (Figure 2.7, Figure 2.8, and Figure 2.9). The

figures give a quick overview of the thermal regime within each polygon and allow warm and cool spots to be easily located. In general we see that the lower, often wet areas tend to have highest MAGT's while the higher, sometimes drier and often with thinner snow cover areas tend to be colder. These figures also show how the snow cover is redistributed during the winter to fill in all the low spots (troughs and low centers) preferentially, leaving the higher areas with a thinner snow cover. The active layer depth tends to follow the microtopography of the polygon.

2.3.3 Active Layer Dynamics

Calculation of the thaw depth throughout the thaw season allows comparison between different active layer parameters with respect to timing (ex. Figure 2.4). The thaw season begins as the snow melts and the surface temperature increases above 0 °C. Then typically, the thaw depth increases quickly at first and slowing as the thawed depth increases. The maximum thaw depth, active layer depth, is reached in late summer. Often shortly after reaching the maximum thaw depth, the active layer begins to refreeze from the bottom. Once air temperatures are sufficiently cool, freezeback of the active layer begins from the surface, as indicated by ground surface temperatures that remain stable below 0 °C. Shortly after initiation of freezeback at the surface, the entire active layer cools to slightly below 0 °C and the so called, "zero curtain" is established. Freezing fronts then progress from both the top and bottom of the active layer until they meet and the active layer is completely refrozen. This point is also marked by the dissipation of the zero curtain as all ground temperatures decrease more rapidly.

The thaw onset for all polygons and positions was found to closely follow the disappearance of snow within a few days (Figure 2.10). From our three years of measurements there is a considerable range in snowmelt (and thaw onset) dates, beginning as early as 23 May in 2015 for the high center of the high-centered polygon and as late as mid-June in 2014 for some troughs and low centers. Within a given year the range of snowmelt / thaw onset dates is not as big but can still be on the order of two weeks between the time when high centers and rims melt out to when the troughs and low centers melt out. Interestingly, the high center of the high-centered polygon is often the first to melt out while the trough of the same polygon is among the last to melt out. The scatter and outliers present in Figure 2.10 is probably a result of patchy snowcover in spring and the snow depth sensors and temperature measurements not being in exactly the same location (Figure 2.1).

Maximum thaw depth is typically reached in late August or early September; however, from our three years of data we find a range of dates spanning mid-August to mid-September (Figure 2.11). Active layer thickness is equally as variable with depths ranging from 30 to 60 cm. Generally, active layer thickness is related to the energy input during the summer, which can be represented by thawing degree days, and then modified by parameters such as vegetation, organic layer thickness, and soil moisture. Using linear regression, a non-significant (R^2 = 0.34) relationship was found when using TDD and TWI to predict active layer thickness. Likely, inclusion of organic layer thickness would improve this relationship. There are some patterns however to the maximum thaw depths and dates. Typically, within a given year, the HCP is among the first to reach maximum thaw depth and tends to have the shallowest thaw depths, while the WP has some of the deepest and the LCP and IP have a mix of shallow and deep active layer depths (Figure 2.11).

The date at which refreezing of the active layer initiates from the surface normally occurred at most positions within a few days of each other (Figure 2.12). In 2014 however, while the freezeback initiation dates within a polygon tend to group together, the spread between polygons is much larger, with the IP and LCP initiating the latest (Figure 2.12). As these two polygon types tend to be the wettest, their late freezeback initiation could be due to large amounts of standing water in their centers and troughs.

The amount of upward freezing is highly variable between polygons and polygon positions, from 5% to almost 70% with a mean near 35%. Since snow timing and duration was expected to an influential factor on the amount of upward freezing (Osterkamp and Romanovsky, 1997), freezeback snow depth days (SDD) were calculated as the sum of daily average snow depth during freezeback period of 1 September to 31 December. Using step-wise linear regression, mean ground temperature at 1 m during freezeback, freezeback SDD, and TWI were found to be good predictors of the amount of upward freezing (R^2 = 0.84, p < 0.05). The strongest predictor is mean ground temperature at 1 m during freezeback (45%) with a negative relationship, thus the colder the permafrost beneath the upward freezing front the more upward freezing that can be expected. Freezeback SDD was also found to be a strong positive predictor (41%), with positions having larger amounts of snow tending to have increased amounts of upward freezing. Lastly, TWI was found to have a positive relationship with upward freezing percent and explaining about 14% of the variation. We find the largest amount of upward freezing in the troughs, which tend to accumulate the most snow (Figure 2.13), while the least amount of upward freezing is found in the

rims (Figure 2.14). The high-centered polygon, while drier, had the highest amount of upward freezing in the trough position.

Also relatively variable is the date at which freezeback of the active layer was complete, with dates as early as late-October to as late as late-December, a range of two months (Figure 2.15). As the amount of time required to refreeze the active layer should be partially attributable to how cold the ground surface is, the freezing degree days (FDD) at the surface (2 cm depth) during the freezeback period, 1 September to 31 December, was calculated. Using a step-wise linear regression it was found that surface FDD during freezeback and TWI were good predictors of freezeback date (R^2 = 0.88, p < 0.05). Surface freezing degree days during freezeback were responsible for approximately 44% of the variation and not surprisingly, the colder the surface the quicker the active layer refroze. TWI explained approximately 56% of the variation and the wetter the position the longer it takes to refreeze. Some of the earliest freezeback dates were in the high-centered polygon, with its center and rim being the first positions to refreeze. The latest positions to refreeze were the wet centers of the low-centered and incipient polygons (Figure 2.15).

2.3.4 Two-dimensional Ground Thermal Dynamics

One of the aspect of a unique dataset like this, is that it allows the visualization of two-dimensional temperature field dynamics as cross-sections through these polygons along our thermal transects. Animations were created to aid in the interpretation of the two-dimensional temperature field dynamics and they are included in the supplementary material as video files for each polygon. Beginning with freezeback, the animations clearly show that the low, wet areas, with more trapped snow take the longest to refreeze. The effect of a skewed snow cover distribution can be seen throughout the rest of the winter, as raised areas (rims and high centers) are often significantly colder than the lower areas that tend to trap more snow. As the snow melts in the spring, the low areas are the last to melt out and thus, the last to begin thawing the ground surface. Additionally, during this time the horizontal temperature differences across the polygons that had been present all winter give way to more uniform temperature with depth that tends to follow the microtopography. The development of the active layer also tends to follow the microtopography. By adding arrows indicating the direction and magnitude of the temperature gradients in this field make it possible to identify times and polygon positions where the horizontal component of heat fluxes might be important (Figure 2.17). We find that most of the year the temperature gradient

(and therefore heat flux) is oriented in the vertical direction. However, during the end of freezeback and the period of time shortly after freezeback, we find a horizontal temperature gradient develops in some troughs and low centers. This effect seems to be strongest in a trough or low center with thick snow cover that is adjacent to a rim with thin snow cover (Figure 2.17).

2.4 Discussion

Recently, it has been shown that the degradation of ice-wedge polygons has increased since the early 1980's in the Alaskan Arctic (Jorgenson et al., 2006; Raynolds et al., 2014). While warmer summer temperatures generally seem to be the culprit, the degradation is likely initiated by extreme warm summer events that push the ecosystem past a critical threshold (Jorgenson et al., 2006; Liljedahl et al., 2016). In the Barrow area several of these type of extreme warm summer events have occurred, as indicated by positive spikes in TDD (1998, 2004, and 2012; Figure 2.5). These sorts of spikes have occurred throughout the almost 100 year temperature record but recently, the magnitude has increased and their impact is likely compounded by increasing winter-time temperatures (FDD; Figure 2.5). The ice-wedge degradation caused by these events initially leads to changes in hydrology (Liljedahl et al., 2012, 2016) due to the changes in local microtopography, which in turn leads to changes in soil moisture (Engstrom et al., 2005), active layer thickness (Shiklomanov et al., 2010), vegetation (Billings and Peterson, 1980; Jorgenson et al., 2015), CO^2 and CH^4 fluxes (Lara et al., 2015; Sachs et al., 2010; Zona et al., 2011), and active layer chemistry (Heikoop et al., 2015; Newman et al., 2015) among others. In this study we find changes in hydrology and microtopography also lead to corresponding changes in the permafrost thermal regime and associated active layer dynamics.

The ground thermal regime in these landscapes is strongly linked to polygon position and polygon type. Interestingly, the HCP, with the most degraded ice-wedges, tended to have the coldest MAGT overall (Figures 2.6, 2.7, 2.8, and 2.9). This is likely due to the highly skewed redistribution of snow in these polygon types, leaving the high centers with very thin snow cover and concentrating the snow in the troughs. This leaves the high centers to act as very effective heat sinks during the winter, cooling the permafrost below. Also important though is the effect the microtopography has had on the local hydrology by transforming the troughs into drainage networks and reducing the active layer soil moisture. With a drier active layer, the organic rich surface layers are much more effective insulators, reducing the degree to which the permafrost is

warmed during the summer. While the IP and LCP tend to be warmer overall due to their wet centers, their rims are often just as cold as the center of the HCP (Figure 2.6), also due to the shallower snow cover over the rims. During most of the year the temperature gradients and therefore the heat fluxes within all the polygon types were vertically directed; however, large differences in ground temperatures between polygon positions during certain times of year lead to the development of horizontal temperature gradients and heat fluxes. The strongest horizontal heat fluxes developed during and immediately following the freezeback period, between low centers and troughs and their adjacent rims. While these horizontal fluxes last for only one or two months, they might be a significant cooling mechanism for these typically wet and slow freezing polygon positions. To our knowledge, these two-dimensional gradients have never before been documented using in-situ data and illustrate the importance of using two and three dimensional models to represent the fine-scale processes in these landscapes.

As a result of the differences in ground thermal regime, snow conditions, and moisture conditions between polygon types and positions, we find large differences in the active layer dynamics. The date of thaw onset is tightly coupled to snow melt (Figure 2.10) since the ground surface must remain at or below the ice point, 0 °C, until the snow melts (Romanovsky and Osterkamp, 1997). However, the date of snow melt and thus thaw onset is quite variable across our study sites due to the large differences in snow depth resulting from the local microtopography. We find that the center of the HCP and rims of WP and LCP become snow free first while the troughs and low centers become snow free as much as three weeks later in some years. This however, does not seem to have an impact on the active layer depth. We find, as did Zhang and Stamnes (1998), that changes in active layer thickness are poorly correlated with changes in MAAT but instead are more related to changes in summer warmth or TDD. While we do not have enough years of observation to demonstrate such a relationship, the strong correlation between active layer depth and TDD has been shown before for our study area (Hinkel et al., 2001). Changes in the wetness of the surface soil layers have a significant impact on the active layer thickness (Zhang et al., 1996). Also an important factor is soil composition, most importantly organic layer thickness but unfortunately these measurements were not included in this study. A thicker organic layer, especially when dry, would have an insulative and protective effect for the underlying permafrost (O'Donnell et al., 2009). The drier surface organic layers of the HCP are likely responsible for the shallower active layer depths observed there.

Almost immediately after the maximum thaw depth (active layer thickness) has been reached, the active layer begins to refreeze from the bottom (upward freezing, Figure 2.4). Previously, amounts of upward freezing between approximately 20 and 45 % have been documented on the north slope of Alaska (Osterkamp and Romanovsky, 1997). While the majority of our measurements fall within this range, we find a much wider, 5 to 70 %, range at our sites (Figures 2.13 and 2.14). This large range appears to be related to differences in permafrost temperature during freezeback and modified by differences in moisture and snow conditions across the landscape. The position with the largest amount of upward freezing is the trough of the HCP, which is undoubtedly due to the early and thick snow cover in this position. An early, thick snow cover insulates the surface, slowing cooling and allowing more time for upward freezing to take place (Osterkamp and Romanovsky, 1997). The moisture content of the active layer is also important as it also acts to slow freezing from the surface due to the high latent heat of fusion for water.

The start of freezeback at the ground surface (downward freezing) is driven mostly by surface boundary conditions (air temperature); thus, in most years initiates at approximately the same date across the landscape (Figure 2.12). In 2014 however, the dates of freezeback imitation at the surface are more spread out, but examination of the climatic data during this time period does not yield any obvious causes. As the downward and upward freezing fronts converge, the complete refreezing of the active layer is reached. The length of time and thus the freezeback date differs dramatically between sites and is mostly related to the surface FDD during freezeback and active layer wetness. The timing and thickness of snow cover is important but its effect is already included by using ground surface FDD, below the snowpack. Due to the large latent heat of fusion for water, we find that very wet positions, like IP and LCP centers, can take over a month longer to refreeze than the dry centers of HCP (Figure 2.15). The insulative effect of snow cover can be seen by comparing the freezeback date of the HCP center to that of the HCP trough, almost two weeks later (Figure 2.15).

Variation in active layer parameters (thaw onset, maximum thaw depth and date, upward freezing and freezeback start and completion dates) combine to produce different sizes and shapes of active layer envelopes (Figure 2.16). Integrating the area contained within an active layer envelope represents the time and depth availability of the active layer for biological processes. Thus, as the maximum thaw depth is approached, the amount of time that layer is unfrozen becomes shorter

and shorter. This is an especially important consideration when scaling measurements that depend on the thawed active layer, such as carbon decomposition and the production of greenhouse gasses. Following the progression of our space for time substitution from IP to LCP to WP and HCP, the HCP clearly stands out as being different from the other polygon types with respect to ground thermal regime and active layer dynamics. It not only has colder MAGT's but also a shorter thawed season and shallower active layer. The most important factor in producing these differences is the drier active layer of the HCP, which reduce the thermal conductivity of the surface layers. This reduces the exchange of energy between the surface and deeper soil layers, protecting the permafrost and ice-wedges from thaw during the summer. The highly skewed snow distribution across the HCP is also an important factor because it leaves the high-centers with relatively thin snow cover during the long winters. The high centers are then able to act as very effective heat sinks, cooling the permafrost below. With colder permafrost, we find more upward freezing during freezeback, further reducing the time the active layer is thawed. Thus, the HCP's have entered a new stable state, where they might be more resistant to a warmer climate. This stabilizing effect was noted by Jorgenson et al. (2015) as one possible outcome of ice-wedge degradation, while the other outcome was development of a thermokarst lake or pond. Under a continued warming scenario however, it would only be a matter of time before this stability was again overcome and ice-wedge degradation resumed once again.

2.5 Conclusion

In our study space for time was substituted along a gradient of ice-wedge polygon development phases to examine how permafrost thermal regime and active layer dynamics might change as degradation of ice-wedges occurs. In these flat, costal landscapes, drainage is often poor leaving the centers and troughs of IP and LCP inundated during the thawed season. Degradation of the ice-wedges in these landscapes leads to subsidence and trough deepening which if continued unimpeded could produce thermokarst ponds or lakes (Jorgenson et al., 2015). However, in some cases, and the case of our HCP study site, the degradation enhances the local drainage and acts to dry the active layer. We found that the HCP had the coldest overall MAGT and shallowest active layer. The HCP also had some of the highest amounts of upward freezing and the earliest freezeback dates. Combining all this produces an active layer in the HCP that is shallower and thawed for a shorter period of time compared to the undegraded IP and LCP sites. With the bulk

of the biological activity occurring when the active layer is thawed, we should expect reduced amounts of decomposition and other biological processes. Thus, degradation of ice-wedge polygon landscapes into HCP's might not initially release large amounts of greenhouse gasses but instead move them into a different stable state with a new threshold that needs to be crossed before they degrade further. This is particularly important given the current focus on the fate of permafrost carbon in these landscapes.

Acknowledgements
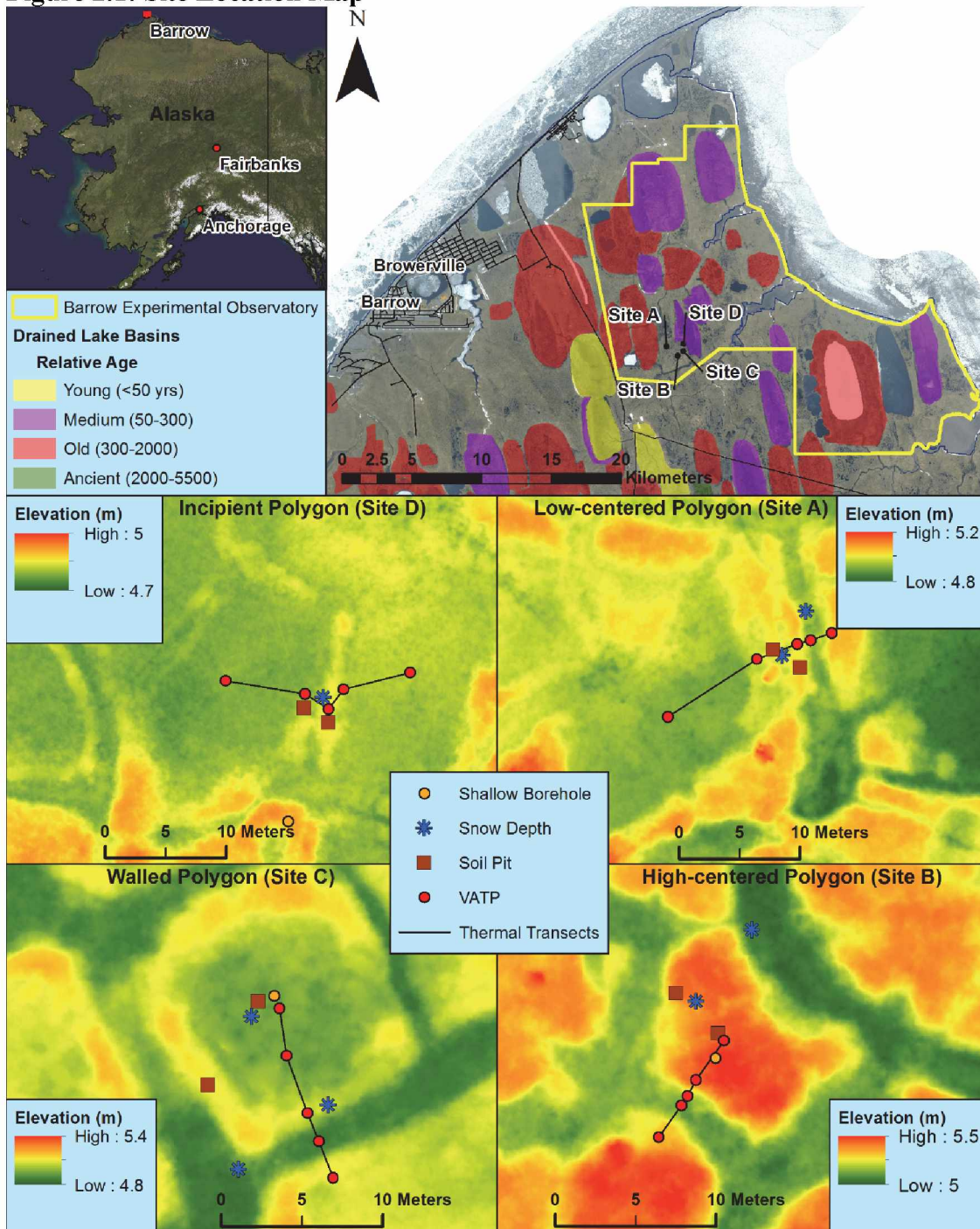
Figure 2.1: Site Location Map

Figure 2.1 The top panel shows the location of our four study sites (A-D) in the Barrow Experimental Observatory in relation to the nearby town of Barrow, AK and to the drained lake basins in the area (Hinkel et al., 2003). The bottom panel gives a detailed view of each study site ordered according to development phase, from least developed ice-wedges (incipient) to degrading ice-wedges (high-centered). The background image is a digital surface model (Cherry and Crowder, 2013) at 5 cm horizontal scale. The location of instrumentation is shown for each study site.

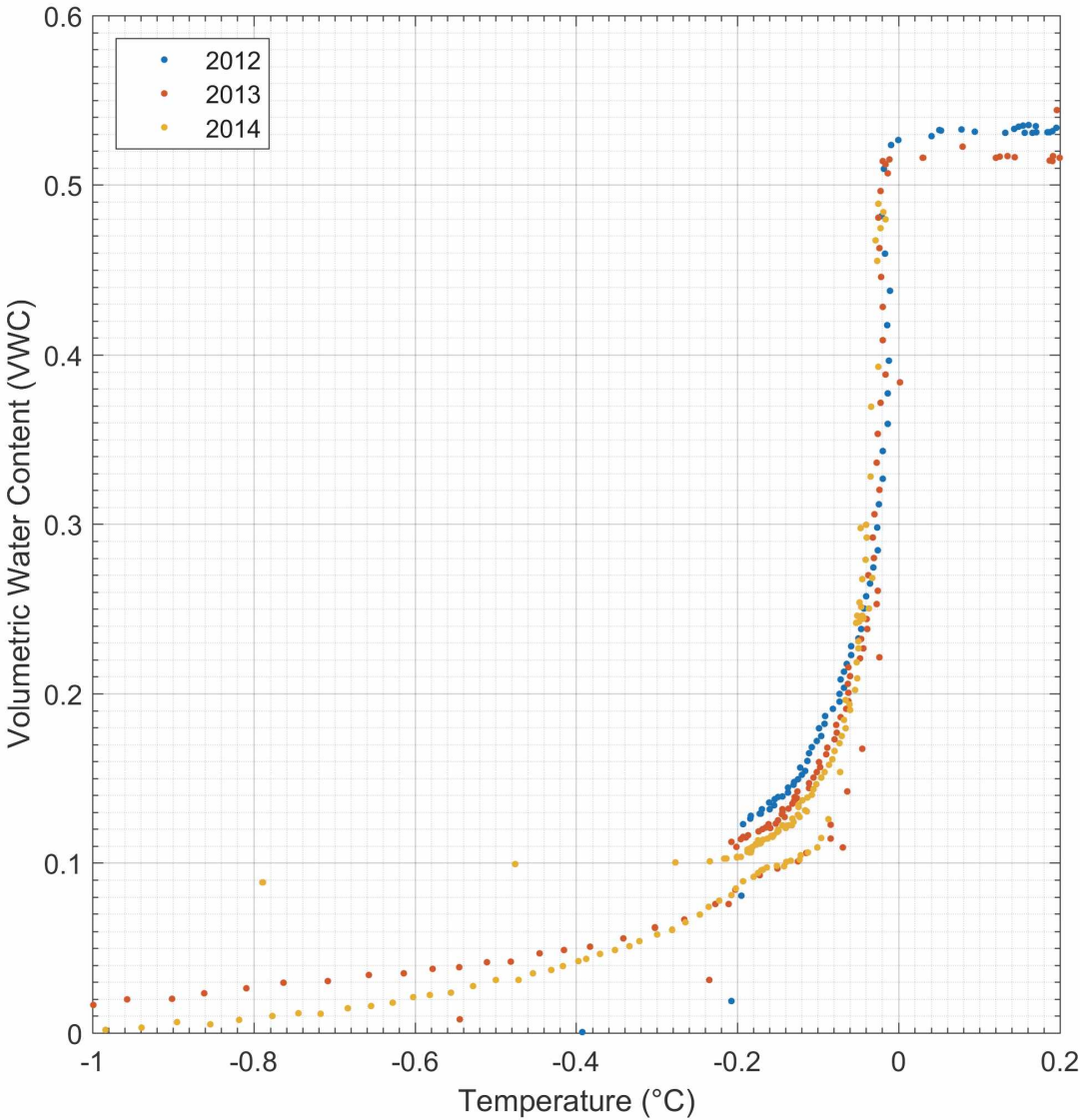**Figure 2.2: Unfrozen Water Content Curve**

Figure 2.2 An example of unfrozen water content curve from the low-centered polygon at 37cm depth.

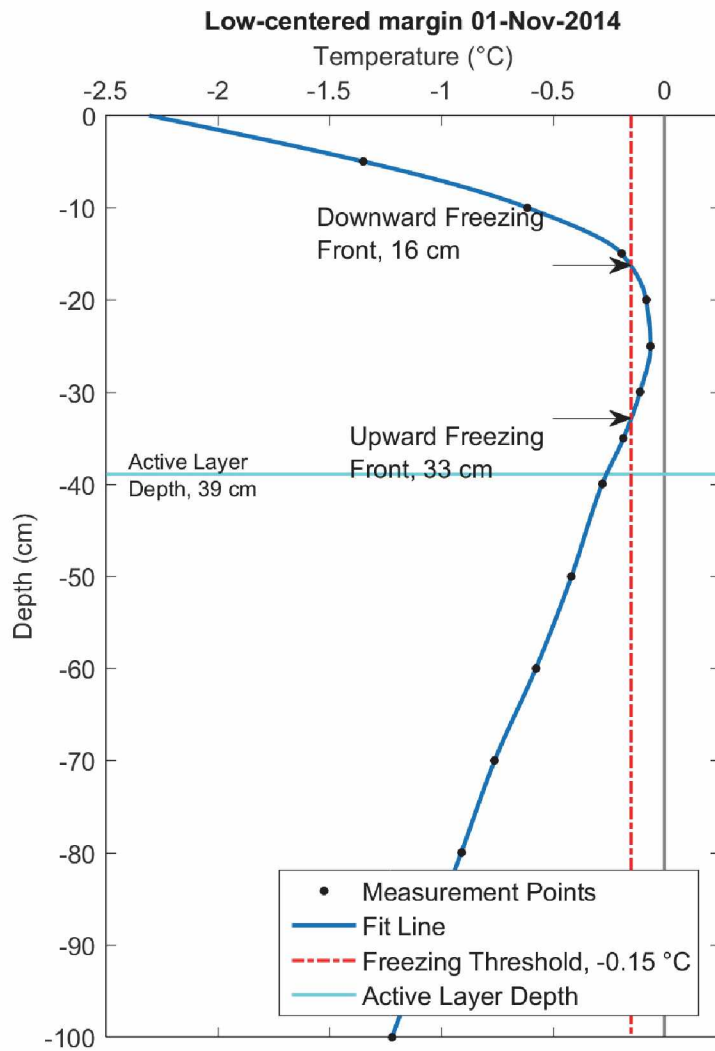**Figure 2.3: Freezing Front Calculation Example**

Figure 2.3 An example of the calculation of the downward and upward freezing fronts. The points at which the fit line cross the freezing threshold show the positions of the downward and upward freezing fronts.
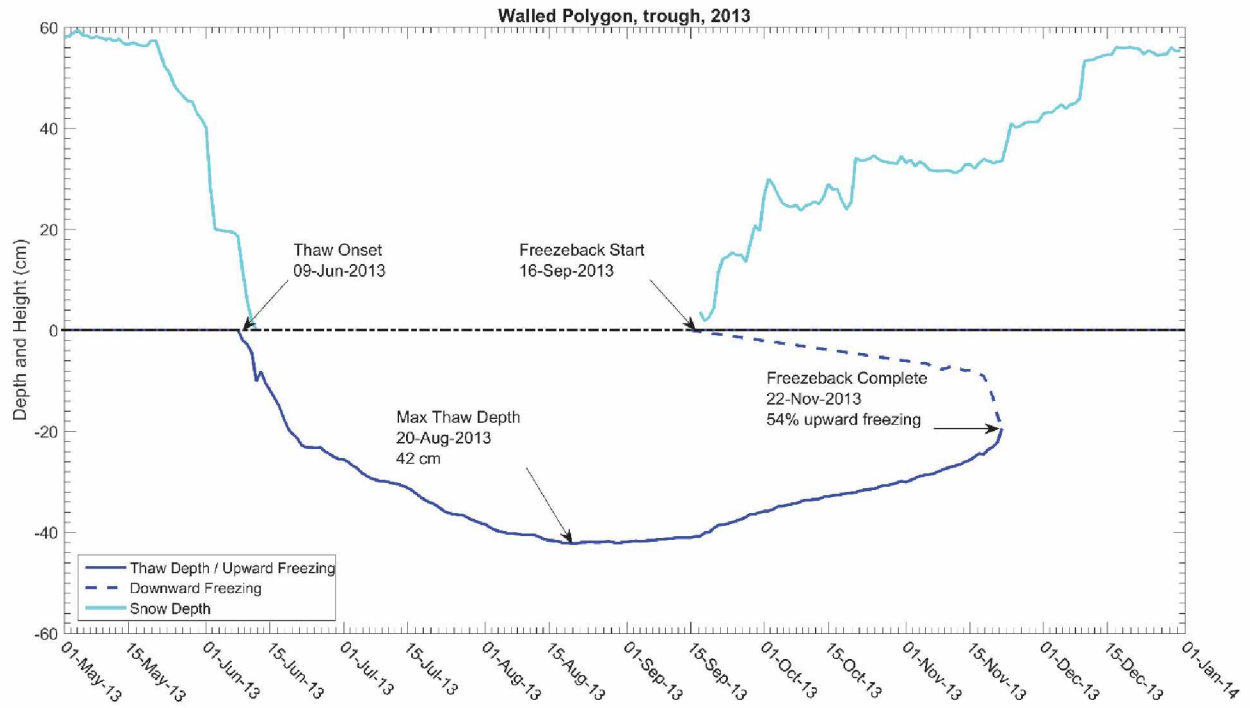
Figure 2.4: Active Layer Dynamics Example

Figure 2.4 An example of the active layer development and refreezing in the trough of the WP in 2013, with the snow depth shown for reference.
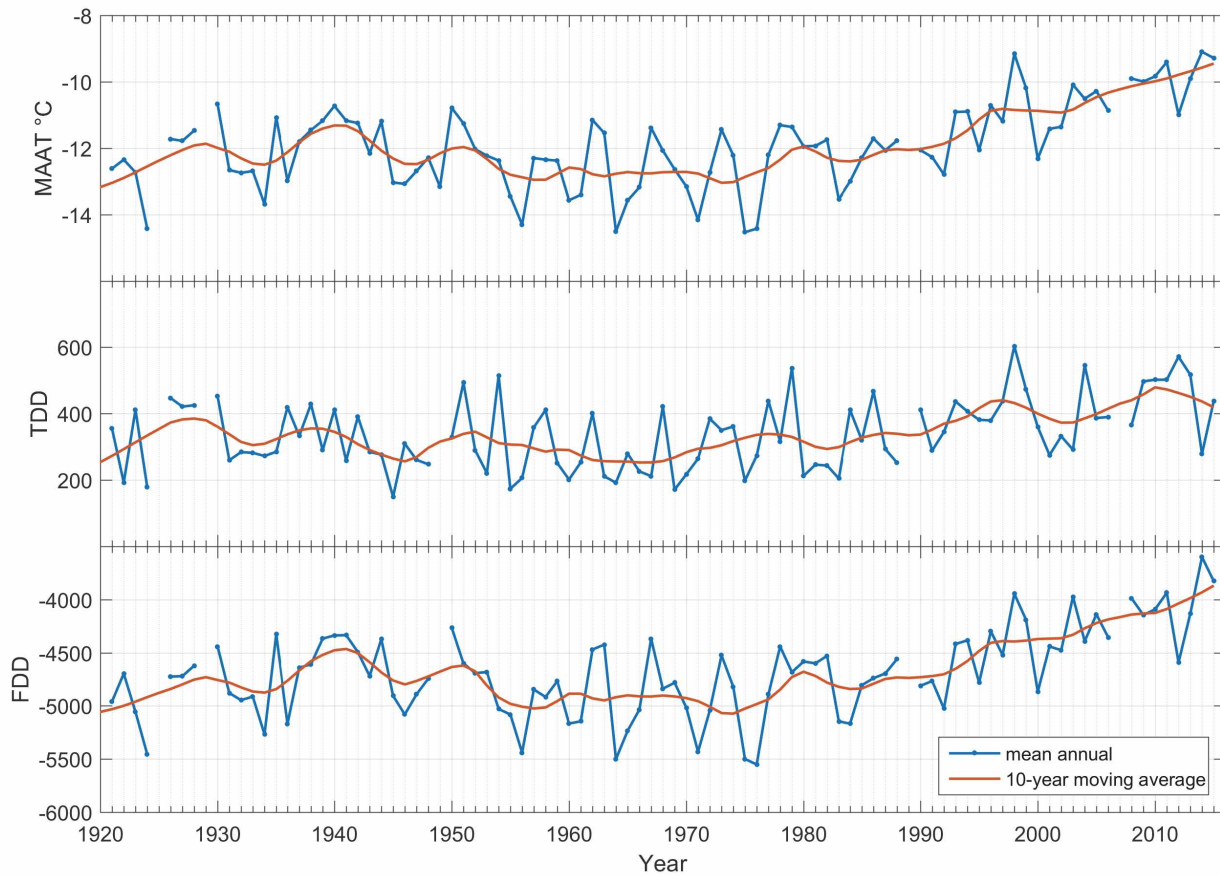
Figure 2.5: Barrow MAAT, TDD, and FDD

Figure 2.5 Mean annual air temperature (MAAT), thawing degree days (TDD), and freezing degree days (FDD) are shown for the Barrow airport since 1920 (Menne et al., 2012). A 10-year moving average is also shown.

Figure 2.6: MAGT at 1 meter

Figure 2.6 Mean Annual Ground Temperature (MAGT) at 1 m depth is shown grouped by year. A box plot is shown for all polygons and positions with each blue box depicting the 25th to 75th percentile, divided by a red line indicating the median. The whiskers extend to the most extreme points not considered outliers (red +). The MAGT's from each polygon position, used to create the boxplot, are shown.
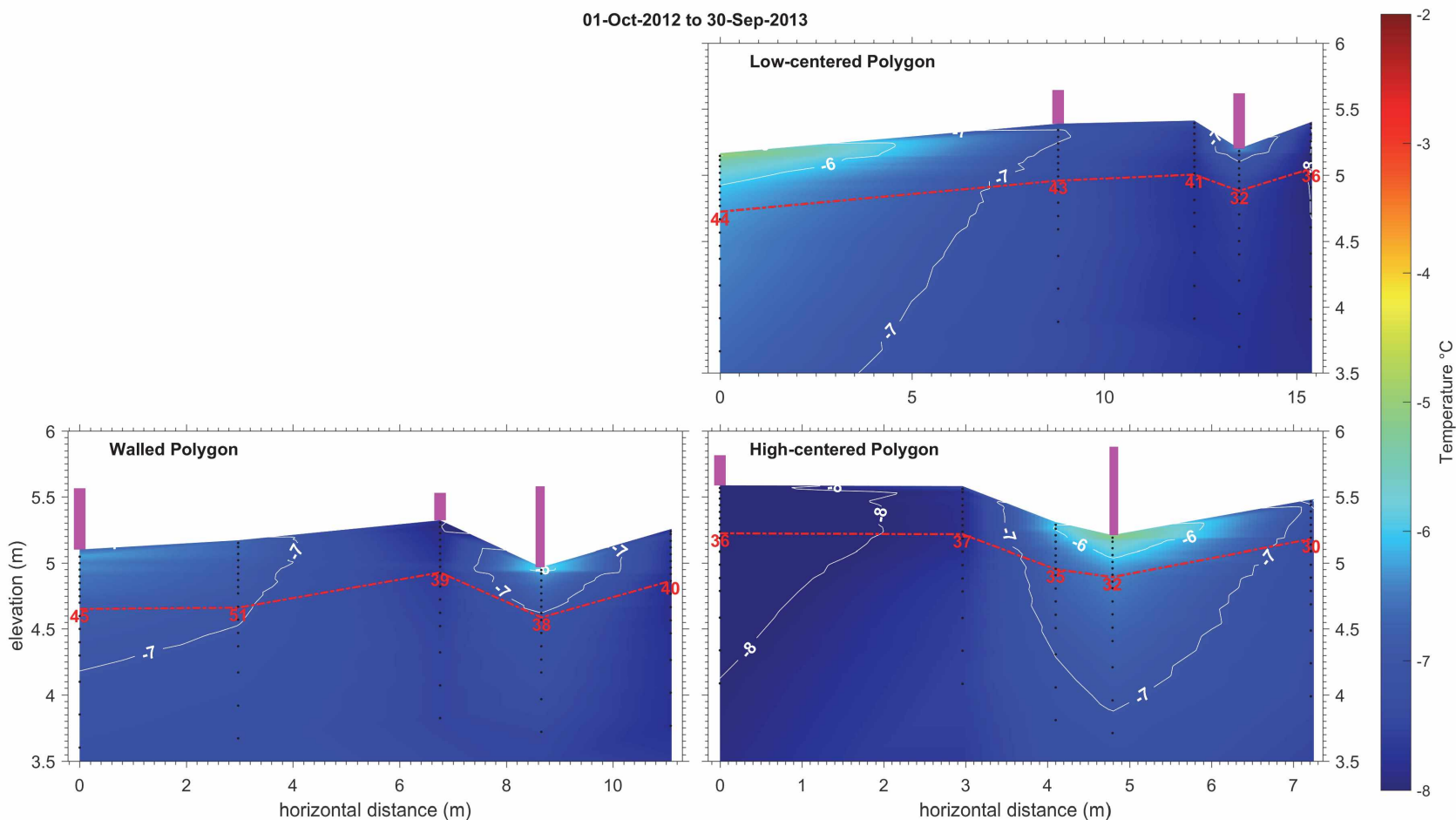
Figure 2.7: MAGT Cross-Sections 2012–2013

Figure 2.7 The mean annual ground temperature (MAGT) is shown for the period 1 Oct. 2012 to 30 Sept. 2013 as a cross-section through each polygon (Incipient Polygon not available this year). The magenta bars indicate the maximum snow depth and the red lines and numbers indicate the active layer depth for the period. The VATP measurement points are shown as black dots. A figure for the incipient polygon is not shown because data collection at this site didn't start until Sept. 2013.
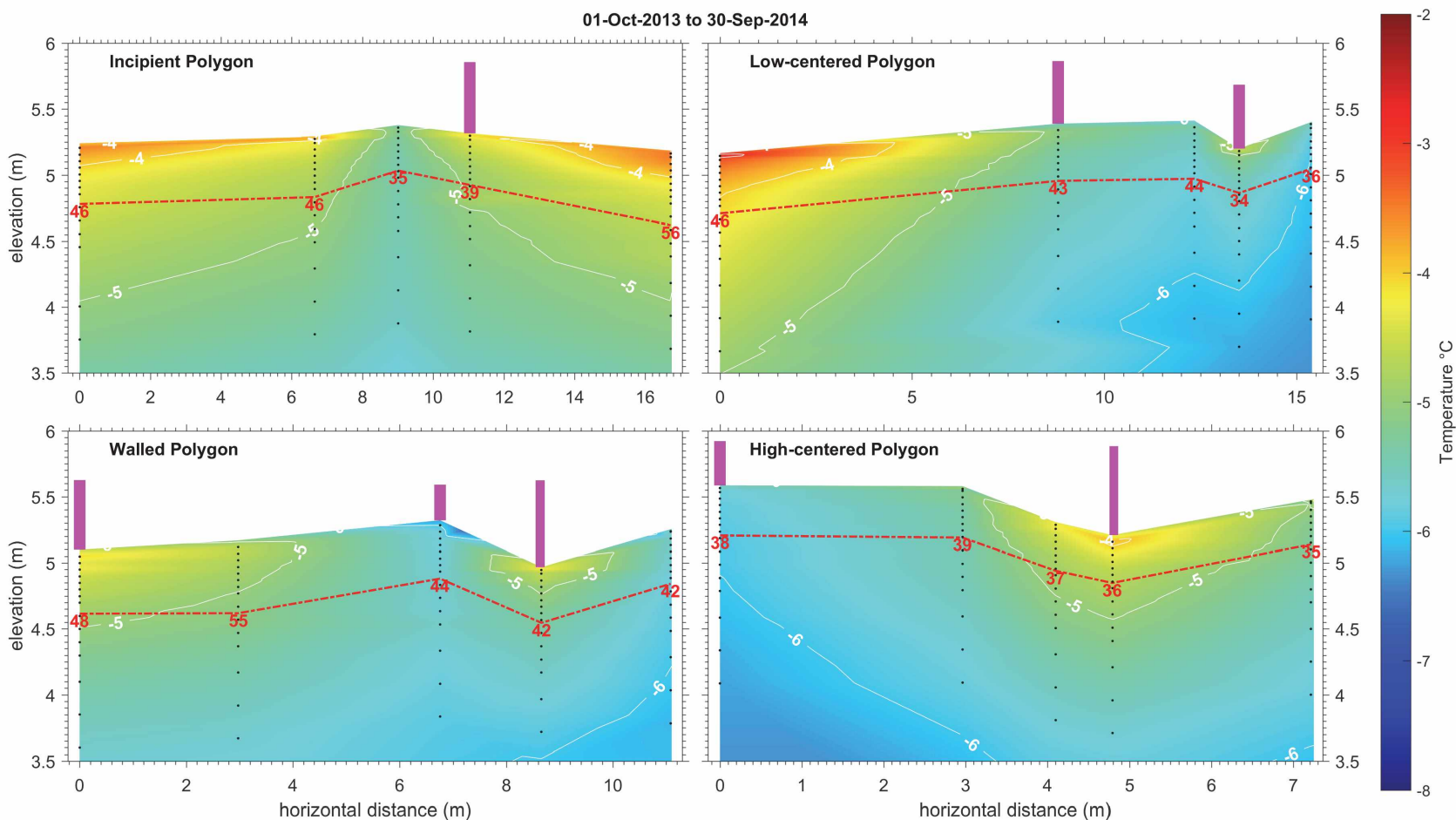
Figure 2.8: MAGT Cross-Sections 2013–2014

Figure 2.8 The mean annual ground temperature (MAGT) is shown for the period 1 Oct. 2013 to 30 Sept. 2014 as a cross-section through each polygon. The magenta bars indicate the maximum snow depth and the red lines and numbers indicate the active layer depth for the period. The VATP measurement points are shown as black dots.

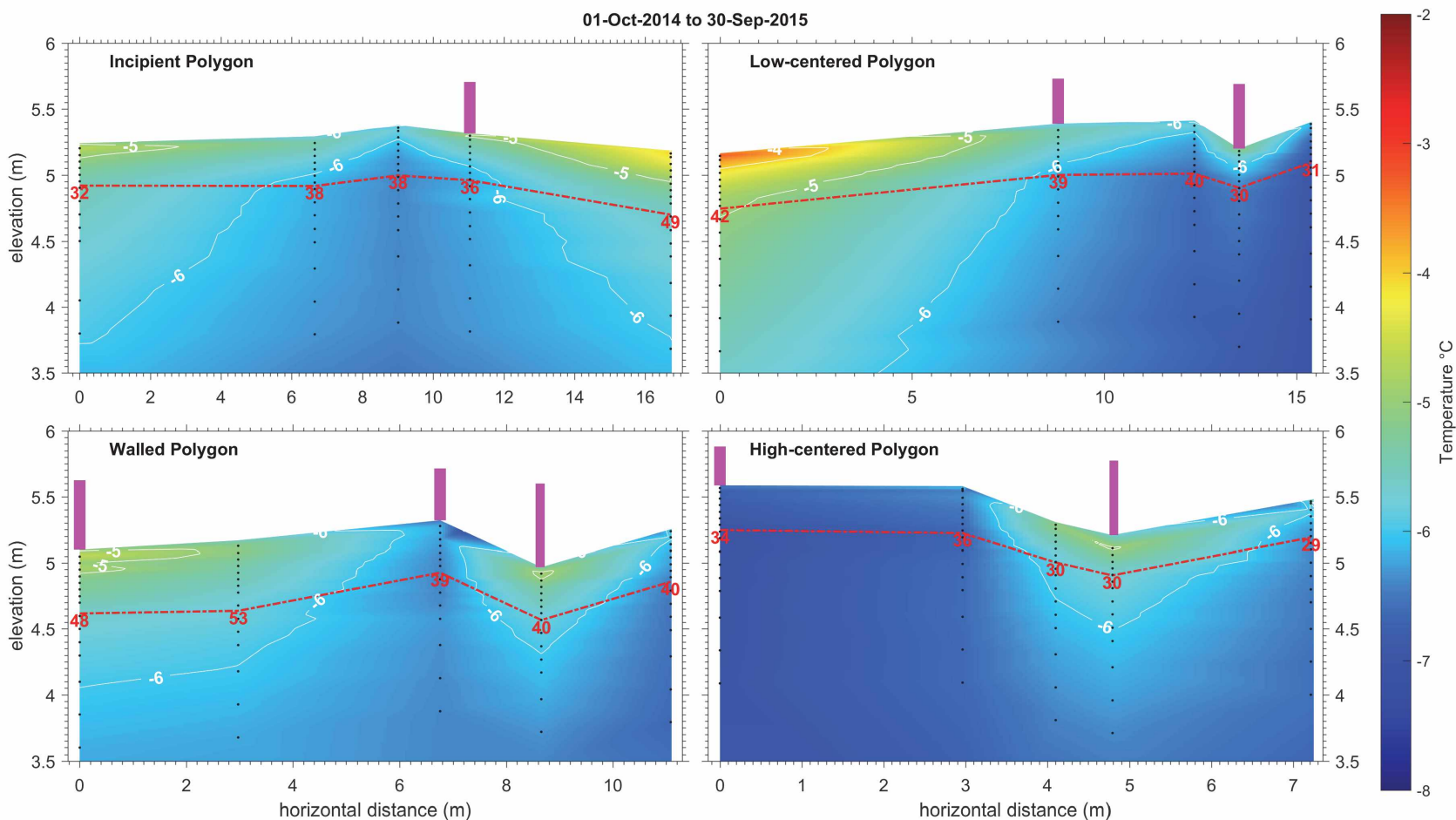**Figure 2.9: MAGT Cross-Sections 2014–2015**

Figure 2.9 The mean annual ground temperature (MAGT) is shown for the period 1 Oct. 2014 to 30 Sept. 2015 as a cross-section through each polygon. The magenta bars indicate the maximum snow depth and the red lines and numbers indicate the active layer depth for the period. The VATP measurement points are shown as black dots.

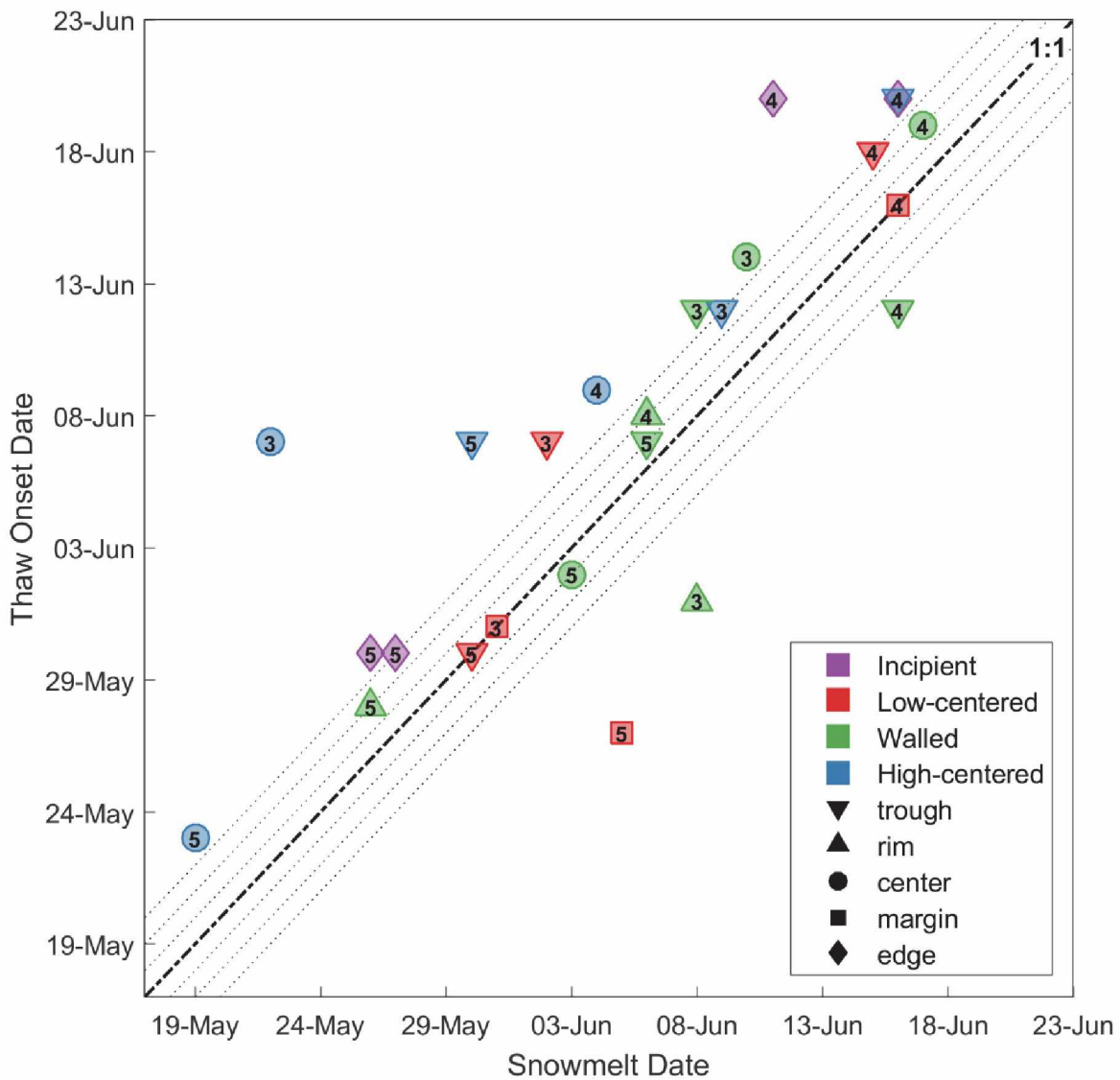**Figure 2.10: Snow Melt vs Thaw Onset**

Figure 2.10 Shown is the relationship between snowmelt date and thaw onset date for all probe positions with snow depth measurements. The numbers in the symbols show the year (i.e. 2015=5). A 1:1 line is shown for reference and the dotted lines on either side indicate plus or minus one day.

Figure 2.11: Active Layer Thickness
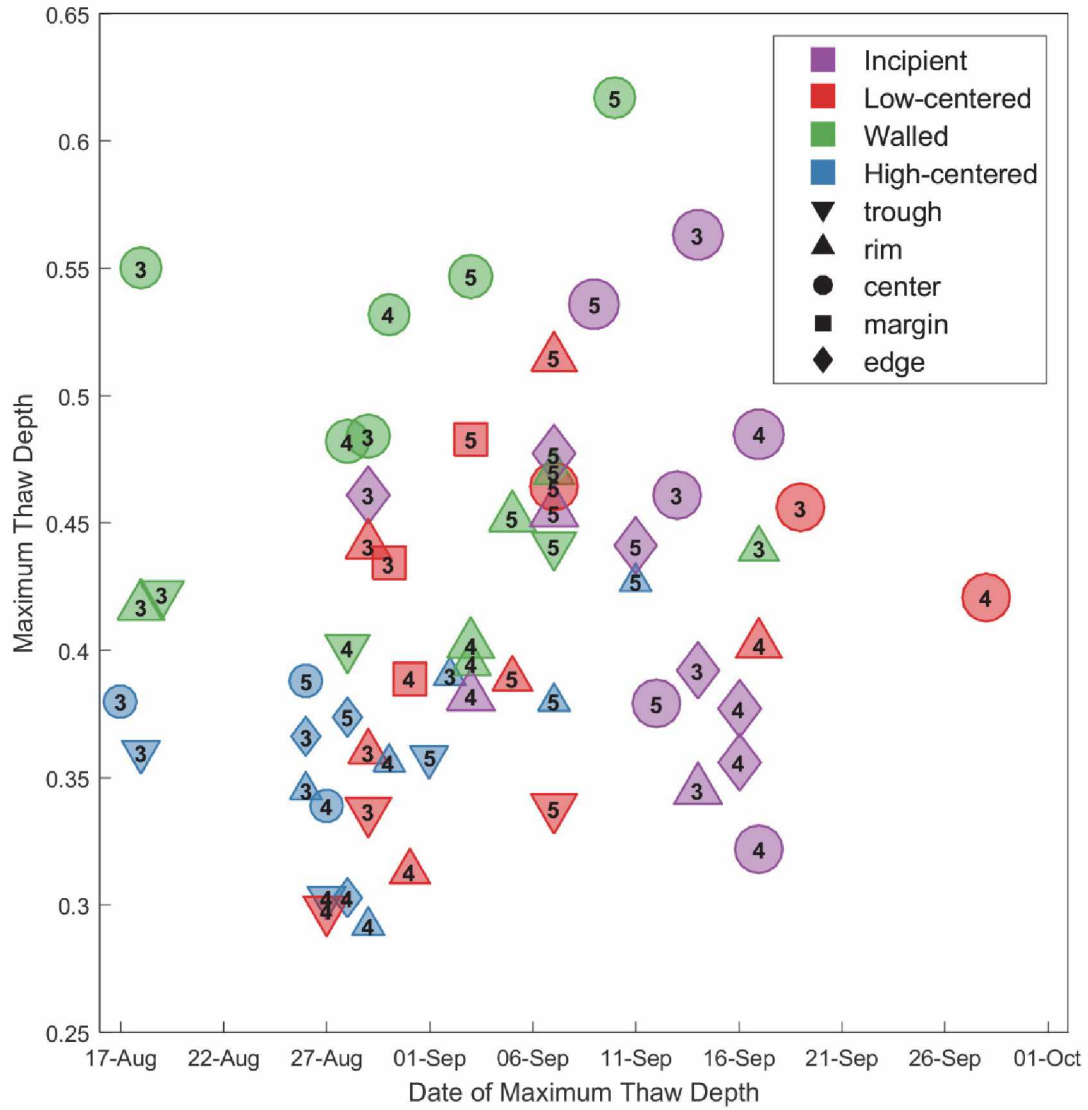
Figure 2.11 The maximum thaw depth is shown as a function of the date of maximum thaw depth. The size of the symbols is related to the TWI, larger is wetter. The numbers in the symbols show the year (i.e. 2015=5).

Figure 2.12: Freezeback Initiation Date
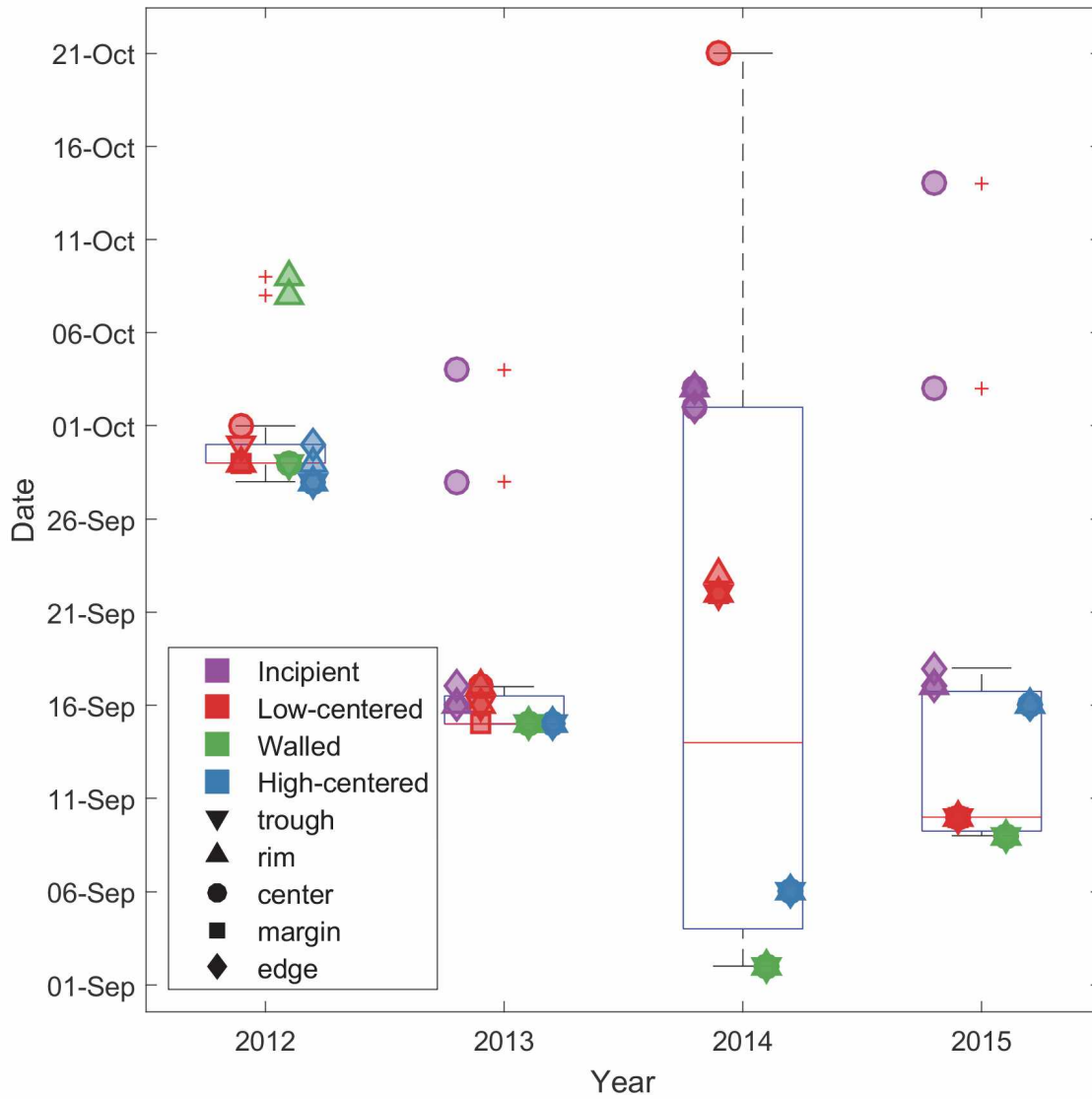
Figure 2.12 A box plot is shown for the initiation date of freezeback. Each blue box shows the 25th and 75th percentile, divided by a red line indicating the median. The whiskers extend to the most extreme points not considered outliers (red +).

Figure 2.13: Upward Freezing as a Function of Ground Temperature and Snow Depth Days

Figure 2.13 The amount of upward freezing is shown as a function of mean ground temperature at 1 m during the freezeback period. The size of the symbols indicates the amount of snow based on the snow depth days during the freezeback period (larger = more snow). A reduced number of polygon positions is shown because snow depth was not measured at all positions.

Figure 2.14: Upward Freezing as a Function of Ground Temperature and TWI
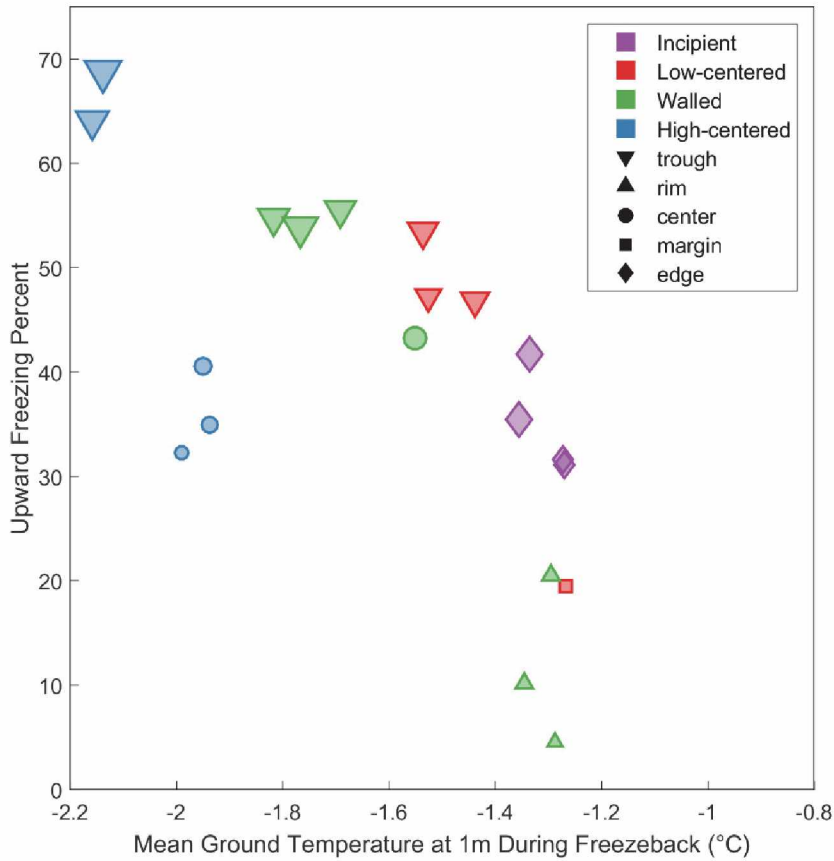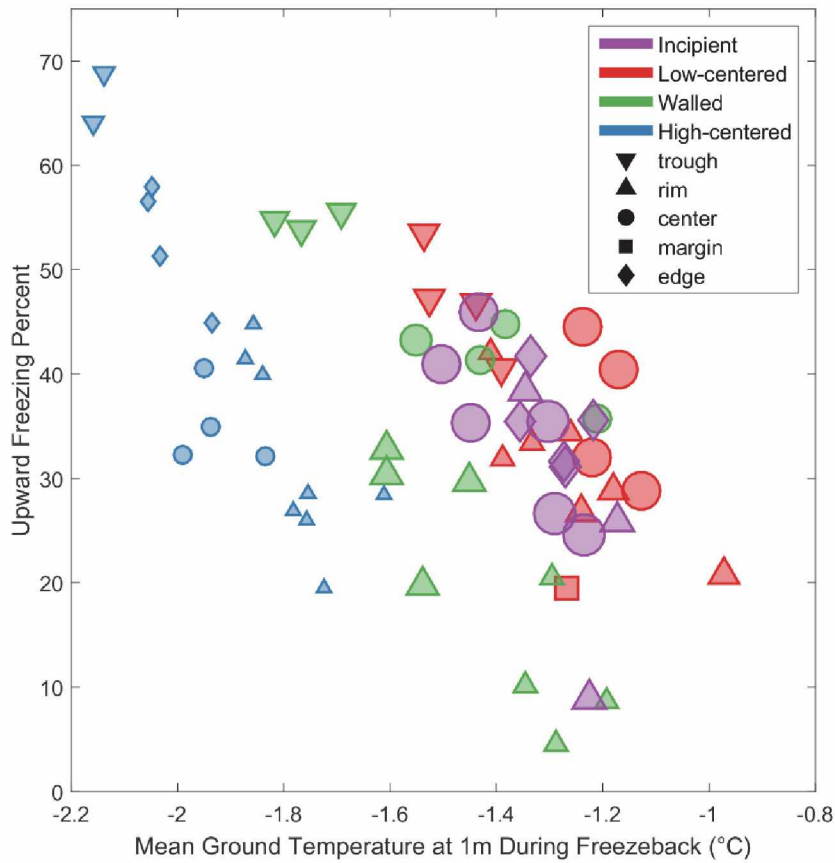

Figure 2.14 The amount of upward freezing is shown as a function of mean ground temperature at 1 m during the freezeback period. The size of the symbols indicates the topographic wetness index (larger = wetter).

Figure 2.15: Freezeback Completion Date
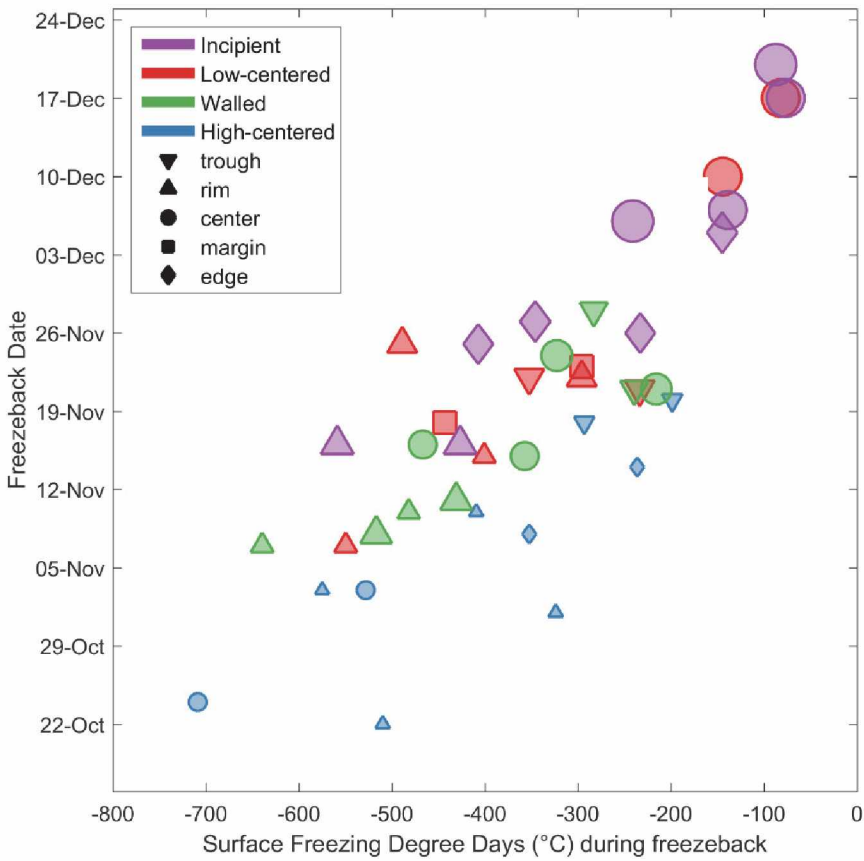
Figure 2.15 The date of freezeback completion is shown as a function of the freezing degree days at the surface during the freezeback period. The size of the symbols indicates the wetness based on the topographic wetness index (larger = wetter).

Figure 2.16: Active Layer Envelopes Example
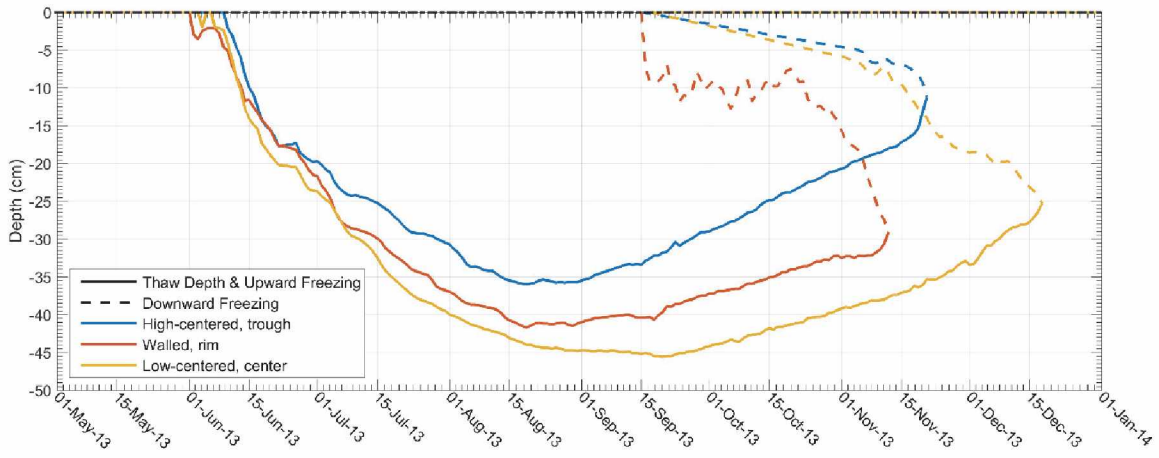
Figure 2.16 Shown is an example of the active layer envelopes for different polygon types and positions during 2013.

Figure 2.17: Two-dimensional Temperature Field Example
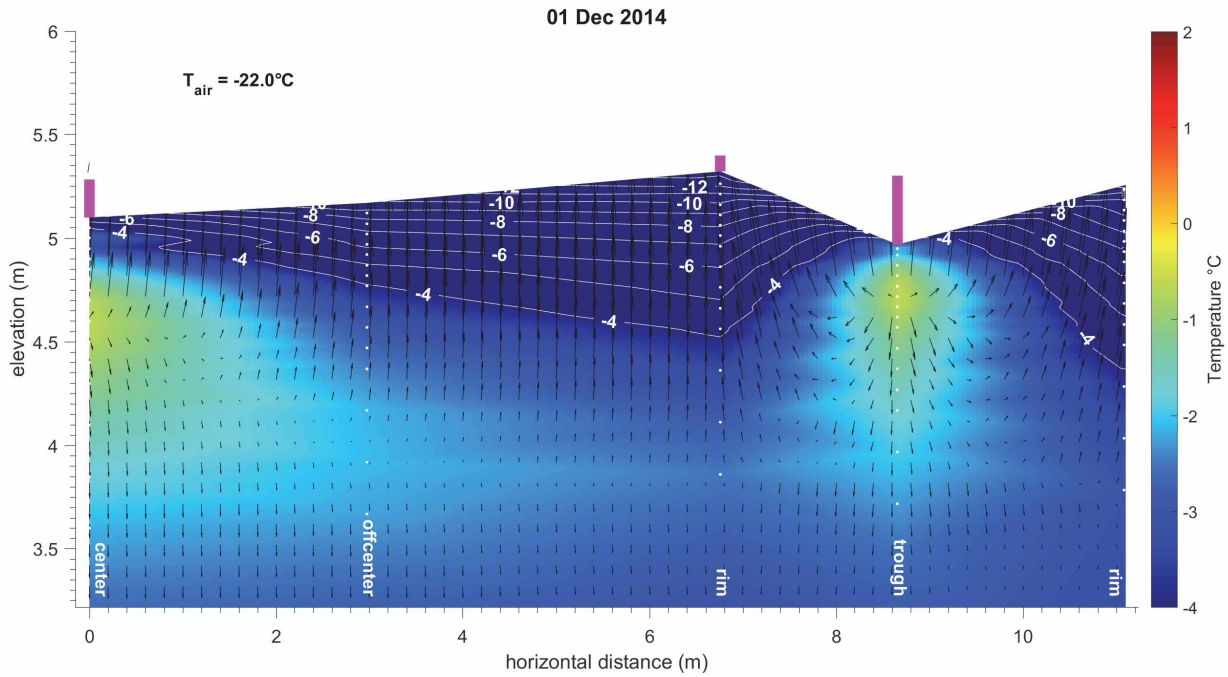
Figure 2.17 Daily average 2D temperature field from the walled polygon. Black arrows point in the direction of decreasing temperature and are proportional to the temperature gradient. Magenta bars are snow depth. VATP measurements, white dots and labels.

Table 2.1: Mean Annual Air Temperature

Mean annual air temperature is given for the Barrow Airport and an average for our four sites. The long-term, 1981-2010 average is also given for the Barrow Airport.

Year	Barrow Airport	Site Average
2012 to 2013	-9.91	-10.83
2013 to 2014	-9.10	-9.86
2014 to 2015	-9.28	-9.83
1981 to 2010	*-11.19*	

References

Billings, W. D. and Peterson, K. M.: Vegetational Change and Ice-Wedge Polygons through the Thaw-Lake Cycle in Arctic Alaska, Arct. Alp. Res., 12(4), 413, doi:10.2307/1550492, 1980.

Bockheim, J. G., Hinkel, K. M. and Nelson, F. E.: Soils of the Barrow region, Alaska, Polar Geogr., 25(3), 163–181, doi:10.1080/10889370109377711, 2001.

Böhner, J. and Selige, T.: Spatial prediction of soil attributes using terrain analysis and climate regionalisation, in SAGA - Analyses and Modelling Applications, vol. 115, edited by J. Böhner, K. R. McCloy, and J. Strobl, pp. 13–28, Göttinger Aeographische Abhandlungen., 2006.

Brown, J.: Tundra Soils Formed over Ice Wedges, Northern Alaska, Soil Sci. Soc. Am. J., 31(5), 686–691, doi:10.2136/sssaj1967.03615995003100050022x, 1967.

Busey, B., Hinzman, L., Romanovsky, V. and Cable, W. L.: Continuous Snow Depth, Intensive Site 1, Barrow, Alaska, Next Gener. Ecosyst. Exp. Arct., [dataset], doi:10.5440/1163347, 2014a.

Busey, B., Hinzman, L., Cable, W. L. and Romanovsky, V.: Surface Meteorology, Barrow, Alaska, Area A, B, C and D, Ongoing from 2012, Next Gener. Ecosyst. Exp. Arct., [dataset], doi:10.5440/1164893, 2014b.

Cable, W. L. and Romanovsky, V.: Subsurface Temperature, Moisture, Thermal Conductivity and Heat Flux, Barrow, Area A, B, C, D, Next Gener. Ecosyst. Exp. Arct., [dataset], doi:10.5440/1126515, 2014.

Cherry, J. and Crowder, K.: Airborne Imagery Collections Barrow 2013, Next Gener. Ecosyst. Exp. Arct., [dataset], doi:10.5440/1167159, 2013.

Conrad, O., Bechtel, B., Bock, M., Dietrich, H., Fischer, E., Gerlitz, L., Wehberg, J., Wichmann, V. and Böhner, J.: System for Automated Geoscientific Analyses (SAGA) v. 2.1.4, Geosci. Model Dev., 8(7), 1991–2007, doi:10.5194/gmd-8-1991-2015, 2015.

Dingman, S. L., Barry, R. G., Weller, G., Benson, C. S., LeDrew, E. F. and Goodwin, C. W.: Climate, Snow cover, Microclimate, and hydrology, in An Arctic ecosystem : the coastal tundra at Barrow, Alaska, edited by J. Brown, P. C. Miller, L. L. Tieszen, and F. Bunnell, pp. 30–65, Dowden, Hutchinson and Ross, Inc., Stroudsburg, Pennsylvania., 1980.

Engstrom, R., Hope, A., Kwon, H., Stow, D. and Zamolodchikov, D.: Spatial distribution of near surface soil moisture and its relationship to microtopography in the Alaskan Arctic coastal plain, Nord. Hydrol., 36(3), 219–234, 2005.

Engstrom, R., Hope, A., Kwon, H. and Stow, D.: The Relationship Between Soil Moisture and NDVI Near Barrow, Alaska, Phys. Geogr., 29(1), 38–53, doi:10.2747/0272-3646.29.1.38, 2008.

Goodrich, L.: The influence of snow cover on the ground thermal regime, Can. Geotech. J., 1982.

Gusmeroli, A., Liljedahl, A. K., Peterson, J. E., Hubbard, S. S. and Hinzman, L. D.: Effects of spatially variable snow cover on thermal regime and hydrology of an Arctic ice wedge polygon landscape identified using ground penetrating radar and LIDAR datasets, AGU Fall Meet. San Fr. USA, 3-7 December 2012, C33C–0668, 2012.

Heikoop, J. M., Throckmorton, H. M., Newman, B. D., Perkins, G. B., Iversen, C. M., Roy Chowdhury, T., Romanovsky, V., Graham, D. E., Norby, R. J., Wilson, C. J. and Wullschleger, S. D.: Isotopic identification of soil and permafrost nitrate sources in an Arctic tundra ecosystem, J. Geophys. Res. Biogeosciences, 120(6), 1000–1017, doi:10.1002/2014JG002883, 2015.

Hinkel, K. M., Paetzold, F., Nelson, F. E. and Bockheim, J. G.: Patterns of soil temperature and moisture in the active layer and upper permafrost at Barrow, Alaska: 1993–1999, Glob. Planet. Change, 29(3-4), 293–309, doi:10.1016/S0921-8181(01)00096-0, 2001.

Hinkel, K. M., Eisner, W. R., Bockheim, J. G., Nelson, F. E., Peterson, K. M. and Dai, X.: Spatial Extent, Age, and Carbon Stocks in Drained Thaw Lake Basins on the Barrow Peninsula, Alaska, Arctic, Antarct. Alp. Res., 35(3), 291–300, doi:10.1657/1523-0430(2003)035[0291:SEAACS]2.0.CO;2, 2003.

Hubbard, S. and Peterson, J.: Active Layer and Moisture Measurements for Intensive Site 0 and 1, Barrow, Alaska, Next Gener. Ecosyst. Exp. Arct., [dataset], doi:http://dx.doi.org/10.5440/1177857, 2016.

IPCC: Climate Change 2014: Synthesis Report. Contribution of Working Groups I, II and III to the Fifth Assessment Report of the Intergovernmental Panel on Climate Change, edited by Core Writing Team, R. K. Pachauri, and L. A. Meyer, IPCC, Geneva, Switzerland. [online] Available from: http://www.ipcc.ch/report/ar5/syr/, 2014.

Jorgenson, M. T., Shur, Y. L. and Pullman, E. R.: Abrupt increase in permafrost degradation in Arctic Alaska, Geophys. Res. Lett., 33(2), L02503, doi:10.1029/2005GL024960, 2006.

Jorgenson, M. T., Kanevskiy, M., Shur, Y., Moskalenko, N., Brown, D. R. N., Wickland, K., Striegl, R. and Koch, J.: Role of ground ice dynamics and ecological feedbacks in recent ice wedge degradation and stabilization, J. Geophys. Res. Earth Surf., 120(11), 2280–2297, doi:10.1002/2015JF003602, 2015.

Koven, C. D., Ringeval, B., Friedlingstein, P., Ciais, P., Cadule, P., Khvorostyanov, D., Krinner, G. and Tarnocai, C.: Permafrost carbon-climate feedbacks accelerate global warming., Proc. Natl. Acad. Sci. U. S. A., 108(36), 14769–14774, doi:10.1073/pnas.1103910108, 2011.

Lachenbruch, A. H.: Mechanics of Thermal Contraction Cracks and Ice-Wedge Polygons in Permafrost, in Geological Society of America Special Papers, vol. 70, pp. 1–66., 1962.

Lara, M. J., McGuire, A. D., Euskirchen, E. S., Tweedie, C. E., Hinkel, K. M., Skurikhin, A. N., Romanovsky, V. E., Grosse, G., Bolton, W. R. and Genet, H.: Polygonal tundra geomorphological change in response to warming alters future CO 2 and CH 4 flux on the Barrow Peninsula, Glob. Chang. Biol., 21(4), 1634–1651, doi:10.1111/gcb.12757, 2015.

Leffingwell, E. de K.: Ground-Ice Wedges: The Dominant Form of Ground-Ice on the North Coast of Alaska, J. Geol., 23(7), 635–654, 1915.

Liljedahl, A. K., Hinzman, L. D. and Schulla, J.: Ice-Wedge Polygon Type Controls Low-Gradient Watershed-Scale Hydrology, in Proceedings of the Tenth International Conference on Permafrost, Salekhard, Russia, 25-29 June 2012, vol. 1, pp. 231–236., 2012.

Liljedahl, A. K., Boike, J., Daanen, R. P., Fedorov, A. N., Frost, G. V., Grosse, G., Hinzman, L. D., Iijma, Y., Jorgenson, J. C., Matveyeva, N., Necsoiu, M., Raynolds, M. K., Romanovsky, V. E., Schulla, J., Tape, K. D., Walker, D. A., Wilson, C. J., Yabuki, H. and Zona, D.: Pan-Arctic ice-wedge degradation in warming permafrost and its influence on tundra hydrology, Nat. Geosci., (March), 1–8, doi:10.1038/ngeo2674, 2016.

MacKay, J. R.: Thermally induced movements in ice-wedge polygons, western arctic coast: a long-term study, Géographie Phys. Quat., 54(1), 41, doi:10.7202/004846ar, 2000.

Menne, M. J., Durre, I., Korzeniewski, B., McNeal, S., Thomas, K., Yin, X., Anthony, S., Ray, R., Vose, R. S., E.Gleason, B. and Houston, T. G.: Global Historical Climatology Network - Daily (GHCN-Daily), Version 3., [USW00027502, Barrow W Post W Rogers Airport, AK US], doi:10.7289/V5D21VHZ, 2012.

Minke, M., Donner, N., Karpov, N., de Klerk, P. and Joosten, H.: Patterns in vegetation composition, surface height and thaw depth in polygon mires in the Yakutian Arctic (NE Siberia): a microtopographical characterisation of the active layer, Permafr. Periglac. Process., 20(4), 357–368, doi:10.1002/ppp.663, 2009.

Newman, B. D., Throckmorton, H. M., Graham, D. E., Gu, B., Hubbard, S. S., Liang, L., Wu, Y., Heikoop, J. M., Herndon, E. M., Phelps, T. J., Wilson, C. J. and Wullschleger, S. D.: Microtopographic and depth controls on active layer chemistry in Arctic polygonal ground, Geophys. Res. Lett., 42(6), 1808–1817, doi:10.1002/2014GL062804, 2015.

O'Donnell, J. A., Romanovsky, V. E., Harden, J. W. and McGuire, A. D.: The Effect of Moisture Content on the Thermal Conductivity of Moss and Organic Soil Horizons From Black Spruce Ecosystems in Interior Alaska, Soil Sci., 174(12), 646–651, doi:10.1097/SS.0b013e3181c4a7f8, 2009.

Osterkamp, T. E. and Romanovsky, V. E.: Freezing of the Active Layer on the Coastal Plain of the Alaskan Arctic, Permafr. Periglac. Process., 8(1), 23–44, doi:10.1002/(SICI)1099-1530(199701)8:1<23::AID-PPP239>3.0.CO;2-2, 1997.

Raynolds, M. K., Walker, D. A., Ambrosius, K. J., Brown, J., Everett, K. R., Kanevskiy, M., Kofinas, G. P., Romanovsky, V. E., Shur, Y. and Webber, P. J.: Cumulative geoecological effects of 62 years of infrastructure and climate change in ice-rich permafrost landscapes, Prudhoe Bay Oilfield, Alaska, Glob. Chang. Biol., 20(4), 1211–1224, doi:10.1111/gcb.12500, 2014.

Romanovsky, V. E. and Osterkamp, T. E.: Thawing of the Active Layer on the Coastal Plain of the Alaskan Arctic, Permafr. Periglac. Process., 8(1), 1–22, doi:10.1002/(SICI)1099-1530(199701)8:1<1::AID-PPP243>3.0.CO;2-U, 1997.

Romanovsky, V. E. and Osterkamp, T. E.: Effects of unfrozen water on heat and mass transport processes in the active layer and permafrost, Permafr. Periglac. Process., 11(3), 219–239, doi:10.1002/1099-1530(200007/09)11:3<219::AID-PPP352>3.0.CO;2-7, 2000.

Romanovsky, V. E., Smith, S. L. and Christiansen, H. H.: Permafrost thermal state in the polar Northern Hemisphere during the international polar year 2007-2009: a synthesis, Permafr. Periglac. Process., 21(2), 106–116, doi:10.1002/ppp.689, 2010.

Sachs, T., Giebels, M., Boike, J. and Kutzbach, L.: Environmental controls on CH4 emission from polygonal tundra on the microsite scale in the Lena river delta, Siberia, Glob. Chang. Biol., 16(11), no–no, doi:10.1111/j.1365-2486.2010.02232.x, 2010.

Schaefer, K., Lantuit, H., Romanovsky, V. E., Schuur, E. a G. and Witt, R.: The impact of the permafrost carbon feedback on global climate, Environ. Res. Lett., 9(8), 085003, doi:10.1088/1748-9326/9/8/085003, 2014.

Schuur, E. A. G., McGuire, A. D., Schädel, C., Grosse, G., Harden, J. W., Hayes, D. J., Hugelius, G., Koven, C. D., Kuhry, P., Lawrence, D. M., Natali, S. M., Olefeldt, D., Romanovsky, V. E., Schaefer, K., Turetsky, M. R., Treat, C. C. and Vonk, J. E.: Climate change and the permafrost carbon feedback, Nature, 520(7546), 171–179, doi:10.1038/nature14338, 2015.

Shiklomanov, N. I., Streletskiy, D. A., Nelson, F. E., Hollister, R. D., Romanovsky, V. E., Tweedie, C. E., Bockheim, J. G. and Brown, J.: Decadal variations of active-layer thickness in moisture-controlled landscapes, Barrow, Alaska, J. Geophys. Res., 115(4), G00I04, doi:10.1029/2009JG001248, 2010.

Stevenson, J. A., Sun, X. and Mitchell, N. C.: Despeckling SRTM and other topographic data with a denoising algorithm, Geomorphology, 114(3), 238–252, doi:10.1016/j.geomorph.2009.07.006, 2010.

Sun, X., Rosin, P., Martin, R. and Langbein, F.: Fast and Effective Feature-Preserving Mesh Denoising, IEEE Trans. Vis. Comput. Graph., 13(5), 925–938, doi:10.1109/TVCG.2007.1065, 2007.

Tarnocai, C., Canadell, J. G., Schuur, E. A. G., Kuhry, P., Mazhitova, G. and Zimov, S.: Soil organic carbon pools in the northern circumpolar permafrost region, Global Biogeochem. Cycles, 23(2), n/a–n/a, doi:10.1029/2008GB003327, 2009.

Wilson, C. J. and Altmann, G. L.: Digital Elevation Model, 0.25 m, Barrow Environmental Observatory, Alaska, 2013, Next Gener. Ecosyst. Exp. Arct., [dataset], doi:10.5440/1224720, 2013.

Wise, J.: NIST Measurement Services: Liquid-In-Glass Thermometer Calibration Service, Washington, DC., 1988.

Zhang, T. and Stamnes, K.: Impact of climatic factors on the active layer and permafrost at Barrow, Alaska, Permafr. Periglac. Process., 9(3), 229–246, doi:10.1002/(SICI)1099-1530(199807/09)9:3<229::AID-PPP286>3.0.CO;2-T, 1998.

Zhang, T., Osterkamp, T. E. and Stamnes, K.: Some Characteristics of the Climate in Northern Alaska, U.S.A., Arct. Alp. Res., 28(4), 509, doi:10.2307/1551862, 1996.

Zona, D., Lipson, D. A., Zulueta, R. C., Oberbauer, S. F. and Oechel, W. C.: Microtopographic controls on ecosystem functioning in the Arctic Coastal Plain, J. Geophys. Res., 116(3), G00I08, doi:10.1029/2009JG001241, 2011.

Conclusion

This study contributes to the development of an approach to scale up ground thermal regime measurements to larger permafrost areas using a combination of thermal monitoring, modelling and up-scaling based on ecotypes and microtopographical position in different ice-wedge polygon phases. These proxies are useful to infer the ground thermal regime and other permafrost properties. In this thesis, the use of surface conditions such as vegetation communities and microtopography were evaluated for their effectiveness as up-scaling parameters for ground thermal regime.

In Chapter 1, ecotypes were found to be an effective way to scale-up the ground thermal regime in the discontinuous permafrost landscapes of Western Alaska. Using a cluster analysis, sites from the same and similar ecotypes grouped together, while ecotypes without near-surface permafrost grouped together but furthest from all permafrost containing ecotypes. Ecotypes composed of grasses, short shrubs, and mosses had the coldest permafrost. As the deciduous shrubs in ecotypes became larger and more dense though, the combine effect of increased snow trapping and increased leaf litter leading to moss absence, resulted in warmer or absence of near-surface permafrost. The presence or absence of a moss layer in some ecotypes was identified as an important indicator of the presence or absence of near-surface permafrost. Thus, through the use of ecotypes, we are able to account for the variability in ground thermal regime in these landscapes.

In Chapter 2, the microtopography created by ice-wedge polygons initiated changes in local hydrology leading to spatial variation in soil moisture and likely organic layer thickness. The microtopography also created local depressions that trapped snow leading to large spatial variations in snow cover. We found that the permafrost thermal regime and active layer dynamics were strongly dependant on snow cover timing and distribution as well as active layer wetness. Thus, the microtopographic position within each polygon (trough, rim, high center, low center, etc.) was found to be a good predictor of the variability in permafrost thermal regime and active layer dynamics. Additionally, we found that the high-centered polygon, with the most degraded ice wedges, tended to have the coldest mean annual ground temperature, likely due to the large high center with thin snow cover during the winter. Also, the active layer of the high-centered polygon was thawed for the shortest period of time and was the shallowest of all polygon types. This suggests that following ice-wedge degradation high-centered polygons stabilize, which is important considering recent reports of increased rates of ice-wedge degradation (Jorgenson et al.,

2006; Liljedahl et al., 2016), which is potentially transforming more landscapes into areas with high-centered polygons.

It is important to point out that the environmental factors that are most important for creating variation in the ground thermal regime differ among regions. For example, at lower latitudes, with warmer and discontinuous permafrost, the ecotype and its interaction with snow cover and hydrology is the most important factor for creating variation in the ground thermal regime. However, at higher latitudes with continuous permafrost, vegetation cover becomes less variable and other factors such as microtopography and its influence on hydrology and snow cover become more important for creating spatial variability in the ground thermal regime. While not studied here, it seems reasonable that in a mountainous region, factors such as aspect and topography might become more important. Therefore, through understanding of the variation in these surface conditions, the variation in permafrost thermal regime can be described and understood.

This approach shows particular promise for modelling and scaling up ground thermal regime as it allows for a much finer resolution than has been possible in the past. If we are able to model the permafrost thermal regime for the ecotypes present in a region, or the microtopographic positions within a polygon network; then it is only necessary to have a detailed map of the ecotypes or microtopography in order to generate a detailed map of the ground thermal regime. The number of model runs can be adapted to the numbers of ecotypes or microtopographic positions, hereby, greatly reducing the computing power needed while increasing the spatial resolution. To use this approach in other areas, more research is needed to understand which environmental factors are the most important in determining variations in ground thermal regime for that area.

References

Brown, J.: Tundra Soils Formed over Ice Wedges, Northern Alaska, Soil Sci. Soc. Am. J., 31(5), 686–691, doi:10.2136/sssaj1967.03615995003100050022x, 1967.

Brown, J., Ferrians, O. J., Heginbottom, J. a. and Melnikov, E. S.: Brown J. 1997 Circum-Arctic map of permafrost and ground-ice conditions.pdf., 1997.

Dingman, S. and Koutz, F.: Relations among vegetation, permafrost, and potential insolation in central Alaska, Arct. Alp. Res., 6(1), 37–47, 1974.

Gold, L. W. and Lachenbruch, A. H.: Thermal conditions in permafrost: a review of North American literature, in Proceedings of the Second International Conference on Permafrost, Yakutsk, USSR, North American Contribution, pp. 3–25, National Academy Of Sciences, Washington, D.C., 1973.

Goodrich, L.: The influence of snow cover on the ground thermal regime, Can. Geotech. J., 1982.

Hinzman, L. D., Kane, D. L., Gieck, R. E. and Everett, K. R.: Hydrologic and thermal properties of the active layer in the Alaskan Arctic, Cold Reg. Sci. Technol., 19(2), 95–110, doi:10.1016/0165-232X(91)90001-W, 1991.

Houghton, R. A.: Balancing the Global Carbon Budget, Annu. Rev. Earth Planet. Sci., 35(1), 313–347, doi:10.1146/annurev.earth.35.031306.140057, 2007.

Hugelius, G., Strauss, J., Zubrzycki, S., Harden, J. W., Schuur, E. A. G., Ping, C.-L., Schirrmeister, L., Grosse, G., Michaelson, G. J., Koven, C. D., O'Donnell, J. A., Elberling, B., Mishra, U., Camill, P., Yu, Z., Palmtag, J. and Kuhry, P.: Estimated stocks of circumpolar permafrost carbon with quantified uncertainty ranges and identified data gaps, Biogeosciences, 11(23), 6573–6593, doi:10.5194/bg-11-6573-2014, 2014.

IPCC: Climate Change 2014: Synthesis Report. Contribution of Working Groups I, II and III to the Fifth Assessment Report of the Intergovernmental Panel on Climate Change, edited by Core Writing Team, R. K. Pachauri, and L. A. Meyer, IPCC, Geneva, Switzerland. [online] Available from: http://www.ipcc.ch/report/ar5/syr/, 2014.

Jorgenson, M. T., Shur, Y. L. and Pullman, E. R.: Abrupt increase in permafrost degradation in Arctic Alaska, Geophys. Res. Lett., 33(2), L02503, doi:10.1029/2005GL024960, 2006.

Jorgenson, M. T., Romanovsky, V. E., Harden, J., Shur, Y., O'Donnell, J., Schuur, E. a. G., Kanevskiy, M. and Marchenko, S.: Resilience and vulnerability of permafrost to climate change, Can. J. For. Res., 40(7), 1219–1236, doi:10.1139/X10-060, 2010.

Koven, C. D., Ringeval, B., Friedlingstein, P., Ciais, P., Cadule, P., Khvorostyanov, D., Krinner, G. and Tarnocai, C.: Permafrost carbon-climate feedbacks accelerate global warming., Proc. Natl. Acad. Sci. U. S. A., 108(36), 14769–14774, doi:10.1073/pnas.1103910108, 2011.

Liljedahl, A. K., Hinzman, L. D. and Schulla, J.: Ice-Wedge Polygon Type Controls Low-Gradient Watershed-Scale Hydrology, in Proceedings of the Tenth International Conference on Permafrost, Salekhard, Russia, 25-29 June 2012, vol. 1, pp. 231–236., 2012.

Liljedahl, A. K., Boike, J., Daanen, R. P., Fedorov, A. N., Frost, G. V., Grosse, G., Hinzman, L. D., Iijma, Y., Jorgenson, J. C., Matveyeva, N., Necsoiu, M., Raynolds, M. K., Romanovsky, V. E., Schulla, J., Tape, K. D., Walker, D. A., Wilson, C. J., Yabuki, H. and Zona, D.: Pan-Arctic ice-wedge degradation in warming permafrost and its influence on tundra hydrology, Nat. Geosci., (March), 1–8, doi:10.1038/ngeo2674, 2016.

Muller, S. W.: Permafrost or permanently frozen ground and related engineering problems., J.W. Edwards, Ann Arbor., 1947.

National Research Council: Opportunities to Use Remote Sensing in Understanding Permafrost and Related Ecological Characteristics, National Academies Press, Washington, D.C., 2014.

Romanovsky, V. E. and Osterkamp, T. E.: Interannual variations of the thermal regime of the active layer and near-surface permafrost in northern Alaska, Permafr. Periglac. Process., 6(4), 313–335, doi:10.1002/ppp.3430060404, 1995.

Romanovsky, V. E., Smith, S. L. and Christiansen, H. H.: Permafrost thermal state in the polar Northern Hemisphere during the international polar year 2007-2009: a synthesis, Permafr. Periglac. Process., 21(2), 106–116, doi:10.1002/ppp.689, 2010.

Schaefer, K., Lantuit, H., Romanovsky, V. E., Schuur, E. a G. and Witt, R.: The impact of the permafrost carbon feedback on global climate, Environ. Res. Lett., 9(8), 085003, doi:10.1088/1748-9326/9/8/085003, 2014.

Schuur, E. A. G., McGuire, A. D., Schädel, C., Grosse, G., Harden, J. W., Hayes, D. J., Hugelius, G., Koven, C. D., Kuhry, P., Lawrence, D. M., Natali, S. M., Olefeldt, D., Romanovsky, V. E., Schaefer, K., Turetsky, M. R., Treat, C. C. and Vonk, J. E.: Climate change and the permafrost carbon feedback, Nature, 520(7546), 171–179, doi:10.1038/nature14338, 2015.

Stoeckeler, E. G.: Investigation of airfield construction in arctic and subarctic regions: identification and evaluation of Alaskan vegetation from airphotos with reference to soil, moisture and permafrost conditions : a preliminary paper, St. Paul, Minn., 1949.

Sturm, M., McFadden, J. and Liston, G.: Snow-shrub interactions in arctic tundra: A hypothesis with climatic implications., J. Clim., 14, 336–344, 2001.

Tarnocai, C., Canadell, J. G., Schuur, E. A. G., Kuhry, P., Mazhitova, G. and Zimov, S.: Soil organic carbon pools in the northern circumpolar permafrost region, Global Biogeochem. Cycles, 23(2), n/a–n/a, doi:10.1029/2008GB003327, 2009.

Viereck, L. A.: Forest Succession and Soil Development Adjacent to the Chena River in Interior Alaska, Arct. Alp. Res., 2(1), 1–26, 1970.

Westermann, S., Duguay, C. R., Grosse, G. and Kääb, A.: Remote sensing of permafrost and frozen ground, in Remote Sensing of the Cryosphere, pp. 307–344., 2014.

Williams, P. J. and Smith, M. W.: The Frozen Earth: Fundamentals of Geocryology, Cambridge University Press, New York., 1991.

Zhang, T., Barry, R. G., Knowles, K., Heginbottom, J. a and Brown, J.: Statistics and characteristics of permafrost and ground-ice distribution in the Northern Hemisphere, Polar Geogr., 31(1-2), 47–68, doi:10.1080/10889370802175895, 2008.

Appendix 1: Approval from M. T. Jorgenson to use Chapter 1

UNIVERSITY
of ALASKA

Bill Cable <wlcable@alaska.edu>

Selawik Ecotype Paper

Torre Jorgenson <ecoscience@alaska.net>   Thu, May 12, 2016 at 7:47 PM
To: wlcable@alaska.edu

Try again, it bounced back. Torre

From: Torre Jorgenson [mailto:ecoscience@alaska.net]
Sent: Thursday, May 12, 2016 9:43 AM
To: 'wlcable@alaska.edu'
Subject: RE: Selawik Ecotype Paper

Hi Bill,

As a co-author of the paper "Scaling-up Permafrost Thermal Measurements in Western Alaska using an Ecotype Approach", I approve of you using the paper in your thesis.

Good luck getting it to publication.

Torre

M. Torre Jorgenson

Alaska Ecoscience

2332 Cordes Dr

Fairbanks, AK 99709

Tel. 907-455-6374

ecoscience@alaska.net

From: Bill Cable [mailto:wlcable@alaska.edu]
Sent: Thursday, May 12, 2016 5:34 AM
To: M. Torre Jorgenson
Subject: Selawik Ecotype Paper

Appendix 2: Approval from R. C. Busey to use Chapter 2

UNIVERSITY
of ALASKA

Bill Cable <wlcable@alaska.edu>

Approval of Manuscript towards thesis

Bob Busey <rcbusey@alaska.edu>   Wed, Jul 6, 2016 at 8:49 AM
To: Bill Cable <wlcable@alaska.edu>

Hi Bill,
As a co-author of the paper "The Impact of Microtopography on Ground Thermal Regime in an Ice-Wedge Polygon Landscape", I approve of you using the paper in your thesis. I think that sounds like a great use of this paper. thanks
-Bob